NUREG/CP-0075
CSNI Report No. 97

Proceedings of the

CSNI/NRC Workshop on Ductile Piping Fracture Mechanics

Held at
San Antonio, Texas
June 21-22, 1984

Compiled by M.F. Kanninen

Sponsored by
Organization for Economic Co-Operation and Development
U.S. Nuclear Regulatory Commission
Oak Ridge National Laboratory

Proceedings prepared by
Southwest Research Institute

Available from

Superintendent of Documents
U.S. Government Printing Office
P.O. Box 37082
Washington D.C. 20013-7082

and

National Technical Information Service
Springfield , VA 22161

NUREG/CP-0075
CSNI Report No. 97
R5

Proceedings of the

CSNI/NRC Workshop on Ductile Piping Fracture Mechanics

Held at
San Antonio, Texas
June 21-22, 1984

Date Published: May 1988

Compiled by
M.F. Kanninen

Sponsored by
Organization for Economic Co-Operation and Development
U.S. Nuclear Regulatory Commission
Oak Ridge National Laboratory

Proceedings prepared by
Southwest Research Institute
P.O. Drawer 28510
San Antonio, TX 78284
NRC FIN B0119

ABSTRACT

This report contains the papers presented at a workshop meeting that was conducted to compare the various different elastic-plastic fracture mechanics analysis methods that can be applied to assess the margin of safety in cracked nuclear plant pipes. A specific problem - a circumferentially cracked Type 304 stainless steel pipe in combined axial tension and bending - was addressed. The applied bending moments at crack growth initiation and at fracture instability were sought. Seven estimation type solutions were performed along with a benchmark elastic-plastic finite element solution.

It was learned that precise specification of the material stress-strain curve must be made to obtain meaningful results. But, when applied under controlled conditions, the different estimation method solutions do provide reasonably consistent results. These results appear to be conservative in comparison with an elastic-plastic finite element solution that was performed to provide a comparison with these results.

Table of Contents

WORKSHOP SUMMARY

- by -

M.F. Kanninen* and J. Strosnider+

INTRODUCTION

Because nuclear plant piping systems employ materials that are ductile and tough, linear elastic fracture mechanics techniques will not usually suffice for fracture assessments when cracks are discovered. Unfortunately, rigorous standardized elastic-plastic fracture mechanics approaches are not yet available for practical applications. The current state-of-the-art centers on the use of deformation plasticity analyses that assume net section plastic flow or other idealized conditions. These approaches, widely known as estimation methods, often give rise to significantly different predictions for the margin of safety when applied to cracked nuclear plant piping systems. A possible reason is that each such approach depends upon many assumptions and idealizations. These are not always recognized by those who must base ignore/repair/remove decisions on cracked pipes based on the results of these analyses.

Recognizing this situation, the U.S. Nuclear Regulatory Commission (NRC) through the Heavy Section Steel Technology program arranged a workshop meeting. This workshop was held on 21-22 June 1984 at the Southwest Research Institute in San Antonio, Texas. The objective of the workshop was to help achieve a better basic understanding of the elastic-plastic analysis methods currently being applied to nuclear plant piping systems. The workshop involved many of the leading elastic-plastic fracture mechanics practitioners together with those having a practical need for this technology. A specific problem was selected as a focal point. To provide a benchmark, an elastic-plastic finite element solution was also obtained. This report summarizes the findings that emerged from the workshop and suggests the further steps that should be taken to expand upon this effort.

*Southwest Research Institute, San Antonio, Texas

+U.S. Nuclear Regulatory Commission, Washington, D.C.

BACKGROUND

The continuing occurrence of cracking in nuclear reactor piping systems, coupled with a desire to eliminate double-ended guillotine breaks as a design basis event, has created the need for reliable ductile piping fracture mechanics analysis techniques. When a crack is detected in the piping of an operating nuclear power plant, it is necessary to determine if the cracked pipe requires immediate repair, or if continued operation can be allowed. In addition to the need for evaluating flaws found in service, there is the possibility that some cracks may go undetected. This makes it necessary to quantify the conditions under which leak-before-break will occur. Ductile piping fracture mechanics models based on elastic-plastic fracture mechanics (EPFM) therefore play a critical role in both flaw evaluation and leak-before-break analyses for insuring nuclear power plant integrity.

The leak-before-break concept also provides the basis for eliminating the postulated double-ended guillotine break (DEGB). The DEGB was originally postulated in the U.S. for the purpose of sizing containment and emergency core cooling systems. But, it has also been used for defining mechanical loads and for evaluating the postbreak consequences of pipe rupture. The mechanical loads resulting from a postulated DEGB, together with seismic and other loads, are used for designing component supports and other structural members. The postbreak consequences resulting from a postulated DEGB produces a need for massive pipe whip restraints and jet impingement shields. These can reduce the reliability of inservice inspections and can increase the radiation exposure associated with in-service inspection and maintenance operations. They also are very expensive to design and install.

The postulated DEGB creates significant difficulties for old as well as new plants. For example, the postulated DEGB at the reactor pressure vessel nozzle led to the axisymmetric loss of coolant accident (LOCA) load issue. The currently proposed basis for eliminating the postulated DEGB relies heavily on deterministic EPFM analyses. These are needed to demonstrate that a through-wall crack of sufficient length to be reliably detected by leakage has an adequate margin against failure under normal and anticipated accident loading conditions.

The NRC, as well as other domestic and foreign organizations, is supporting efforts to develop the necessary elastic-plastic fracture mechanics analyses and to provide appropriate experimental data for thair validation. The Ductile Piping Fracture Mechanics Workshop described herein, organized in conjunction with CSNI, resulted from the NRC recognition that many different

approaches and solutions currently exist for performing ductile piping fracture analyses. Unfortunately, these too often give disparate predictions. Consequently, it is difficult for the NRC and the plant operators to make the appropriate decision on pipes with real or postulated cracks. These issues clearly illustrate the need for accurate and reliable ductile piping fracture mechanics analysis techniques.

APPROACH

The workshop approach was to have each of several EPFM practitioners lead the workshop participants to a complete and thorough understanding of their approach. The objective was to obtain a more complete understanding of the various closed-form EPFM analysis methods that are available. A common benchmark problem, against which the various analytic schemes can be evaluated, was also included. This evaluation included particular emphasis on the assumptions associated with each method and the effects of those assumptions on the calculated results.

The workshop was not intended to be competitive. Rather, it was intended to provide a forum where the applications and limitations of the various analytic methods could be identified and understood.

The problem to be evaluated was that of a large diameter pipe containing a through-wall crack located in a girth-weld. The pipe was to be subjected to a constant axial stress and a monotonically increasing bending moment. The pipe was made of a power law hardening material assumed to have a true-stress, true-strain curve of the Ramberg-Osgood form with the constants chosen to represent the stress strain behavior of wrought Type 304 stainless steel at 550°F. Because of the sensitivity of some analysis methods to the precise form of the curve, as an option, alternative representations (e.g., piece-wise linear) were also permitted.

The problem was to first calculate the applied J value as a function of bending moment up to the limit moment of the pipe. The second part of the problem was to use the base metal J-integral resistance curve to predict the applied bending moments at crack initiation and at load controlled instability. Third, it was to be assumed that the pipe is connected at each end to large rigid masses and that the pipe ends are subject to unlimited monotonically increasing rotation. Finally, as an optional exercise, consideration was to be given to incorporating distinct stress-strain and J-resistance curves for the weldment.

Elastic-plastic finite element analyses of these problems, both for a monolithic pipe and for a pipe with a discrete weld region, under both load-controlled and displacement controlled conditions, were requested for provide benchmark solutions. (The discrete weld problem is of interest since stainless steel weld material has been shown to have lower ductile fracture toughness than wrought stainless steel base metal). It was not possible to obtain these solutions in time for presentation at the workshop. But, the solutions for the monolithic pipe and the welded pipe are now in hand.

For the readers convenience, the workshop problem in the form presented to the workshop attendees is given as Appendix A of this report. The workshop agenda (note that some minor changes in this schedule, necessitated by travel schedule difficulties) is given as Appendix B. Appendix C contains a complete list of those who participated in the workshop. Finally, Appendix D provides the points suggested by Ian Milne of the UK CEGB for the piece-wise linear stress-strain curve used in some estimation solutions and in the finite element solution.

RESULTS AND DISCUSSION

A total of seven organizations presented closed-form analysis results at the workshop. Of these, three also addressed the weld problem. With some exceptions, the results were fairly consistent, but appeared in all cases to be relatively conservative. Owing to the difficulties encountered in performing a finite element simulation of this problem, the benchmark solutions that were being developed were not available at the time of the workshop. However, one solution was subsequently obtained and is discussed in the following.

The workshop problem that was posed to the workshop participants in April, 1984 is contained in Appendix A of this report. It was subsequently amended when it was pointed out by Ian Milne of CEGB that the power law hardening formulation would not provide truely representative results. Accordingly, as an option, it was decided that other forms of the stress-strain curve would be acceptable. One such was the piecewise linear representation formulated by CEGB that is given in Appendix D. As it turned out, all of the workshop solutions used either the power law hardening curve suggested in the original formulation of the workshop problem or the piecewise linear representation suggested by Milne. A comparison of these two curves is given as Figure 1.

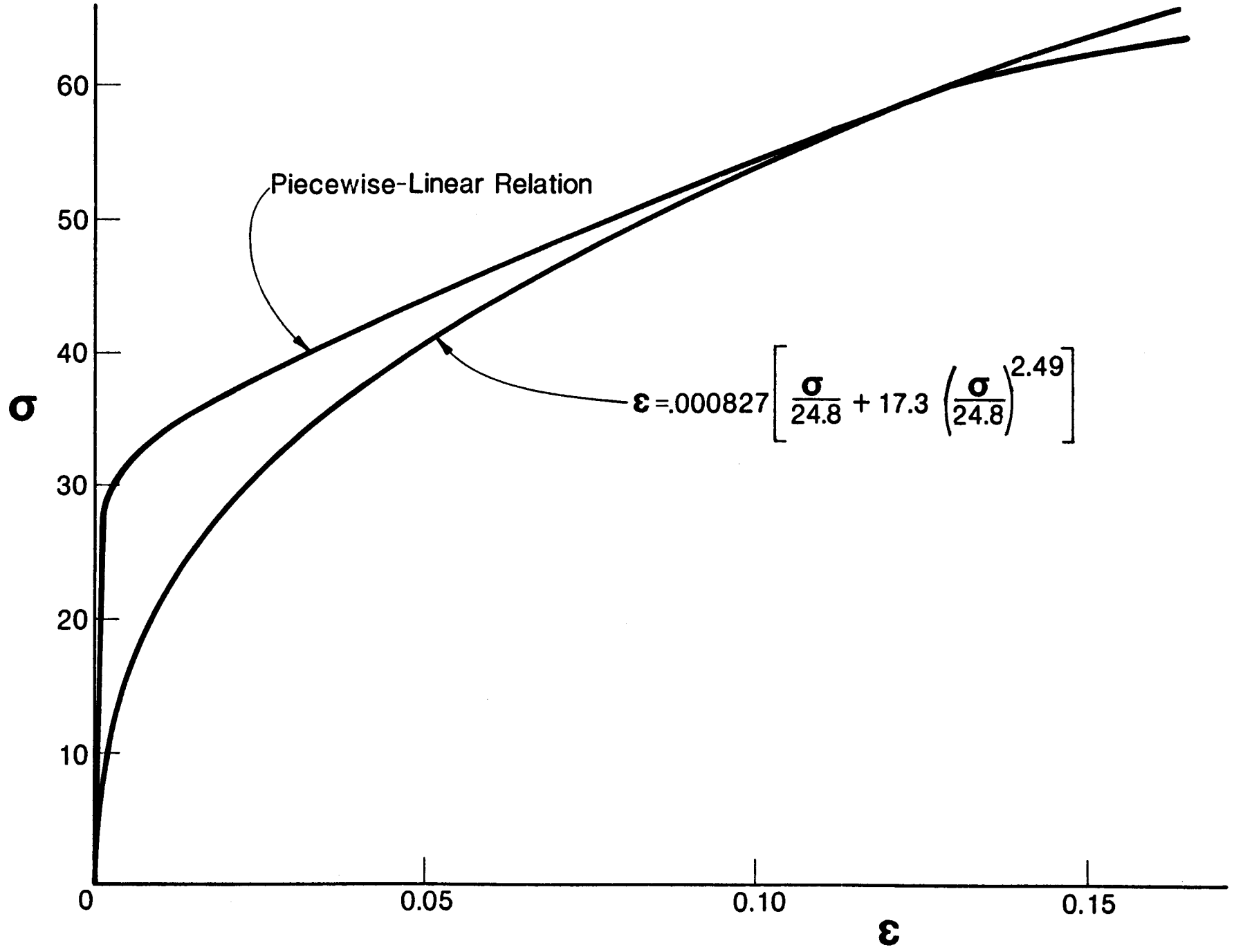

FIGURE 1. TYPE 304 STAINLESS STEEL STRESS-STRAIN CURVES
USED FOR CSNI WORKSHOP PROBLEM SOLUTIONS

In view of the relatively modest amount of difference that apparently exists between the two curves shown in Figure 1, it is perhaps surprising that the analysis predictions are significantly different. The result that best clarifies this finding is one taken from the CEGB workshop contribution presented by R. A. Ainsworth, given as Figure 2. This shows J as a function of the applied bending for the two different stress-strain curves. It can be seen that the prediction of crack growth initiation (i.e., when $J=J_{IC}$) is indeed markedly different for the two cases.

Table 1 displays the names of those giving formal presentations at the workshop. Note that not all of those listed presented solutions to the workshop problem per se. While seven solutions were presented, an equal number provided elaborations on one aspect or another of the general problem. Table 2 summarizes the specific solutions to the workshop problem that were actually received.

The contributed solutions shown in Table 2 have been delineated in terms of the particular analysis technique and the stress-strain curve representation. In the former category the technique designed as "FAD" is the failure analysis diagram (also known as the R6) approach while "J-T" implies the tearing instability approach. Results are given in Table 2 for both crack growth initiation and for fracture instability, both for the base metal monolithic case and for the two-phase weldment/base metal case.

For comparison with the results in Table 2, the elastic-plastic finite element solution developed by Cardinal and Polch at SwRI is of interest. Their solution predicts an applied bending moment at initiation of 2010 in-kips with a value of 2290 in-kips at instability. Figure 3 shows the plastic zones computed with the finite element model at crack growth initiation. This shows that net section yielding is being approached, consistent with the experimental findings. This result also indicates that the estimation method results using the power law hardening curve are conservative by roughly a factor of four at initiation and by at least a factor of two at fracture instability.

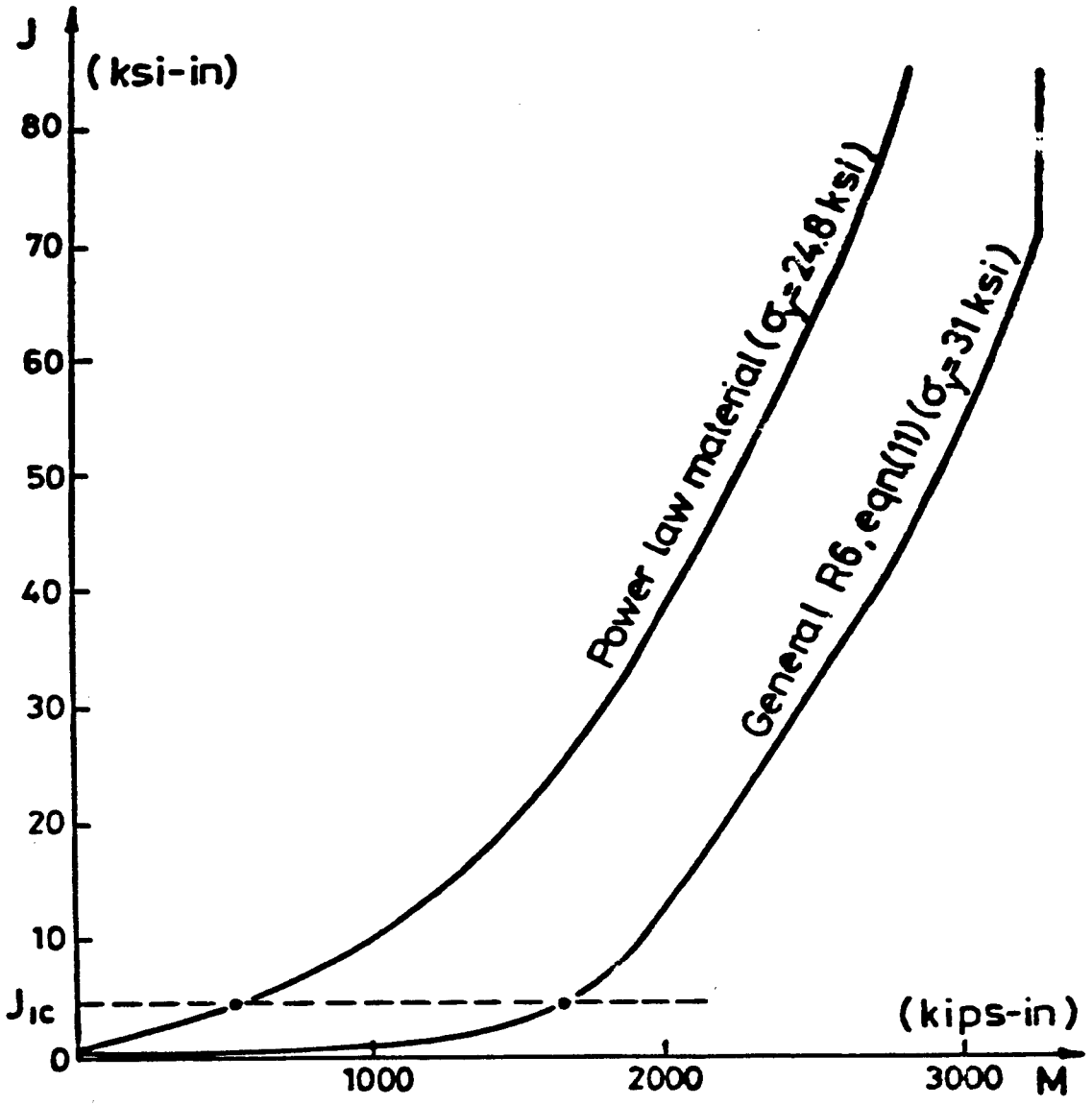

FIGURE 2. COMPARISON OF APPLIED BENDING MOMENT PREDICTED FOR INITIATION OF CRACK GROWTH USING TWO DIFFERENT STRESS-STRAIN REPRESENTATIONS AFTER AINSWORTH, et al.

TABLE 1. NRC/CSNI DUCTILE FRACTURE MECHANICS WORKSHOP PRESENTATIONS

Contributed Solutions

- R. Ainsworth ..... CEGB
- V. Kumar ..... GE
- D. Norris ..... EPRI
- J. Bloom ..... B&W
- P. Riccardella ..... SIA
- R. Packeiser* ..... BAM
- G. Wilkowski ..... BCL

Other Presentations

- J. Strosnider..... NRC
- K. Cotter..... FPDC
- A. Okamoto..... EPRI
- J. Pan..... BCL
- D. Broek..... FRI
- A. Zahoor..... IC
- R. Bass..... ORNL

- J. Cheissoux ..... CEA

Finite Element Solution

- J. Cardinal/Z. Polch ..... SwRI

*Solution submitted by telex – presentation made by M.F. Kanninen

CONCLUSIONS AND RECOMMENDATIONS

As a result of the workshop, progress was achieved towards a better understanding of ductile fracture mechanics methods for nuclear plant piping. This progress has led to several conclusions. These, together with the recommendations that they engender, can be summarized as follows.

First, the estimation methods that are now available are highly sensitive to the exact representation of the material stress-strain curve. The power law hardening representation, chosen mainly because of its utility in deformation plasticity estimation method solutions, was clearly shown to give predictions that are significantly different than those obtained with more exact representations; e.g., a piece-wise linear fit. It is therefore recommended that attention be given to the generalization of the estimation methods to admit more precise stress-strain behavior, assuming that this can be accomplished without an inordinate increase in complexity.

ORGANIZATION	TECHNIQUE	STRESS-STRAIN CURVE	BASE METAL		WELD METAL	
			INITIATION MOMENT (IN-KIPS)	INSTABILITY MOMENT (IN-KIPS)	INITIATION MOMENT (IN-KIPS)	INSTABILITY MOMENT (IN-KIPS)
CEGB	FAD	POWER LAW	527	1067	-	-
		MILNE	1655	1850	1364 / 2225	1565 / 2716
GE	GE/EPRI HANDBOOK	POWER LAW	450	980	-	-
EPRI	DPFAD	POWER LAW	321	765	1889	2437
	J-T	POWER LAW	321	651	1889	2474
	J-L	POWER LAW	321	784	1889	2456
	LIMIT LOAD	POWER LAW	-	2881	-	2881
B&W	DPFAD	POWER LAW	286	755	1843	2360
BCL	GE/EPRI HANDBOOK	POWER LAW	560	1025	-	-
BAM	LEFM		3070	3310	-	-
STRUCTURAL INTEGRITY ASSOCIATES	J ESTIMATION (BENDING APPROX) J-T	POWER LAW	-	700	-	2600
SOUTHWEST RESEARCH INSTITUTE	ELASTIC-PLASTIC FINITE ELEMENT	MILNE	2013	2535	1578	2013

TABLE 2. SUMMARY OF CSNI/NRC DUCTILE PIPING FRACTURE MECHANICS WORKSHOP PROBLEM SOLUTIONS

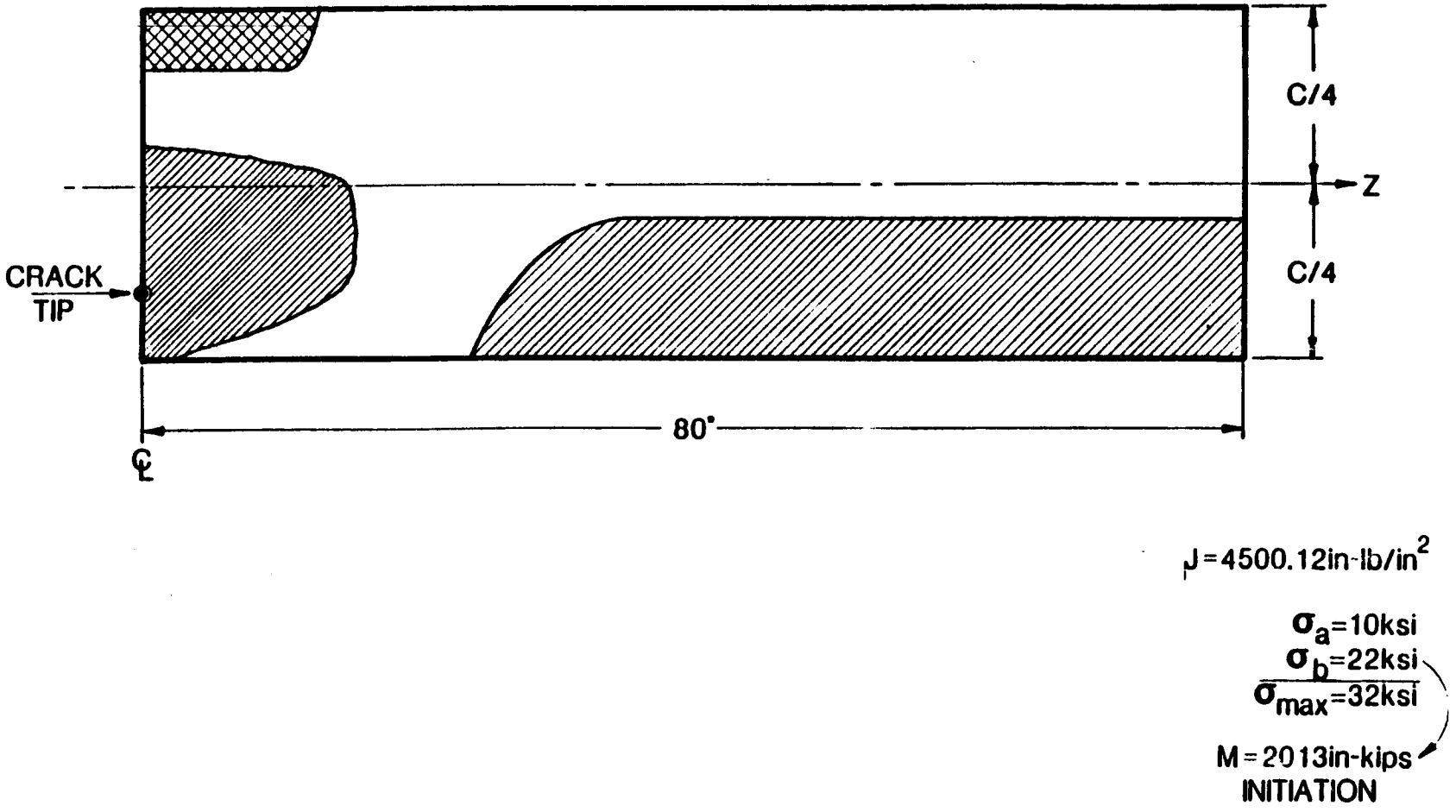

FIGURE 3. PLASTIC ZONES AT CRACK INITIATION
PREDICTED WITH THE FINITE ELEMENT MODEL

The second conclusion stemming from the workshop is that there is a definite need for an experimental data base that can be used to assess the ductile fracture techniques that have been (and will be) used for nuclear plant piping systems. A large program supported by the NRC is now in progress. However, it must be recognized that neither this or any other similar program will be able to encompass all possible piping system cracking scenarios. Accordingly, the focus of any such program is properly on obtaining results that can be used to test and validate analysis methods. These, in turn, can be used in a much more cost-effective manner to address the myriad of service problems that can be expected. The experimental pipe fracture effort must of course be cognizant of the nature of the pipe cracking problems that can be anticipated in service. But, of possibly more importance, attention must also be placed on providing results that properly define an elastic-plastic boundary value problem. It is recommended that all current and anticipated experimental pipe fracture programs be planned with this as a foremost consideration.

The third conclusion stems from the clear inadequacies of the current approaches to problems in which the weldment is to be considered explicitly; i.e., with stress-strain and resistance curve properties that are distinct from those of the base metal. The effect of prior plastic deformation and material microstructural alterations induced by the welding procedure, while largely ignored in current work, should be considered to quantify those effects. At this point it would appear that only elastic-thermoplastic, multi-phase, finite element analyses offer the possibility of approaching such problems. It is recommended that these be undertaken in conjunction with experiments guided by analysis considerations (see above).

Finally, it can be concluded that the workshop accomplished its objective in that, (1) a quantitative comparison of several different approaches to a common problem was achieved, and (2) the participants enhanced their understanding of the approaches that are now in use. More particularly, the assumptions and idealization necessarily underlying such approximate methods were clearly revealed and assimilated by the participants. But, it should also be recognized that the physical problem that was the focus of the analysis efforts was a very simple one. Three obvious complications that could be considered to make such a problem more representative of actual service conditions would be to consider; (1) a part-through-wall crack, (2) that the crack is in a weld or in a nearby heat affected zone, and (3) that the loading is not monotonic but could be cyclic and dynamic. On the basis that this workshop proved to be an effective vehicle for advancing this

technology, it is recommended that a similar workshop be organized to address a more complicated problem incorporating one or more of these more realistic features. The CSNI would be the logical agency to sponsor such an activity.

ACKNOWLEDGEMENTS

This workshop was made possible by support extended by the U.S. Nuclear Regulatory Commission through the Heavy Section Steel Technology Program conducted by the Oak Ridge National Laboratory. The author would like to thank Charles Serpan and Jack Strosnider of the NRC and Claud Pugh of ORNL for giving him the opportunity to organize and conduct the workshop. He also would be exceedingly remiss in not acknowledging the several contributions of Jack Strosnider in providing background material on the underlying issues and for his enthusiastic participation in the workshop itself.

SOLUTION TO THE WORKSHOP PROBLEM USING THE CEGB FRACTURE ASSESSMENT PROCEDURE [R6]

- by -

R.A. Ainsworth*, G.G. Chell+ and I. Milne+

SUMMARY

The workshop problem has been specified as a large diameter stainless steel pipe with a part-circumferential through-wall crack. The pipe is subjected to a constant axial stress and an increasing bending moment. This paper presents a standard R6 solution to define the bending moments at crack initiation and load controlled instability using the failure assessment line developed for materials with a high capacity for work hardening. An addendum briefly describes the background to the R6 approach and its validation for stainless steels. The addendum also uses the R6 procedure to derive additional information about the workshop problem and illustrates the sensitivity of the problem to the input material deformation data.

INTRODUCTION

The solution of any problem by the CEGB failure assessment procedure R6[1] follows a series of well-defined steps. These have been illustrated by the worked examples given by Harrison et al. [2]. The solution of the CSNI Workshop problem is given in the main text of this paper and follows these steps which are:

1. Definition of the problem - this is not always simple in practical situations, but has, of course, been provided for the workshop problem.

* Central Electricity Generating Board, Berkeley Nuclear Laboratories, Berkeley, Gloucestershire, UK.

+ Central Electricity Generating Board, Central Electricity Research Laboratories, Leatherhead, Surrey, UK.

2. Characterization of the flaw and geometry - here it is necessary to characterize the flaw and geometry into a form for which limit load and stress intensity factors are available or can be calculated. This is straightforward for the workshop problem, but can be much more difficult in plant applications.

3. Establishing the material properties - both flow and fracture properties are required.

4. Stress analysis - this is usually done by establishing elastic stresses for the uncracked body.

5. Calculation of the plastic yield load ratio L_r for a range of crack sizes. This requires only a knowledge of the plastic collapse load as a function of crack size.

6. Calculation of the stress intensity factor ratio K_r for a range of crack sizes. This comes from a knowledge of the elastic stress intensity factor.

7. Perform an assessment using the calculated values of L_r and K_r compare an assessment point (L_r, K_r) with a specified failure assessment curve.

8. Sensitivity analysis - this is omitted for the workshop problem.

The failure assessment curve used in step 7 has recently been modified for materials with a high capacity for work hardening such as the stainless steel of the workshop problem. The background to these changes is given in an addendum to this paper. This also includes further details about the workshop problem which are not part of the normal procedure given above but which can be derived from the R6 solution.

1. PROBLEM DEFINITION

The geometry of interest is that of a large diameter pipe containing a simple through-wall crack as shown in Figure 1. The pipe is subjected to a constant axial stress of 10 ksi which does not vary as a result of any crack growth or end rotation of the pipe. The problem is to predict the applied bending moments at crack initiation and at load controlled instability following ductile crack growth.

2. GEOMETRY AND FLAW CHARACTERIZATION

The geometry and notation are given in Figure 1. The important dimensions are:

Mean radius of pipe	R	= 7.75 in
Thickness of pipe	t	= 0.50 in
Initial semi-crack angle	θ_o	= 0.645 radians
Initial crack length	$a_o=R\theta_o$	= 5.00 in
Semi-pipe length	L	= 420 in

For the purposes of analysis the flaw is characterized by its mean semi-length $a=R\theta$ and is assumed to extend equally at both crack tips.

3. MATERIAL PROPERTIES

For the purposes of this example, parent material properties appropriate for Type 304 stainless steel are taken. Discussion of relevant material properties and the inclusion of weld data are given in the addendum.

Lower bound yield (proof) stress, $\sigma_y = 31$ ksi

Lower bound ultimate stress, $\sigma_u = 75$ ksi

Lower bound flow stress, $\bar{\sigma} = \frac{1}{2}(\sigma_y + \sigma_u) = 53$ ksi

Initiation fracture toughness, $K_i = 367 \text{ ksi } (\text{in})^{1/2}$

Fracture resistance, $K_\Omega(\Delta a) = 741(\Delta a)^{0.21} \text{ ksi}(\text{in})^{1/2}$

The initiation toughness corresponds to an initiation value of $J_i=K_i^2/E=4.5$ ksi-in with Young's modulus E = 30,000 ksi. The fracture resistance K_Ω corresponds to $J = 18.3\ (\Delta a)^{0.42}$ ksi-in and is compared to the data supplied in Figure 2. The power law fit gives exact agreement at the quoted initiation toughness, and reasonable agreement over the first one inch of crack growth. Representation of toughness data by a power law is not necessary in order to use the R6 method but, has been adopted here for convenience.

4. STRESS ANALYSIS

The applied axial stress is given as σ_z=10 ksi. The nominal bending stress due to the applied moment M is

$$\sigma_b = M/\pi R^2 t$$

5. EVALUATION OF L_r

The plastic collapse load of a circular cross-section containing a through-wall crack under tension and bending has been given by Ranta-Maunus and Achenbach [3]. The value of L_r is the ratio of the applied loading to that required to cause plastic yielding (the load factor against plastic yielding is $1/L_r$ and applies equally to σ_z and σ_b). The value of L_r is given by:

$$\frac{\pi\sigma_b}{2L_r\sigma_y} = 2 \sin\left[\frac{\pi}{2}\left(1 - \frac{\sigma_z}{L_r\sigma_y}\right) - \frac{1}{2}\theta\right] - \sin\theta$$

Calculations are continued to the value $L_r = L_r^{max}$ defined by:

$$L_r^{max} = \bar{\sigma}/\sigma_y = 53/31 = 1.71$$

and this defines the cut-off on the R6 diagram, Figure 3. Values of L_r as a function of σ_b (i.e. M) can readily be evaluated for the initial crack size ($\theta=\theta_o=0.645$) and some results are given in Table 1. Plastic collapse corresponds to $L_r = L_r^{max}$ at a value M=3270 in-kips.

6. EVALUATION OF K_r

For the axial stress the stress intensity factor has been obtained from Delale and Erdogan [4] as:

$$K_z = \sigma_z(\pi a)^{1/2}\, Y_1(a/(Rt)^{1/2})$$

where

$$Y_1(x) = 1 + 0.\,19x + 0.01x^2$$

is an approximate quadratic fit to the tabulated values of Delale and Erdogan. For the bending stress, the stress intensity factor has been obtained from the axial stress result, but scaled according to the bending/axial K-ratio given by Sanders [5]. This gives:

$$K_b = \sigma_b(\pi a)^{1/2}\, Y_1(a/(Rt)^{1/2})\;\; Y_2(\theta)$$

where

$$Y_2(\theta) = \frac{1/2 \sin\theta \{4 \cot[(\pi-\theta)/\sqrt{2}] + 3\sqrt{2}\cot\theta + \sqrt{2}\,\theta\cot^2\theta + \sqrt{2}\,\theta\}}{2\,\theta\cot[(\pi-\theta)/\sqrt{2}] + \sqrt{2}\,\theta\cot + \sqrt{2}}$$

and

$$K_r = (K_z + K_b) \;/\; K_\Omega(\Delta a)$$

where K_z and K_b are evaluated for a crack length $a_o + \Delta a$. For initiation assessments K_Ω is replaced by $K_c = 367$ ksi $(\text{in})^{1/2}$ and K_z and K_b are evaluated for a crack size a_o. These results are listed in Table 1.

7. ASSESSMENT

7.1 Assessment for Crack Initiation

The assessment points as a function of applied moment are plotted in Figure 3 for the initial crack size a_o (i.e. the tabulated values of L_r and K_r in Table 1). The intersection of the locus of assessment points with the failure assessment line occurs at the point $L_r = 1.09$, $K_r = 0.44$ and this gives

Bending moment at crack initiation:

$$M_i = 1655 \text{ kips-in}$$

7.2 Assessment for Load-Controlled Instability

The calculations which gave values of K_r and L_r in Table 1 can easily be repeated for postulated crack extensions Δa giving a total crack length $a = a_o + \Delta a$. Results are given in Table 2 for an applied bending moment equal to 1850 kips-in. For this bending moment the locus of assessment points as a function of crack extensions is tangential to the failure assessment curve. Thus

Bending moment at load-controlled instability:

$$M_{max} = 1850 \text{ kips-in}$$

Points on the assessment curve between the points for crack initiation and instability correspond to increasing amounts of crack growth. The points can be established, in the same way as the initiation load, by constructing a locus of assessment points for increasing applied moment for postulated amounts of crack growth. Results are given in Table 3. The crack extension at the maximum load is:

$$\Delta a_t = 0.29 \text{ in}$$

8. OBSERVATIONS

The solution to the problem has been obtained by hand calculation using stress intensity factor and limit load solutions available in the literature. The accuracy of the solution is, of course, dependent on the accuracy of these input solutions. In real problems, where there are uncertainties in the input data, a conservative result can be obtained by using upper bound estimates of stress intensity factor, lower bound estimates of collapse load, and lower bound material properties. It is worth remarking that the failure assessment curve is taken as geometry independent and that calculations are only required to establish assessment points and not to establish this curve.

The above sections have presented a standard R6 assessment, apart from an analysis of the sensitivity of the result to variations in the input data which has been omitted. The R6 analysis is, however, equivalent to a J-analysis as described in the addendum and further information about the solution can therefore be derived. The addendum presents this information for: J as a function of applied moment; rotation results as a function of

applied moment; and an assessment of the sensitivity of the solution to the interpretation of the basic stress-strain data.

REFERENCES

[1] R.P. Harrison, K. Loosemore, I. Milne and A.R. Dowling, Assessment of the integrity of structures containing defects, CEGB Report R/HR6 - Rev. 2 (1980).

[2] R.P. Harrison, K. Loosemore, I. Milne, A.R. Dowling and R.A. Ainsworth, Assessment of the integrity of structures containing defects, supplement 2 - worked examples, CEGB Repoprt R/H/R6 - Supplement 2 (1983).

[3] A.K. Ranta-Maunus and J.D. Achenbach, Nucl. Eng. and Design 60, 339 (1980).

[4] F. Delale and F. Erdogan, Quarterly Appl. Maths. 37 239 (1983).

[5] J.L. Sanders, ASME J. Applied Mechanics, 50, 221 (1983).

ACKNOWLEDGEMENT

This paper is published by permission of the Central Electricity Generating Board.

TABLE 1. ASSESSMENT POINTS FOR INITIAL CRACK SIZE, a_o = 5 in

M (kips-in)	σ_b (ksi)	L_r	K_r
0	0	0.54	0.17
100	1.06	0.57	0.18
500	5.3	0.69	0.25
1000	10.6	0.86	0.33
1500	15.9	1.04	0.42
2000	21.2	1.22	0.50
2500	26.5	1.41	0.58
3000	31.8	1.60	0.66
3270	34.7	1.71	0.71

TABLE 2: ASSESSMENT POINTS FOR MOMENT M = 1850 kips-in

a_o (in)	Δa (in)	a (in)	K_Ω ksi(in)$^{1/2}$	L_r	K_r
5.0	0	5.0	367	1.17	0.47
5.0	0.26	5.26	574	1.21	0.31
5.0	0.52	5.52	656	1.25	0.29
5.0	0.78	5.78	710	1.30	0.28
5.0	1.04	6.04	746	1.35	0.27

TABLE 3: GROWTH LOCUS

a (in)	Δa (in)	M (kips-in)
5.0	0	1655
5.06	0.06	1768
5.12	0.12	1811
5.20	0.20	1840
5.29	0.29	1850

TABLE 4: VALUES OF J AS A FUNCTION OF APPLIED MOMENT FOR INITIAL CRACK SIZE, a_o = 5 in.

M (kips-in)	σ_b (ksi)	$J^{(1)}$ ksi-in
0	0	0.14
100	1.06	0.17
500	5.3	0.36
1000	10.6	0.88
1500	15.9	2.87
2000	21.2	12.3
2500	26.5	31.4
3000	31.8	53.6
3270	34.7	71.6

(1) Obtained using the general R6 Equation (11) with σ_y = 31 ksi

ADDENDUM - BACKGROUND TO THE CEGB APPROACH [R6] FOR STRAIN HARDENING MATERIALS

1. J-ESTIMATES

Without loss of generality, the value of J for a crack in a component under load can be expressed as:

$$J = \sigma_{ref}\ \varepsilon_{ref}\ R$$

where σ_{ref} is some nominal or reference stress due to the applied load, ε_{ref} is the corresponding strain from uniaxial tensile data, and R is a characteristic dimension. This dimension can be related to the elastic solution:

$$J_{el} = K^2/E' \qquad (1)$$

so that J becomes:

$$J = J_{el}\ (E\ \varepsilon_{ref}/\sigma_{ref}) \qquad (2)$$

Thus the calculation of J under elastic-plastic conditions is equivalent to the determination of the elastic K plus the evaluation of a reference stress. Clearly, under elastic conditions the value of reference stress is arbitrary as $E\ \varepsilon_{ref}/\varepsilon_{ref} = 1$ for elastic behavior.

Values of reference stress to describe fully plastic behavior may be obtained from the results of Kumar et al [A1] who give, in their notation:

$$J = \alpha\sigma_o\varepsilon_o\ c(a/b)\ h_1\ (a/b,\ n)\ (P/P_o)^{n+1} \qquad (3)$$

for a material with

$$\varepsilon/\varepsilon = \alpha(\sigma/\sigma_o)^n$$

Noting that n=1 corresponds to an elastic solution, Equations (3) and Equation (2) are identical for the reference stress defined by:

$$\sigma_{ref}(a/b),\ n = P\sigma_o/\mu P_o$$

where

$$\mu^{n-1} = h_1\ (a/b,\ 1)/h_1(a/b,\ n)$$

It transpires [A2] that h_1 does not vary strongly with n given the normalization used by Kumar et al. [A1] and the value of μ is close to unity and sensibly independent of n for large n. Thus, in general Equation (2) can be used to evaluate J for fully plastic behavior with the reference stress defined by:

$$\sigma_{ref} = P\sigma_o/P_L(\sigma_o) \tag{4}$$

where $P_L(\sigma_o)$ is the plastic collapse load for a rigid plastic material of yield stress σ_o. The value μP_o has been replaced by P_L as this gives a better normalization than P_o for reference stress purposes, particularly where some authors have used a net section stress unrelated to plastic collapse and produced a strong dependence of h_1 on n (see [A2] for further details).

The use of Equation (2) with the reference stress defined by Equation (4) is adequate for elastic and fully plastic behavior. However, in the intermediate elastic-plastic regime some plastic zone correction is required for $\sigma_{ref} < \sigma_y$, the yield stress. Based on the empirical solution of [A1], Equation (2) can be modified to describe the whole range of behavior giving [A2]

$$J/J_{el} = E\varepsilon_{ref}/\sigma_{ref} + \tfrac{1}{2}(\sigma_{ref}/\sigma_y)^2/[1 + (\sigma_{ref}/\sigma_y)^2] \tag{5}$$

with

$$\sigma_{ref} = P\sigma_o/P_L(\sigma_o)$$

2. THE [R6] APPROACH FOR STRAIN HARDENING MATERIALS

Failure is avoided provided J is less than some critical material value J_c and provided the load is less than the collapse load, i.e.

$$J \leq J_c$$
$$P \leq P_L(\sigma_{flow}) \tag{6}$$

where plastic collapse has been assumed to be governed by a flow stress, usually the mean of the 0.2% proof stress and the ultimate stress. In [R6] these limits are written in terms of non-dimensional variables K_r and L_r defined as:

$$K_r = K/K_c \tag{7}$$

$$L_r = P/P_L(\sigma_y) \tag{8}$$

where σ_y is the yield or 0.2% proof stress. With these definitions and J defined by Equation (5) the failure avoidance limits of (6) are:

$$K_r \leq [E\,\varepsilon_{ref}/\sigma_{ref} + \frac{1}{2}\,L_r^2/\,(1+L_r^2)]^{-1/2}$$

$$L_r \leq L_r^{max} = \sigma_{flow}/\sigma_y \tag{9}$$

where $\sigma_{ref} = L_r\sigma_y$

Equations (9) with the variables L_r and K_r defined by Equations (7) and (8) represent the basic CEGB failure assessment method for strain-hardening materials. The method may be represented on the failure avoidance diagram shown schematically in Figure A1. For a component, if an assessment point (L_r, K_r) defined by Equations (7, 8) lies inside the curve then the crack will not lead to failure under the given applied loads. It should be noted that, although the approach of [A1] has been used in the derivation of Equation (9), the failure assessment curve is geometry independent and does not require values of the h-functions used in [A1].

2.1 The R6 Procedure for Stable Tearing

Stable tearing from a crack of initial size a_o is included in R6 by evaluating K_r and L_r for a range of postulated crack extensions Δa. In this case Equations (7) and (8) become:

$$K_r = K(a_o + \Delta a)/K_\Omega(\Delta a)$$

$$L_r = P/P_L(a_o+\Delta a, \sigma_y)$$

where $K_\Omega(\Delta a)$is the material resistance derived from the J-resistance by $K_\Omega^2(\Delta a) = E'J_R(\Delta a)$. Values of K_r and L_r can be evaluated for a range of loads and postulated crack extensions as shown schematically in Figure A1.

For the initial crack size (i.e. $\Delta a = 0$) assessment points move along the line OA under increasing load and crack initiation is predicted at the load $P = P_2$ where the locus intersects the failure assessment line at C. At a higher load $P = P_3$, the assessment point lies outside the failure assessment line for $\Delta a = 0$ but lies inside the line for $\Delta a = \Delta a_1$: thus, at this load the crack is predicted to behave stably with a crack extension $\Delta a < \Delta a_1$. For the load $P = P_5$, all assessment points lie outside the failure assessment line and it is predicted that application of this load would lead to failure. At the load $P = P_4$ the locus of assessment points for increasing Δa is tangential to the failure assessment curve at D: this is the predicted maximum tolerable load and the corresponding crack extension at maximum load is $\Delta a = \Delta a_2$. The R6 prediction under increasing load can be summarized as follows: Assessment points follow the line OA until crack initiation occurs at the load $P = P_2$ at the intersection, C, of OA with the failure assessment curve; thereafter under increasing load crack growth occurs with assessment points following the portion CD of the failure assessment curve until load controlled instability occurs at the point D at a load P_4 and crack extension Δa_2.

The above analysis procedure is completely equivalent to a tearing analysis using J and defining load controlled instability by dJ/da(structure) $\geq dJ_R/da$. The simplification in the R6 procedure arises through the adoption of the approximate estimate of J given by Equation (5) which is reflected in the failure assessment curve of Equation (9).

2.2 The Failure Assessment Curve

It is apparent that adopting the normalization of Equations (7) and (8) leads to a geometry independent curve in Equation (9). Geometry dependence is, of course, included in the stress intensity factor and limit load functions of Equations (7) and (8). The failure assessment curve can be established if stress-strain data is available, and this is a possible option in the proposed strain hardening failure assessment procedure. However, other options are available if detailed stress-strain data is not available. One option is for materials with a low capacity for strain hardening. For elastic-perfectly plastic materials ($E\,\varepsilon_{ref}/\sigma_{ref} = 1$, $\sigma_{ref} < \sigma_y$; $\varepsilon_{ref} \to \infty$, $\sigma_{ref} = \sigma_y$) Equation (9) defines a simple plastic zone correction with a cut-off at collapse. This was the basis of the original R6 procedure [A3], except that the plastic zone correction was based on the Bilby-Cottrell-Swinden model rather than the first-order Irwin correction used in Equation (9) (see Chell [A4] for further discussion). This led to the failure assessment curve:

$$K_r \leq S_r \{(8/\pi^2) \ln \sec (\pi S_r/2)\}^{-1/2} \qquad (10)$$

with

$$S_r = P/P_L\,(\sigma_{flow})$$

being used to include work hardening in an approximate manner. The simplification is adequate for materials with the ratio σ_u/σ_y less than about 1.3.

For materials with a higher capacity for work hardening, an approximate lower bound curve to Equation (9) has been obtained by plotting data for a range of materials, including stainless steels. This has led to the approximate failure assessment line

$$K_r \leq (1 - 0.14L_r^2)[0.3 + 0.7 \exp(-0.65L_r^6)] \qquad (11)$$

used in the basic workshop problem. Where material stress-strain data is available, however, it is better to use Equation (9) rather than either of the simple formulae (10) and (11).

2.3 Validation of the Procedure for Stainless Steels

Akhurst and Milne [A5] have tested a range of stainless steel geometries (SENT, DENT, CCP, 3PB) with a range of crack depths (a/w = 0.4, 0.6, 0.8) and derived experimental J values from the load-displacement records. The experimental results showed no systematic effect of crack depth and typical results for a/w = 0.6 are shown in Figure A2 and compared with Equation (11). It can be seen that Equation (11) is a good and slightly conservative line for bend type geometries, although somewhat more conservative for tension geometries (CC and SENT at large deflections). This may be due to an actual conservatism or it may reflect uncertainties in J estimates derived from load-displacement records for these last geometries.

3. FURTHER CALCULATIONS FOR THE WORKSHOP PROBLEM

3.1 The Failure Assessment Curve

In order to derive the failure assessment curve of Equation (9) it is necessary to have material stress-strain data. The stress-strain curves obtained from the two power laws given for the workshop problem are shown plotted in Figure A3 together with their respective $(\varepsilon_o, \sigma_o)$ co-ordinate points. Neither of these points lie on the power-law curves. The largest disagreement is for parent material where at σ_o the strain represented by the power law is some eighteen times ε_o. The $(\varepsilon_o, \sigma_o)$ coordinates do, however, lie on the elastic modulus line and the values of σ_o given are typical of proof stresses for the respective types of material. The 0.2% proof stresses derived from the power laws are 11.3 ksi and 49.8 ksi for the parent and weld material respectively. The proof stress defines the value to use for σ_y in Equation (9) and the resulting assessment diagram for the parent material is shown as curve 2 in Figure A4. An additional stress-strain curve with properties more closely representing the low-strain behavior of stainless steels is also shown in Figure A3. This curve passes through the $(\varepsilon_o, \sigma_o)$ point for the parent material and was constructed to provide the given flow stress of 53 ksi and to converge to the given power-law curve at 10% strain. The curve has a proof stress of 31 ksi and results in the assessment diagram given by curve 4 in Figure A4. It approximates to curve 3 in Figure A4, the curve validated by the experimental results shown in Figure A2 (Ref. [A5]). Also included for illustration in Figure A4 is curve 1 obtained by arbitrarily taking σ_y as the value of σ_o used in the power law (i.e. σ_o = 24.8 ksi).

It is contended that for the parent material, the additionally derived stress-strain curve is more representative of the behavior of stainless steels in the important low strain region than the power-law curve. As this derived data produces a failure assessment curve very similar to the general curve of Equation (11), this general curve has been used to produce the basic solution to the workshop problem. However, in order to demonstrate the results that would be obtained if the power-law given in the workshop problem data were relevant, an R6 solution for curve 1 is given below.

The curves of Figure A4 show that very different failure assessment diagrams are obtained for different stress-strain curves. It must be emphasized that this is not some peculiarity of the R6 approach. It is merely a reflection that the calculated value of J, which is essentially a strain-based quantity in the plastic region, depends strongly on material strain data at low strains. Thus the two curves of Figure A3 for parent material, which show large differences in strain for stress levels in the region of σ_o, may be expected to exhibit large differences in calculated values of J for nominal component stresses in the region of σ_o. Therefore, in any component assessment, whether by R6 or some J-estimation approach, a realistic representation of the material stress-strain data over the full range of strain should be employed.

For weld metal the stress-strain data is shown in Figure A3 and the corresponding failure assessment lines are shown in Figure A5. Here σ_o is close to the 0.2% proof stress and the curves differ little from Equation (11). For assessments given below, this general curve (curve 3) has been adopted with yield data arbitrarily taken as σ_y = 50 ksi, σ_u = 62 ksi giving a cut off at L_r^{max} = 1.12.

3.2 R6 Solution for Power-Law Material

The assessment proceeds in an identical manner to Section 7 of the main text, but the yield stress is taken as 24.8 ksi to define L_r and the failure assessment curve has been taken as curve 1 in Figure A4. For the initial crack size, the locus of assessment points as a function of applied moment intersects this curve at point A in Figure A4 giving K_r = 0.25, Lr = 0.88 and a bending moment at crack initiation

$$M_i = 527 \text{ kips-in}$$

Stable tearing proceeds from point A to point B in Figure A4 until the moment at instability

$$M_{max} = 1067 \text{ kips-in}$$

and a corresponding crack extension

$$\Delta a_t = 0.82 \text{ in}$$

It is apparent that the result is very sensitive to the input stress strain data, particularly at crack initiation where there is a factor of three difference between the above value of M and that in the main text. Even at instability the maximum load predictions differ by a factor of 1.7.

3.3 Value of J as a Function of Applied Moment for the Initial Crack Size

Part of the workshop problem is to calculate the applied J value as a function of bending moment up to the limit moment of the pipe. These are readily deduced for the results of Table 1 by noting that Equation (11) implies:

$$J/J_{el} = \{(1-0.14L_r^2)[0.3 - 0.7 \exp(-0.65L_r^6)]\}^{-2}$$

and

$$J_{el} = K^2/E = (367\ K_r)^2/E$$

The first of these equations arises from Equation (11); the second equation is simply because K_r is defined for a toughness of 367 ksi(in)$^{1/2}$ in Table 1. Combining these equations with the tabulated values of K_r and L_r leads to the required solution in Figure A6 and Table 4.

Using the R6 assessment line of sub-section 3.2 in conjunction with the yield stress of 24.8 leads to the line on Figure A6 for the power-law material. The differences in the two curves primarily reflect the differences in the two stress-strain curves of Figure A3. The points for crack initiation at J = 4.5 ksi-in are marked and these correspond to the values, M_i.

3.4 Calculation of End Rotations

The end rotation is made up of two parts, that for the uncracked pipe plus the contribution for the crack:

$$\phi = \phi_{uc} + \phi_c \tag{12}$$

For the applied bending moment at instability, the nominal bending stress σ_b is below yield so that the uncracked rotation can be obtained elastically as

$$\phi_{uc} = ML/\pi R^3 tE$$

where L is the pipe semi-length and ϕ_{uc} is the rotation at each end of the pipe (see Figure 1).

The rotation due to the presence of the crack can be deduced from the definition of J as

$$J = \frac{1}{t} \int_0^M (\partial\phi/\partial a) dM$$

This gives

$$\phi_c = t \int_0^a (\partial J/\partial M) da \tag{13}$$

Using R6 to evaluate J as previously described for crack depths from zero to the crack size, a, the required rotation can be obtained. The stress intensity and limit load functions of Section 5 and 6 have been assumed valid over this range of crack depths and numerical integration has been used to calculate ϕ_c. This can be further sub-divided into an elastic part and a plastic part (the elastic part from equation (13) with $J = K^2/E$). Results are given below for both the R6 solution of the main text and for the R6 solution for a power-law material of Section 3.2 above.

R6 Solution of Main Text

$$M_i = 1655 \text{ kips-in} \quad \phi_{uc} = 0.032 \quad \phi_c^{el} = 0.001 \quad \phi_c^{pl} = 0.004$$

$$\phi_i = \phi_{uc} + \phi_c^{el} + \phi_c^{pl} = \underline{0.037}$$

$$M_{max} = 1850 \text{ kips-in} \quad \phi_{uc} = 0.035 \quad \phi_c^{el} = 0.001 \quad \phi_c^{pl} = 0.012$$

$$\phi_f = \phi_{uc} + \phi_c^{el} + \phi_c^{pl} = \underline{0.048}$$

Power-Law Hardening Solution

$$M_i = 527 \text{ kips-in} \quad \phi_{uc} = 0.010 \quad \phi_c^{el} = 0 \quad \phi_c^{pl} = 0.007$$

$$\phi_i = \underline{0.017}$$

$$M_{max} = 1067 \text{ kips-in} \quad \phi_{uc} = 0.020 \quad \phi_c^{el} = 0.001 \quad \phi_c^{pl} = 0.022$$

$$\phi_f = \underline{0.043}$$

It can be seen that although the power-law hardening leads to a much lower prediction of maximum load, the rotations at instability are in close agreement for the two solutions. Note, however, that for the specified power-law properties the uncracked pipe will not behave elastically even at low stresses so that the uncracked rotations given above may be in error. This problem does not arise using the more realistic properties which produce genuine elastic behavior at low stresses.

3.5 Effect of Weld Properties

This problem is not considered in detail here but two bounding solutions are obtained. The first assumes that the pipe deformation is governed by parent material flow properties but that failure is governed by the weld toughness properties (given by the power-law fit of Figure 2 of the main text). The second assumes that the weld flow properties govern the deformation in the vicinity of the weld and therefore govern failure.

Parent Flow Properties (σ_y = 31 ksi)/Weld Toughness (J_{1c} = 2 ksi-in)	
Bending moment at crack initiation	M_i = 1364 kips-in
Bending moment at instability	M_{max} = 1565 kips-in
Crack extension at instability	Δa_t = 0.20 in

Weld Flow Properties (σ_y = 50 ksi)/Weld Toughness (J_{1c} = 2 ksi-in)	
Bending moment at crack initiation	M_i = 2225 kips-in
Bending moment at instability	M_{max} = 2716 kips-in
Crack extension at instability	Δa_t = 0.29 in

It can be seen that the two solutions are widely different. Which governs will depend on the thickness of the weld. A possible approach to determine the relevant solution would be to compare the plastic zone size to the weld thickness although this is not pursued here.

SENSITIVITY ANALYSIS OF FLAW GROWTH INSTABILITY

- by -

A. Okamoto*, D. M. Norris+

ABSTRACT

A solution is presented to the CSNI workshop problem. We describe parameteric studies that test the sensitivity of the instability load to constants of the Ramberg-Osgood stress-strain description, the J resistance curve, and the crack and pipe geometry. The assumption of linear interaction line for combined tension and bending is checked with new solutions. We compare failure analysis diagram solutions with an analogous graphic procedure in J-T space, and with a graphic method based only on J-Load space. The three solution methods gave about the same instability loads.

Our solution of the CSNI problem showed that the tearing instability load is higher for the lower toughness weldment material than for the tough base metal. This is probably due to an inappropriate base material description. We find that the instability load increases with material strength and is more sensitive to changes in this strength than to equivalent changes in the J resistance curve. Finally, comments are given on appropriate fitting ranges for stress - strain data.

INTRODUCTION

Our research shows that wrought stainless steel pipe with circumferential or axial cracks fails by plastic collapse of the pipe cross section reduced by the crack area. Failure occurs when the net section forms a plastic hinge. Based on this work, acceptable flaw size tables were generated for different loading conditions and included in the Winter 1983 Edition the ASME Boiler and Pressure Vessel Code [1]. The tables were specified for pipe and pipe fittings (and associated weld materials) that are made of wrought stainless steel, Ni-Cr-Fe alloy, or cast stainless steel with a ferrite level less than 20%.

* I.H.I., Yokohama, Japan
+ Electric Power Research Institute, Palo Alto, California

Further confidence in this simple plastic collapse methodology was given by bounding crack-growth instability analyses [2] that showed that nuclear stainless steel piping systems were fracture proof. These conclusions were based on the early work of Paris and his associates[3] for a single length of pipe and the extension later (e.g., see Ref. [4]) to complicated nuclear piping systems. This work assumed perfectly plastic material behavior and displacement controlled loads of magnitude sufficient to cause the cracked cross section to be fully yielded.

The recent recognition that flux welds showed lower tearing resistance and that fracture might occur before the cracked cross section was fully yielded, suggested that the method of NNUREG/CR-0838[3] was inappropriate and a more detailed elastic-plastic analysis is required. This new analysis conservatively assumed load control and made use of the elastic-plastic analysis methodology developed by Kumar et al. [5]. This methodology is the basis of the work reported here.

This paper reports our round-robin results with parametric studies that relate to this low toughness weldment issue. Our CSNI problem solution showed a higher instability load for a material with lower tearing resistance than for the tough base metal. To understand this unexpected result we conducted computer experiments where we varied the J-resistance curve, the stress-strain law, and the geometry of the crack and pipe. Using new solutions for combined tension and bending of circumferentially cracked pipe, we were able to assess the conservatism in a linear interpolation between results for pure tension and pure bending.

SOLUTION OF THE WORKSHOP PROBLEM

We solved the CSNI problem [6] three ways: (1) by direct application of the estimation scheme of Kumar et al.[5] in a procedure first suggested by Zahoor[7], (2) using the failure analysis diagram described by Bloom[8] based on earlier work of Harrison, Loosemore, and Milne[9], generally known as the R6 method, and (3) a new method based on tracking the crack growth in J and load space. We describe the three methods as JT, FAD, and JL, respectively. These were automated in the FLET computer program.

Our results for the three computations are summarized in Figure 1. We find that the three methods predict the critical load for instability to within 7 percent with the FAD method giving the highest instability load. The computed differences in critical crack size are significantly larger.

The JT method uses the estimation formulas [5] to compute applied J and T for the initial crack length as a function of increasing load. Plotting these with the J resistance curve in J versus T space gives the critical value of J. The associated critical load is then determined from a plot of J versus load. General formulas are only available for pure tension and for pure bending. For mixed loading the assumption of linear interpolation is made (see Figure 1).

The FAD method uses the procedure described by Bloom[8] that derives the assessment line from the estimation scheme of Ref. [5]. The method has advantages in that the results may be presented in a single plot of fracture toughness versus fraction of collapse load. Crack growth is naturally included in the method. Bending and tension interpolation is required. The results are the same as for the JT method on which it is based if crack growth is accounted for in the JT method.

The JL method again uses the estimation scheme formulas in J versus load space with a set of curves representing increments of constant crack length, starting from the initial value. The actual crack growth with increasing load can then be plotted on this curve set and the instability value determined from the slope of the J versus load curve. The procedure is applied for pure bending and pure tension and the interpolation assumption employed.

TENSION AND BENDING INTERACTION

The tension-bending assumption was checked with new fully plastic combined tension and bending solutions for through-the-wall cracks by Kumar and German[10]. We computed the instability load for the CSNI 16-inch diameter circumferentially cracked pipe for five values of normalized bending to tension ratio M/NR and total crack angle = 90 degrees. We chose a stress-strain curve compatible with the available estimation scheme solutions (yield stress = 24.8 ksi, alpha = 2, and n = 5) and used the CSNI base metal J-resistance curve. The results, given in Figure 2, show some limited conservatism in a linear interaction assumption.

SENSITIVITY TO THE J RESISTANCE CURVE

The sensitivity to J resistance is shown in Figure 3. We chose five (rather arbitrary) resistance curves clustered about the CSNI base metal curve as shown in Figure 3a. The three interaction curves shown in Figure 3b bound our calculational results obtained by FAD. We find that only small changes occur in instability load for substantial changes in J resistance. We used the base-metal stress-strain law for these calculations.

SENSITIVITY TO THE STRESS-STRAIN CURVE

The solution methods described above are based on the J estimation scheme that requires the true stress-true strain curve to be fit by the Ramberg-Osgood relation

$$\frac{\varepsilon}{\varepsilon_o} = \frac{\sigma}{\sigma_o} + \alpha\left(\frac{\sigma}{\sigma_o}\right)^n \qquad (1)$$

To check the sensitivity of the instability load to the Ramberg-Osgood constants, we computed instability loads for three sets of stress-strain curves; each set varied yield stress and α and around the specified base-metal curve. We chose ε_o to correspond to the yield stress σ_o and took $\sigma = E\varepsilon\phi$. We used the CSNI base-metal resistance curve. The results are given in Figure 4.

Changes in one of these variables affect characteristics normally associated with another parameter, and it was difficult to sort out the independent effects. However, if one chooses the stress at one percent strain in the curves of Figure 4a, there is a strong correlation with instability load (see Figure 5). A higher stress at one percent strain gives a higher instability load.

CRACK AND PIPE GEOMETRY

We used the CSNI base-material description to determine how increasing crack length and increasing pipe diameter affect the instability load. The results for crack length are shown in Figure 6 replotted on results given by Ranganath and Mehta[11]. For crack growth with constant load, the instability

load decreases with increasing pipe diameter when the crack angle is kept constant (see Figure 7).

DISCUSSION AND CONCLUSIONS

The work reported here shows that increasing the yield strength actually increases the load required for ductile crack growth instability (see Figure 5) if the material tearing resistance, measured by the J resistance curve, remains constant. Lower J resistance may be offset by higher yield strength. A low yield strength allows more plastic work to be done on the material at a given load. This can result in a large contribution to the plastic part of J and earlier instability. This may have important implications for the weldment toughness issue because of the high yield strength present in these weldments.

The low tearing instability resistance shown here for the CSNI base material is inconsistent with measurements of pipe failure load. Figure 8 shows results of Kanninen et al.[12] on bending of wrought stainless steel pipe with circumferential through-wall cracks. The data falls approximately on the plastic collapse line and well above the predicted instability loads for this type of material.

The disagreement is associated with an inappropriate Ramberg-Osgood fit to the data. Stainless steel data plotted by Yukawa[13] on logarithmic coordinates show bilinear behavior. He computed the load-displacement curve obtained from a stainless steel compact specimen by fitting stress-strain data at about 1% strain. Yukawa's data show that the CSNI fit may be appropriate for stainless steels, but at only very high strains.

It appears that the large value of α specified in the round-robin problem description of Ref. [6] gives too much weight to the plastic part of J. Since the estimation scheme of Ref. [5] defines σ_o as the 0.2% offset yield stress, and since σ_o is taken as E times ε_o, the strain at σ_o is 18.3 times the yield strain as seen from Equation (1). The result is a higher J for a given load and lower instability limit.

The analyses performed here are all strongly dependent on the estimation scheme

$$J = J_e + J_p \qquad (2)$$

and the calibration functions for J_p given in Ref. [5]. These methods have been closely checked by prediction of laboratory specimen behavior for both ferritic and stainless steels. Since the calibration functions for piping have been developed only recently, there is limited verification analysis. While this work is underway, it is probable that comparisons with data will point out some weaknesses in the methodology that may affect the conclusions reached here.

REFERENCES

1. American Society of Mechanical Engineers Boiler and Pressure Vessel Code, Section XI IWB-3640, Winter Addenda 1983.

2. Cotter, K.H., Chang, H-Y, and Zahoor, A., Application of Tearing Modulus Stability Concepts to Nuclear Piping, EPRI report NP-2261, February 1982.

3. Tada, H., Paris, P., and Gamble, R., Stability Analyses of Circumferential Cracks in Reactor Piping Systems, NUREG/CR-0838, June 1979.

4. Zahoor, A. and Gamble R., Leak-Before-Break Analysis for BWR Recirculation Piping Having Cracks at Multiple Weld Locations, EPRI report NP-3522-LD, April 1984.

5. Kumar, V., German, M., et al., Further Developments in the Engineering Approach for Elastic-Plastic Fracture Analysis, EPRI Report NP-3607, Final Report on Contract RP1237-1, September 1983.

6. CSNI Ductile Piping Fracture Mechanics Workshop, Workshop Problem Description, Southwest Research Institute, San Antonio, Texas, June 1984.

7. Zahoor, A. and Gamble, R., Presentation to the ASME Task Group on Piping Flaw Analysis, Vancouver, Canada, May 1983.

8. Bloom, J., Procedure for the Assessment of the Integrity of Nuclear Pressure Vessels and Piping Containing Defects, EPRI Report NP-2431, June 1982.

9. Harrison, R.P., Loosemore, K., and Milne, I., Assessment of the Integrity of Structures Containing Defects, Central Electricity Generating Board, R/H/R6-Rev 1, April 1977.

10. Kumar, V. and German, M., Private communication to D. M. Norris, June 1984.

11. Ranganath, S. and Mehta, H., Engineering Methods for the Assessment of Ductile Fracture Margin in Nuclear Power Plant Piping, in Elastic Plastic Fracture, Volume II, ASTM STP 803, Philadelphia, PA, October 1981.

12. Kanninen, M. F. et al., Instability Predictions for Circumferentially Cracked Type-304 Stainless Steel Pipes Under Dynamic Loading, Vols. 1 and 2, EPRI Report NP-2347, April 1982.

13. Yukawa, S., Notes on Ramberg-Osgood Fit to Stainless Steel Stress-Strain Data, presentation to the Task Group on Piping Flaw Evaluation, ASME Code, Pittsburgh, Pa., July 1984.

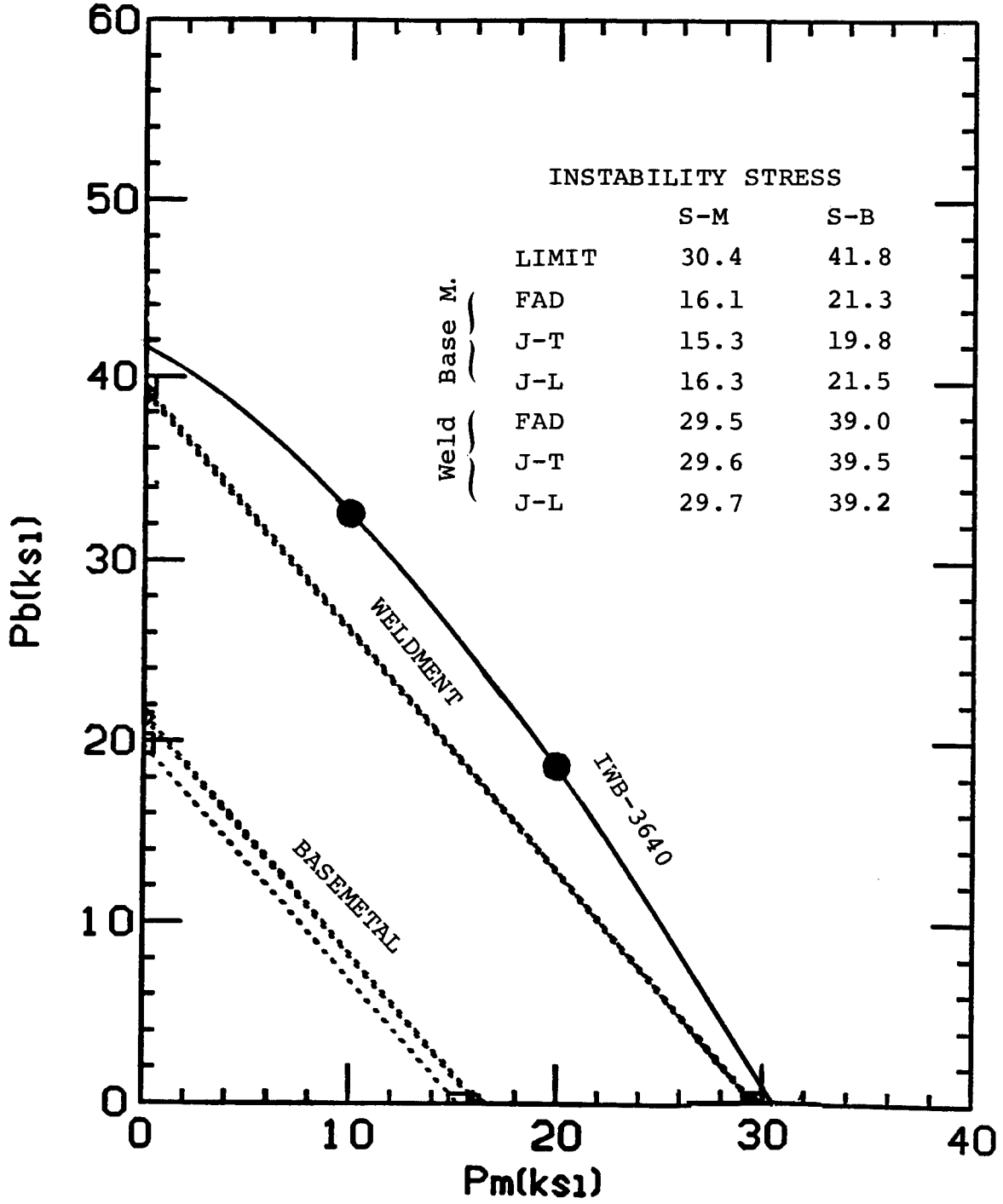

FIGURE 1. ROUND ROBIN RESULTS FOR THE JT, FAD, AND JL METHODS. THE STRAIGHT LINE SHOWS THE LINEAR INTERPOLATION FOR COMBINED TENSION AND BENDING; THE UPPER CURVE IS THE PLASTIC COLLAPSE LINE PREDICTED BY ASME CODE, SECTION XI, IWB-3640.

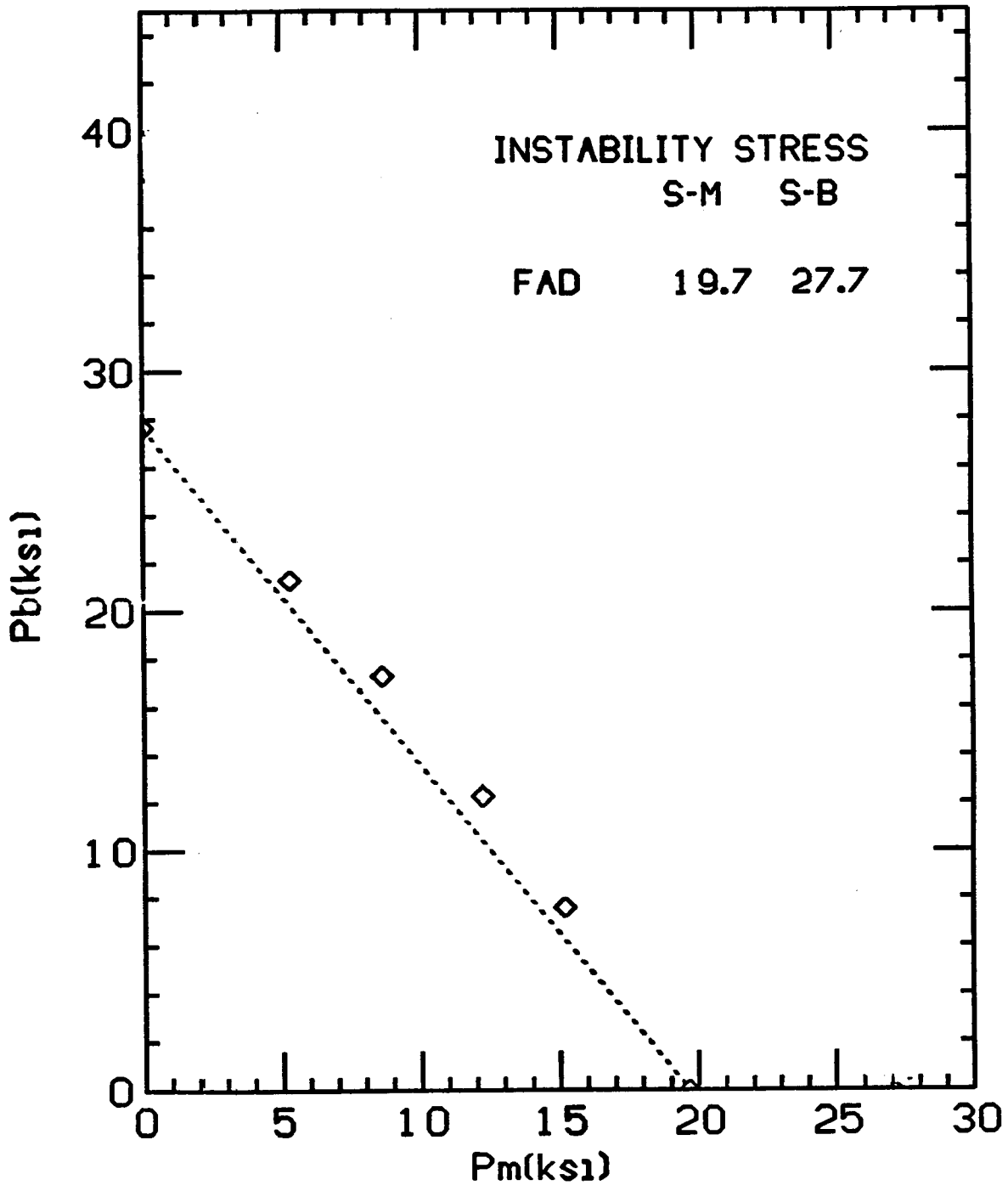

FIGURE 2. COMPARISON OF LINEAR INTERPOLATION FOR COMBINED TENSION AND BENDING WITH JT SOLUTIONS USING SOLUTIONS GENERATED FOR BENDING TO TENSION RATIOS (M/NR) OF 0.0, 0.25, 0.5, 1.0, 2.0, AND FININITY.

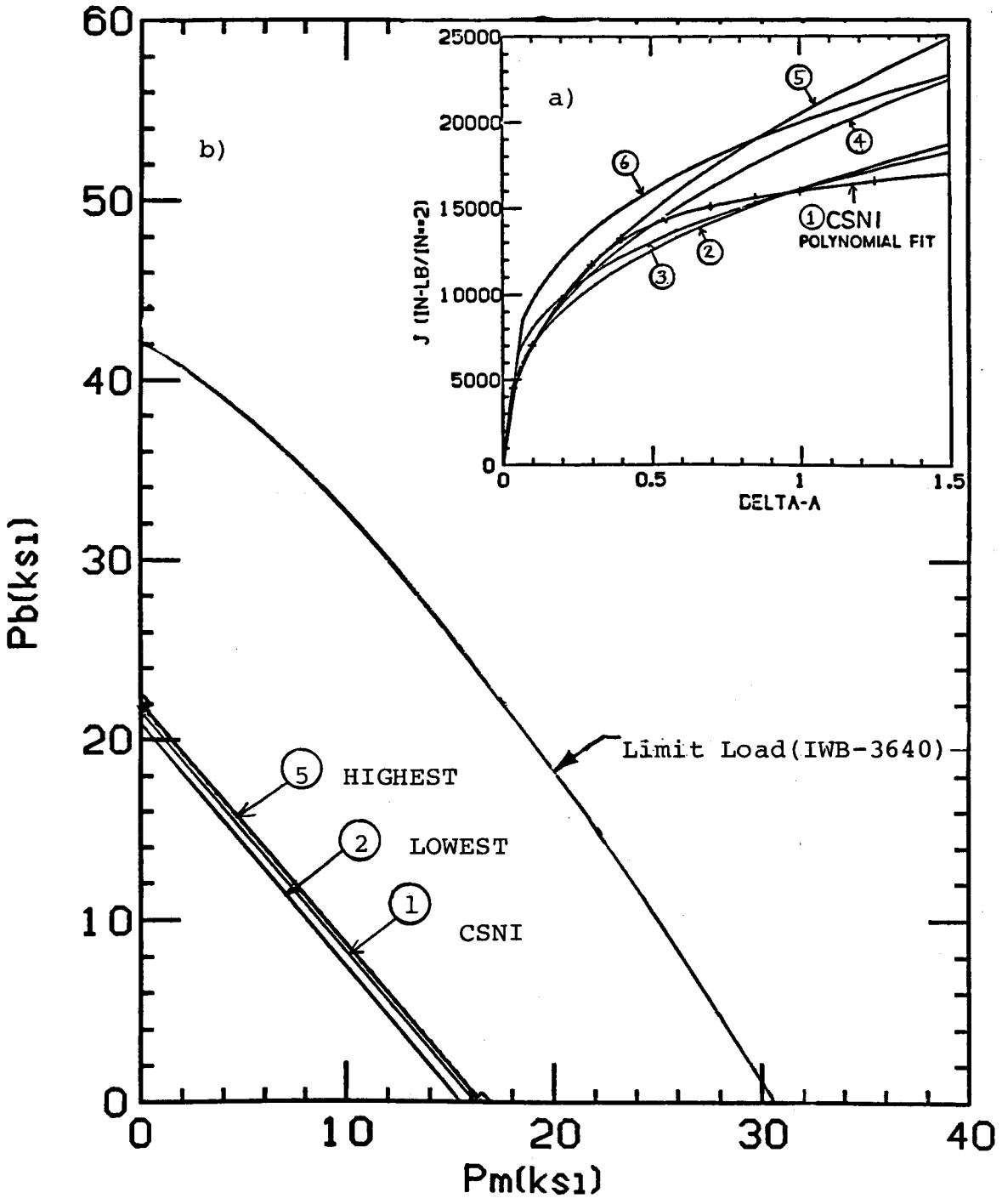

FIGURE 3. SENSITIVITY OF TEARING INSTABILITY LOAD TO THE J-RESISTANCE CURVE (FAD METHOD). a) SIX SAMPLE J-RESISTANCE CURVES; b) LOAD VERSUS MEMBRANE STRESS

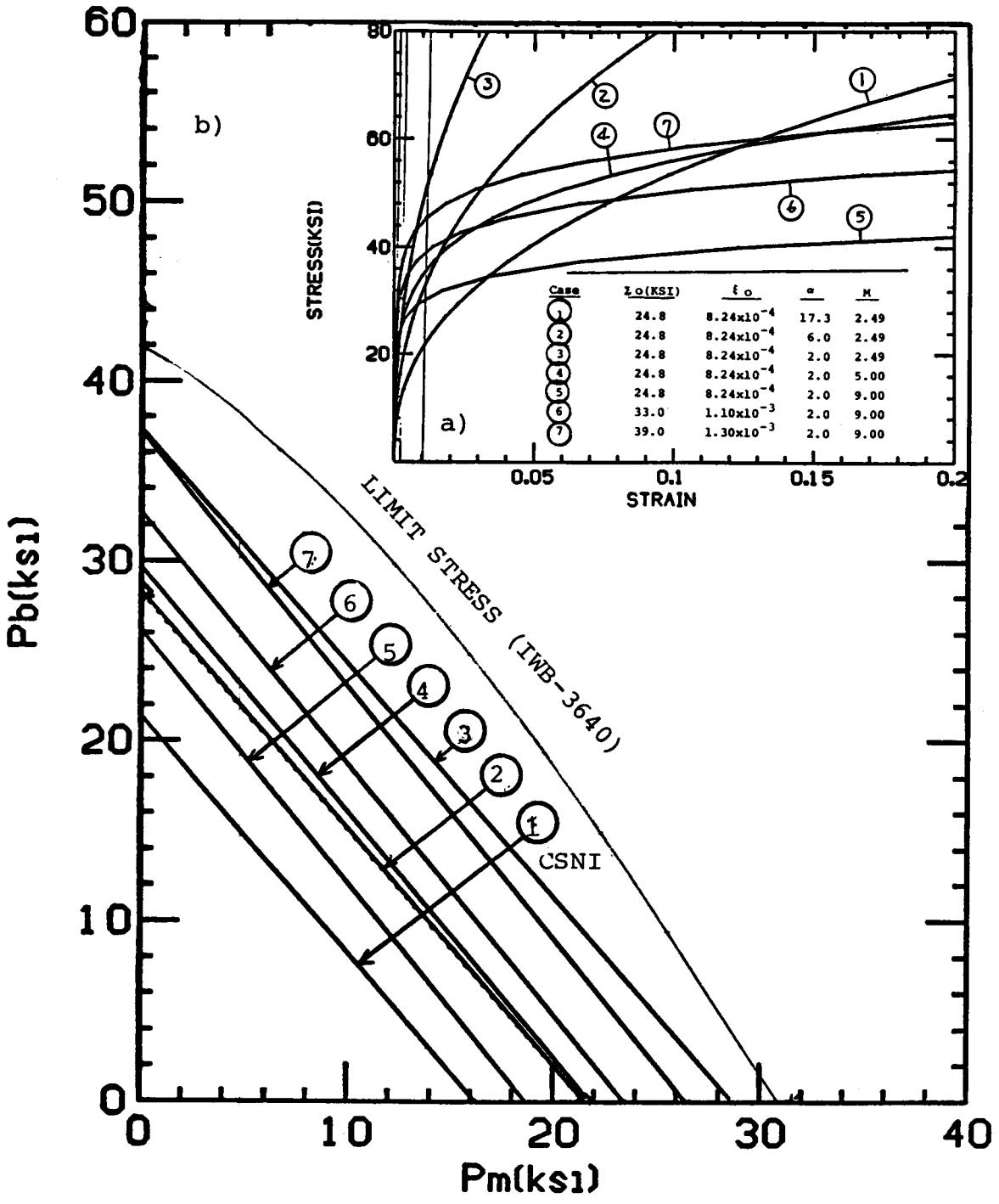

FIGURE 4. SENSITIVITY OF TEARING INSTABILITY LOAD TO THE RAMBERG-OSGOOD PARAMETERS (FAD METHOD). a) WORK HARDENING CURVES; b) BENDING LOAD VERSUS BENDING STRESS

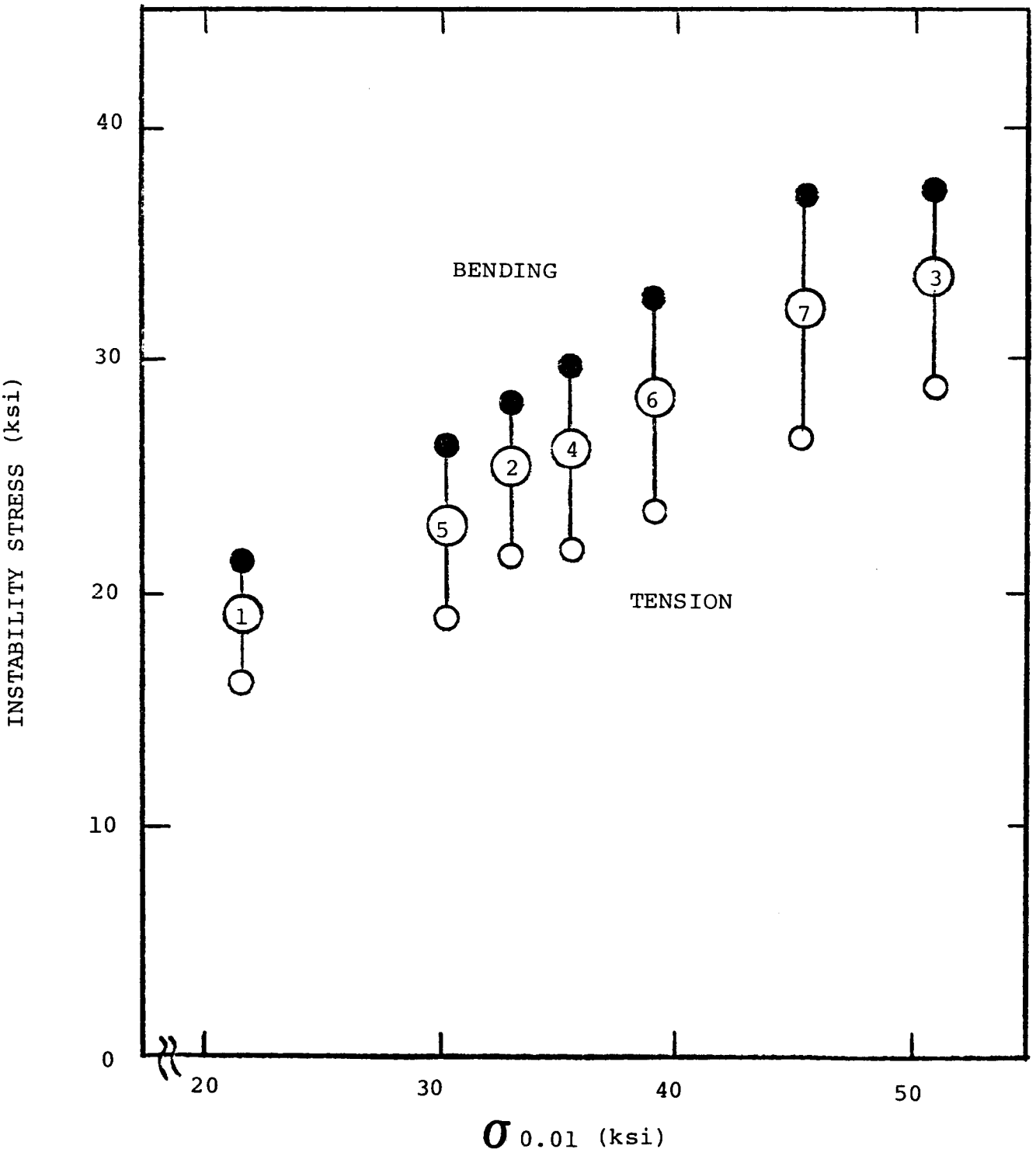

FIGURE 5. CORRESPONDENCE OF INSTABILITY LOAD WITH STRESS MEASURED AT ONE-PERCENT STRAIN (FAD METHOD).

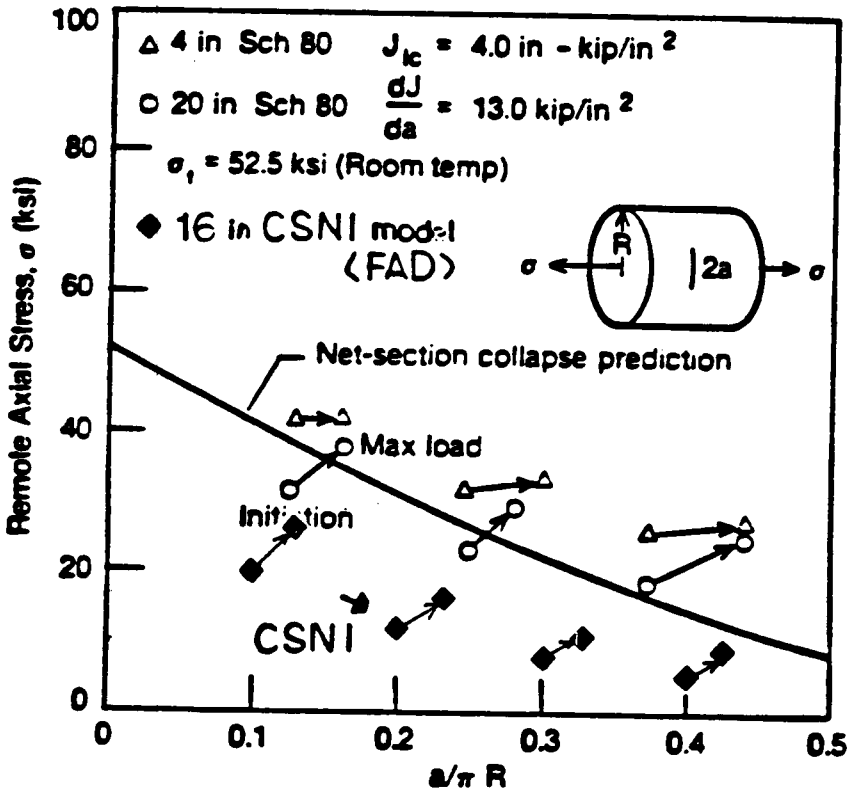

FIGURE 6. COMPARISON OF INITIATION AND INSTABILITY LOADS WITH NET-SECTION COLLAPSE CRITERIA FOR DIFFERENT CRACK LENGTHS (FAD METHOD).

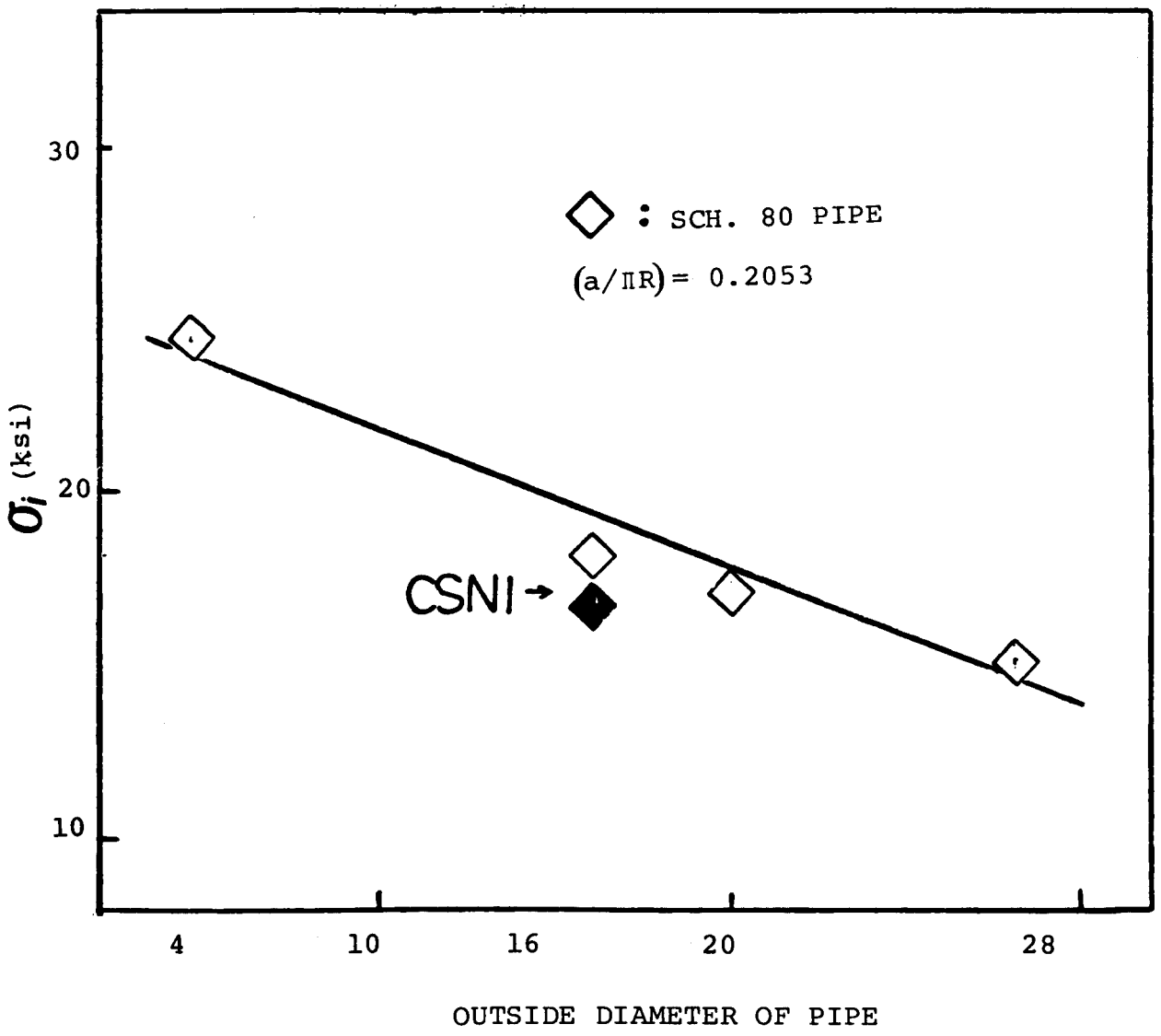

FIGURE 7. VARIATION OF INSTABILITY TENSION LOAD WITH PIPE DIAMETER (FAD METHOD).

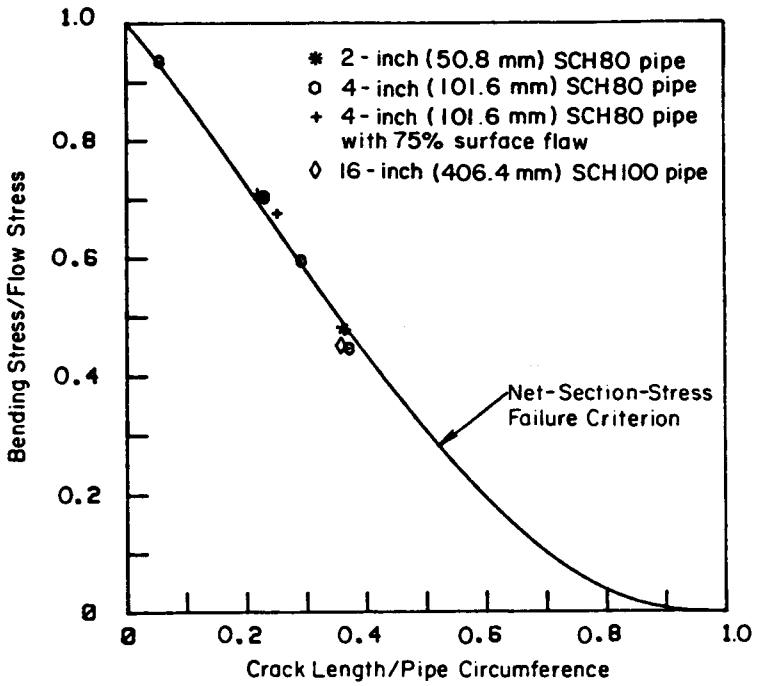

FIGURE 8. COMPARISON OF NET-SECTION COLLAPSE CRITERIA WITH PURE BENDING DATA ON STAINLESS STEEL PIPES WITH THROUGH-WALL FLAWS.

DEFORMATION PLASTICITY FAILURE ASSESSMENT DIAGRAM APPROACH

- by -

J. M. Bloom

INTRODUCTION

There are several methods which can be used to address ductile tearing of cracked piping. The CSNI/NRC Ductile Piping Fracture Mechanics Workshop problem is readily adaptable, in particular to the deformation plasticity failure assessment diagram (DPFAD) approach. This approach can easily be used for the prediction of instability of nuclear piping containing simple through-wall cracks as given in the workshop problem. In essence, the DPFAD approach recognizes both brittle fracture and net section collapse of a flawed structure and is given in the form of a safety/failure plane defined by the stress intensity factor/fracture toughness ratio as the ordinate and the applied stress/net section plastic collapse stress ratio as the abscissa. For a particular stress level and defect size, these coordinates can be readily calculated. If the calculated assessment point lies inside the failure assessment curve, no crack growth can occcur. If the assessment point lies on the curve, stable crack growth is possible. If the assessment point lies outside the curve, unstable crack growth and failure is predicted. Further discussion of the "DPFAD" approach can be found in Refs. [1], [2], [3], and [4].

WORKSHOP PROBLEM

The problem to be solved is of a large diameter pipe (16 inches) containing a through-wall crack circumferentially oriented as shown in Figure 1. The pipe is subjected to a constant axial stress of 10 ksi and is made of a power law hardening material which has a true-stress, true-strain curve which can be represented by the Ramberg-Osgood expression

*Babcock & Wilcox Company, Research & Development Division, Alliance, Ohio

$$\frac{\varepsilon}{\varepsilon_o} = \frac{\sigma}{\sigma_o} + \alpha\left(\frac{\sigma}{\sigma_o}\right)^n \qquad (1)$$

The Problem is to predict the applied bending moments at crack initiation and at load controlled instability. The material properties are given in Table 1 and Figure 2 for both weld metal and base metal.

PROBLEM FORMULATION

Before applying the DPFAD approach to the workshop problem, several assumptions were made:

1. The analysis was based upon a load-controlled model. This assumption leads to a lower bound result and enables the DPFAD approach to use existing fully-plastic solutions for a through-wall cracked pipe under pure axial loads and pure bending loads.[5]

2. Since only pure axial and pure bending solutions are available, a linear interpolation will be used to determine the instability moment for an applied axial stress of 10 ksi. This assumption is illustrated schematically in Figure 3. Note that this assumption is clearly conservative since it is expected that the actual interaction curve between axial (membrane) loading and bending loading is highly nonlinear and concave upward.

3. The material properties as given in the workshop problem were used directly. Two problems were solved:

   a. The crack located entirely in the base metal with base metal stress-strain and J_R properties.

   b. The crack located entirely in the weld metal with both stress-strain and J_R properties being that of the weld metal. The actual J_R data shown in Figure 2 was used directly to calculate the individual assessment points per (Δa, J_R) data point sets.

4. Crack extension due to stable crack growth was assumed to proceed equally along the circumference of the pipe at both crack ends (fronts).

5. Since the fully plastic calibration functions "h_1" and the elastic stress intensity correction factor "F(a/t, R/t)" were only available[5] for

- R/t = 5, 10, 20

and

- $a/_{\pi R}$ or (a/b) = 1/16, 1/8, 1/4, 1/2,

the "h_1" and "F" functions were determined for R/t = 15.5 and a/b = .205 using Lagranagian polynomial interpolations.[6] The K_I expressions are given later in the text while the "h_1" values are given on the DPFAD plots along with the resultant instability stresses.

PROBLEM SOLUTION

The "DPFAD" approach for predicting instability loads for nuclear piping (plane stress model) consists of the following steps:

1. DPFAD Curve Generation

The total J-integral response of the cracked pipe configuration is first obtained using the GE estimation scheme[7] for a power law strain-hardening material where

$$J = J_I^e\ (a_{eff}, P) + J^P\ (a, P, n) \qquad (2)$$

J_I^e is the elastic contribution based on Irwin's plasticity-adjusted crack size (a_{eff}), a is the physical crack size, P is the applied remote load, and J^P is the deformation plasticity or fully plastic solution. The J_I^e expression for the workshop problem is given by

$$J_I^e = K_I^2/E \qquad (3)$$

where K_I is the linear elastic fracture mechanics (LEFM) stress intensity factor and E is Young's modulus.

For R/t = 15.5

$$K_I = \sigma_m \sqrt{\pi a}\, F_m \qquad \text{for tension} \tag{4}$$

and

$$F_m = 0.7\ (1 + 6.97\ a/b) \qquad 1/16 \leq a/b \leq 1/4$$

while

$$K_I = \sigma_b \sqrt{\pi a}\, F_b \qquad \text{for bending} \tag{5}$$

and

$$F_b = 0.8\ (1 + 4.74\ a/b) \qquad 1/8 \leq a/b \leq 1/4$$

The fully plastic solution taken from Ref. [5] is

$$J_p = \frac{\pi\alpha\sigma_o^2 R(1-a/b)(a/b)h_1[P/P_o]^{n+1}}{E} \tag{6}$$

for membrane (axial) loading

and

$$J_p = \frac{\pi\alpha\sigma_o^2 R(1-a/b)(a/b)h_1[M/M_o]^{n+1}}{E} \tag{7}$$

for bending loading

where

$$P_o = 2\sigma_o R t \pi \Gamma \tag{8}$$

and

$$\Gamma = [1-a/b-2/\pi \sin^{-1}(1/2 \sin a/b\pi)]$$

and

$$M_o = 4\sigma_o R^2 t \, [\cos(a\pi/2b) - 1/2 \sin (a\pi/b)] \quad (9)$$

The DPFAD curve is obtained by normalizing the sum of the elastic and plastic response [Equation (2)] by the "elastic" J-integral of the cracked pipe in terms of "a" given by Equation (3). The normalized J-response is then defined by

$$K_r = \sqrt{J_I^e/J} = f(S_r) \quad (10)$$

where

$$S_r = \sigma/\sigma_L(a) \quad (11)$$

σ is the remote applied stress and σ_L is the reference plastic collapse stress or limit stress, a function of "a" and the material yield strength, σ_o.

For membrane loading, Equation (8) should be used and S_r defined by

$$S_r = P/P_o \quad (12)$$

while for bending, Equation (9) should be used and

$$S_r = M/M_o \quad (13)$$

Equations (10) and (11) define a curve which is a function of the flaw geometry, structural configuration, and stress-strain behavior of the material of interest. This curve, in terms of K_r, S_r, is independent of the magnitude of the applied loading.

2. Assessment Point Evaluation

To determine the instability load of a flawed pipe, a locus of assessment points corresponding to some postulated stable crack growth must first be calculated in terms of K_r,S_r coordinates. The assessment point coordinates will be denoted by K_r',S_r' to differentiate them from the K_r,S_r coordinates of the DPFAD curve defined by Equations (10) and (11). For stable crack growth, K_r' and S_r' are defined by

$$K_r' \ (a_o+\Delta a) = \sqrt{J_I^e \ (a_o+\Delta a)/J_r \ (\Delta a)} \qquad (14)$$

and

$$S_r' = (a_o+\Delta a) = P/P_o \ (a_o+\Delta a) \quad \text{or} \quad M/M_o \ (a_o+\Delta a) \qquad (15)$$

where J_I^e, J_R , and P_o or M_o are all functions of the amount of postulated slow stable crack growth. The reference plastic collapse load (P_o or M_o) is now a function of the current crack size, "$a_o + \Delta a$". For actual crack initiation, $J \geq J_{IC}$ [where J_{IC} is determined from ASTM Standard E813-81[8]], Equations (10) and (11) define the boundary between no crack growth and crack growth. For actual stable crack growth, $J = J_R$ [where J_R is obtained from the experimentally measured J_I-R data[9]] and

$$K_r' = K_r$$

and (16)

$$S_r' = S_r$$

and the curve defined by Equation (3) becomes the actual stable crack growth path in the K_r,S_r plane, as shown schematically in Figure 4. If $J > J_R$, load instability results and the crack growth path goes outside the K_r-S_r curve for load-controlled structures.

Note that stable crack growth is taken into account by the assessment points using Equations (14) and (15), but that the DPFAD curve itself is based on the initial crack length, a_o.

The DPFAD curve defined by Equations (10) and (11) for $a = a_o$ (the initial crack size) becomes a conservative lower bound approximation for the exact failure assessment diagram curve ($a = a_o + \Delta a$) provided $\Delta a << a_o$.

3. Instability Load Prediction

The first step in the prediction of the instability load is to assume that constant load is applied to the pipe such that at the initiation of crack growth, the K_r', S_r' point lies inside the DPFAD curve.

The assessment point locus (illustrated in Figure 5 by the L_1 locus) is calculated by incrementing Δa using the corresponding J_R (Δa) value to calculate K_r'. The instability or maximum load is determined by taking the ratio of the distance from the origin of the diagram to the DPFAD curve passing through the assessment point farthest from the curve by the distance to the assessment point itself. This ratio of distances (sometimes denoted as the safety factor [S.F.]) times the assumed constant load gives the equilibrum load (where crack growth is stable). At the instability load (L_m), the locus of assessment points is tangential to the failure assessment curve as shown in Figure 5. In the K_r,S_r space this is identical to the R-curve approach.[10]

The initiation J value denoted by J_{Ic} is given in the workshop problem (Figure 2) and the corresponding assessment point is denoted by L_i in Figure 4 and Figure 5.

RESULTS

Tables 2 through 5 present the coordinates of the assessment locus for a constant pure axial load of 10 ksi and a pure bending load of 10 ksi for both the base metal and weld metal. Initiation stresses denoted by σ_i are given in each table as well as the instability stresses denoted by σ_{max}. The values were obtained by multiplying 10 ksi by the approximate safety factor given in these tables. Figures 6 through 9 present this information graphically. The individual results for both pure axial loading and pure bending as well as the combined loading are summarized in Tables 6 and 7. The method used for the combined loading case is illustrated in Figure 3.

Note that the maximum stress point is fairly flat, so Δa at instability cannot be precisely predicted, therefore, a range is given in Tables 6 and 7.

DISCUSSION AND CONCLUSIONS

The DPFAD approach can be applied to the full range of structural behavior from linear elastic to fully plastic or net section collapse (NSC) including elastic plastic fracture mechanisms (EPFM). The DPFAD approach presents an excellent visualization of these significant predominate failure mechanisms: LEFM, EPFM, and NSC. Figure 10 schematically illustrates the relevant failure mechanistic zones for the weld metal. A similar figure can be constructed for the base metal. The construction of these failure zones is based on methods discussed in detail in Ref. [11].

With Figure 10 in mind, it can be seen from Figures 8 and 9 that the base metal instability results are not very sensitive to the fracture toughness of the base metal as measured by the $J_R(\Delta a)$ curve, but are sensitive to the material stress-strain curve, in particular, the σ_o(yield strength) and strain hardening properties of the base metal (net section collapse failure mechanism regime). The weld metal, however, being more typical of ferritic pressure vessel steel is sensitive to both stress-strain and toughness properties of the weld metal (EPFM failure regime).

Margins on stress (load) are easily visualized and are more significant than margins on J-integral or Tearing modulus. Design engineers are more familiar with loads (stresses) than J-integral values. The J-T approach[12] requires two diagrams in order to determine the load margins while the DPFAD approach only requires one diagram. Unlike the J-T approach, stable crack growth due to both structural crack extension and increased toughness due to ductile tearing are included in the DPFAD approach and needless extracting of J-integral derivatives with respect to crack growth are not required. The instability point is the point on the constant load locus farthest from the diagram curve in the DPFAD approach.

POST WORKSHOP COMMENTS

The assumption of linear interpolation of the pure tension and pure bending results can led to possible large conservatisms in the prediction of both initiation moment and instability moment as shown schematically in Figure 3 by the nonlinear interaction curve denoted by "?".

The following comments are made with regard to the Ramberg-Osgood relationship. This relationship is a function of only two parameters as originally set forth. Fixing any two σ_o, n fixes the third parameter, α. If σ_o is arbitrarily chosen (as a reference stress in the GE estimation scheme), α must be set such that the true-stress/true-strain data is approximately fit in a least square sense. This is discussed in more detail in Ref. [1]. The only unique parameter is the slope of the log of the true-stress/true-strain curve, n.

ACKNOWLEDGEMENT

The author wishes to acknowledge the Babcock & Wilcox Owners Group for supporting his participation in the CSNI/NRC Ductile Piping Fracture Mechanics Workshop and for their support in preparing this paper for inclusion in the planned NRC NUREG Report. In addition, the author wishes to acknowledge C. J. Hudson, Project Manager at Babcock & Wilcox, Utilities Power Generation Group (Nuclear), Lynchburg, Virginia for his support on this project.

REFERENCES

1. J. M. Bloom and S. N. Malik, "A Procedure For The Assessment of the Integrity of Nuclear Pressure Vessels and Piping Containing Defects", EPRI Report NP-2431, June 1982.

2. J. M. Bloom, "Validation of a Deformation Plasticity Failure Assessment Diagram Approach to Flaw Evaluation", Elastic-Plastic Fracture: Second Symposium, Volume II - Fracture Resistance Curves and Engineering Applications, ASTM STP 803, 1983.

3. J. M. Bloom, "A Procedure for the Assessment of the Structural Integrity of Nuclear Pressure Vessels", Journal of Pressure Vessel Technology, February 1983.

4. J. M. Bloom, "Deformation Plasticity Failure Assessment Diagram", ASTM E24.06.02 Task Group Report, December 1983 (submmitted for publication as a paper in a future ASTM STP).

5. V. Kumar and M. German, "Further Developments in the Engineering Approach for Elastic-Plastic Fracture Analysis", EPRI Report NP-3607, July 1984.

6. A. Okamoto, Private communication, June 1984.

7. V. Kumar, et al., "An Engineering Approach for Elastic-Plastic Fracture Analysis", EPRI Report NP-1931, July 1981.

8. E813-81 Standard Test Method for J_{Ic}, A Measure of Fracture Toughness, ASTM Standards, American Society for Testing and Materials, Vol. 03.01, 1981.

9. P. Albrecht, et al., "Tentative Test Procedure for Determining the Plane Strain J_IR Curve", Journal of Testing and Evaluation Vol. 10, No. 6, Nov. 1982.

10. "Fracture Toughness Evaluation by R-Curve Methods", ASTM STP-527, April 1973.

11. J. M. Bloom and J. L. Hechmer, "Limits of Linear Elastic Fracture Mechanics", Journal of Pressure Vessel Technology. Vol. 106, No. 2, May 1984.

12. P. C. Paris, et al., "Instability of the Tearing Mode of Elastic-Plastic Crack Growth", ASTM STP-668, 1979.

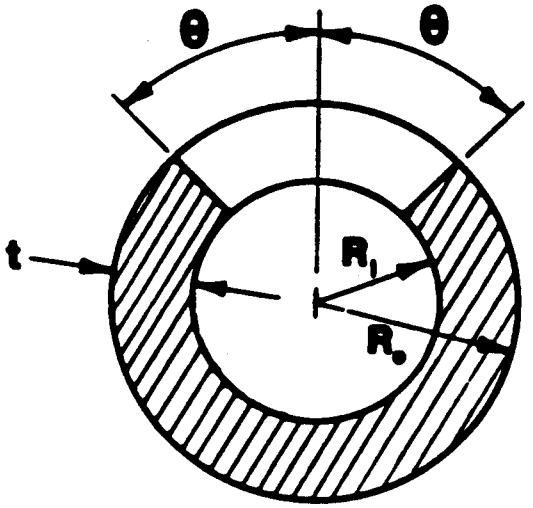

θ = 0.645 radians
R_i = 7.5 inches
R_o = 8.0 inches
t = 0.5 inches

FIGURE 1. CRACKED PIPE GEOMETRY

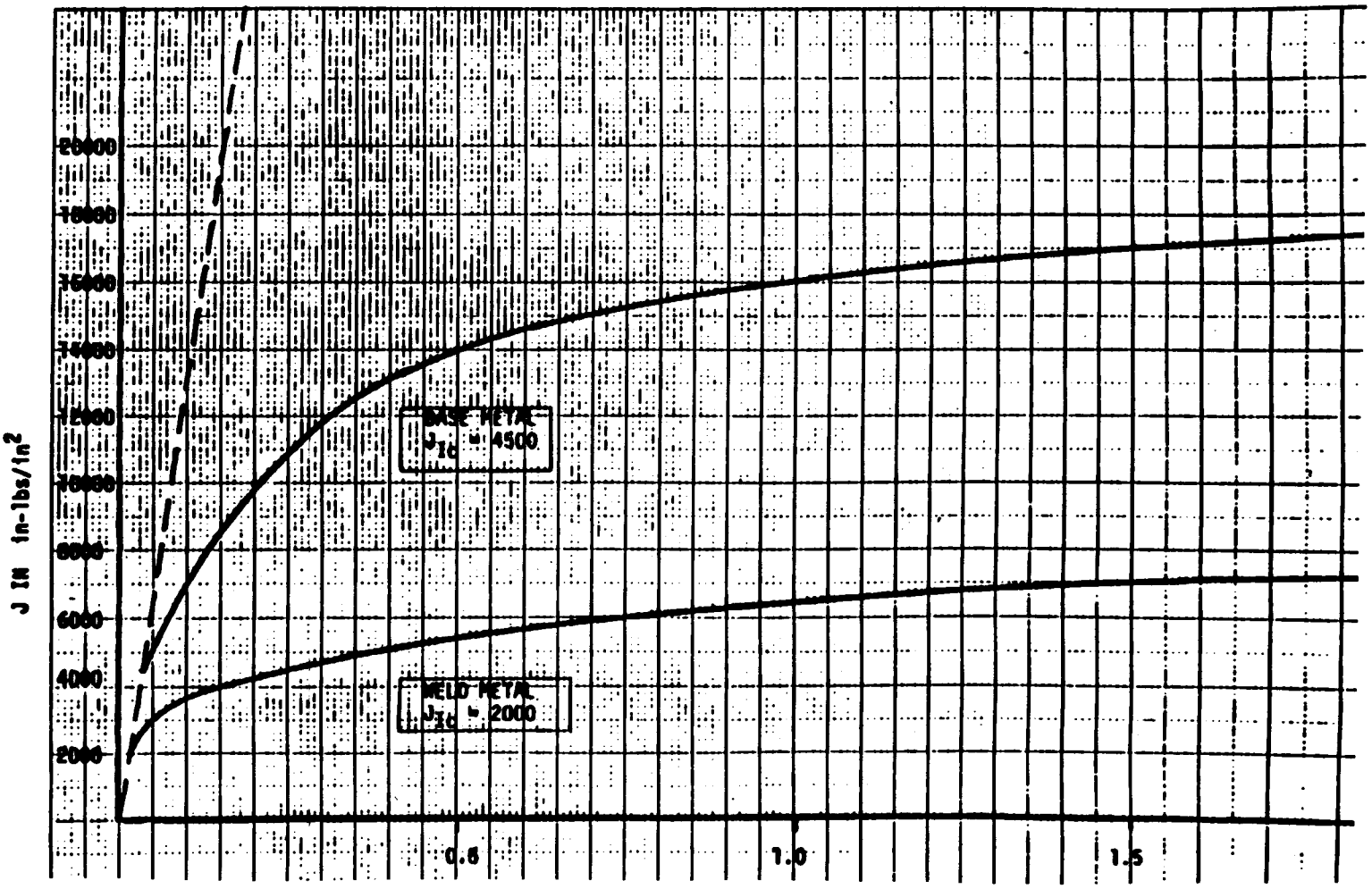

CRACK EXTENSION IN INCHES

FIGURE 2. J-INTEGRAL RESISTANCE CURVES

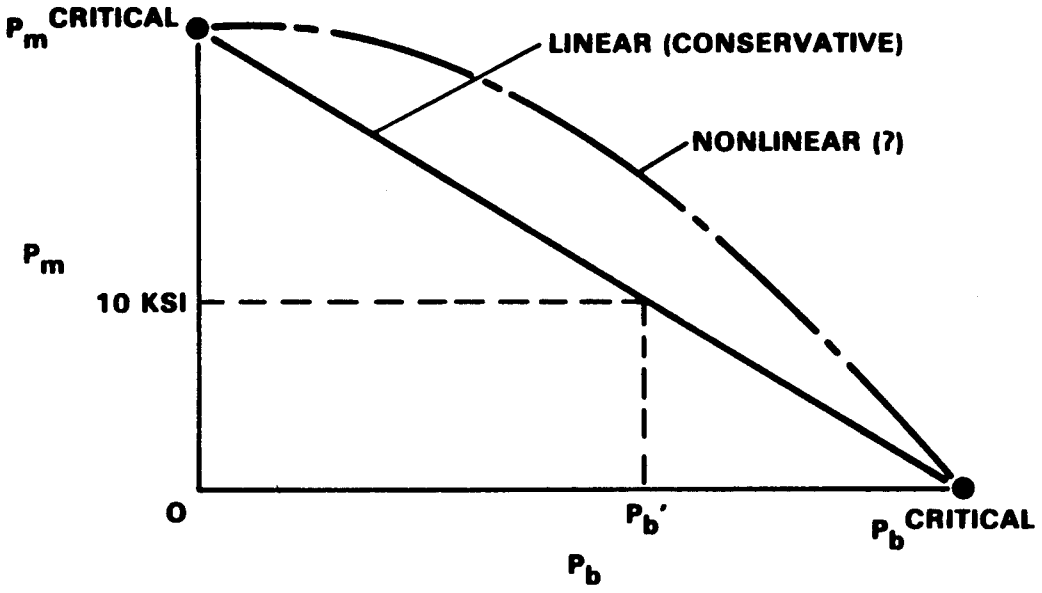

FIGURE 3. LINEAR INTERPOLATION FOR COMBINED MEMBRANE PLUS BENDING STRESSES FOR P_m = 10 KSI

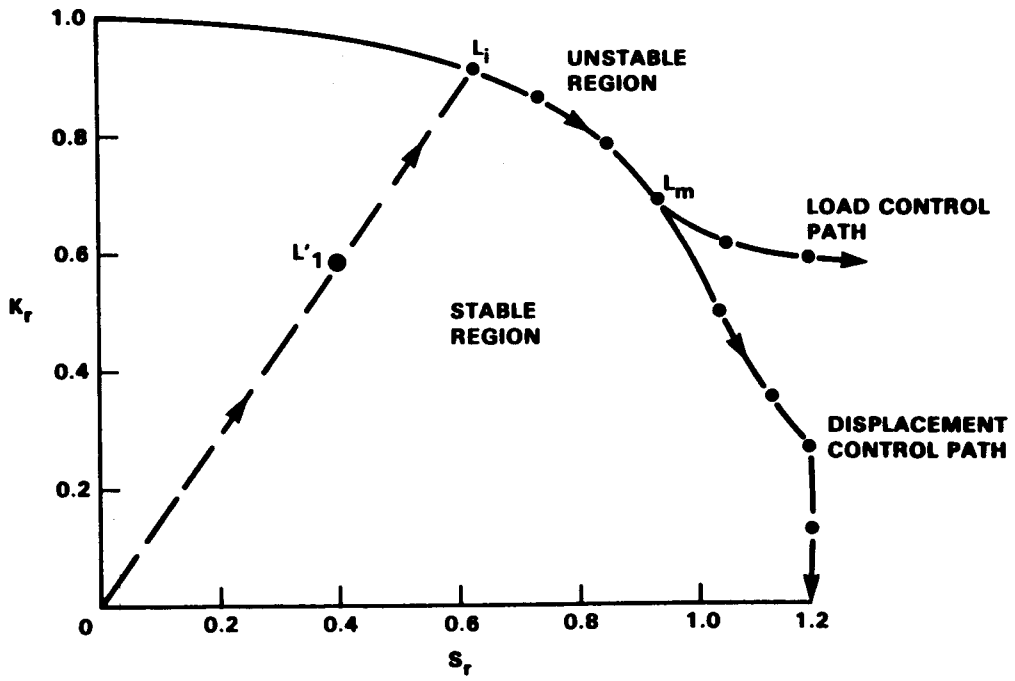

FIGURE 4. FAILURE ASSESSMENT DIAGRAM IN TERMS OF STABLE CRACK GROWTH

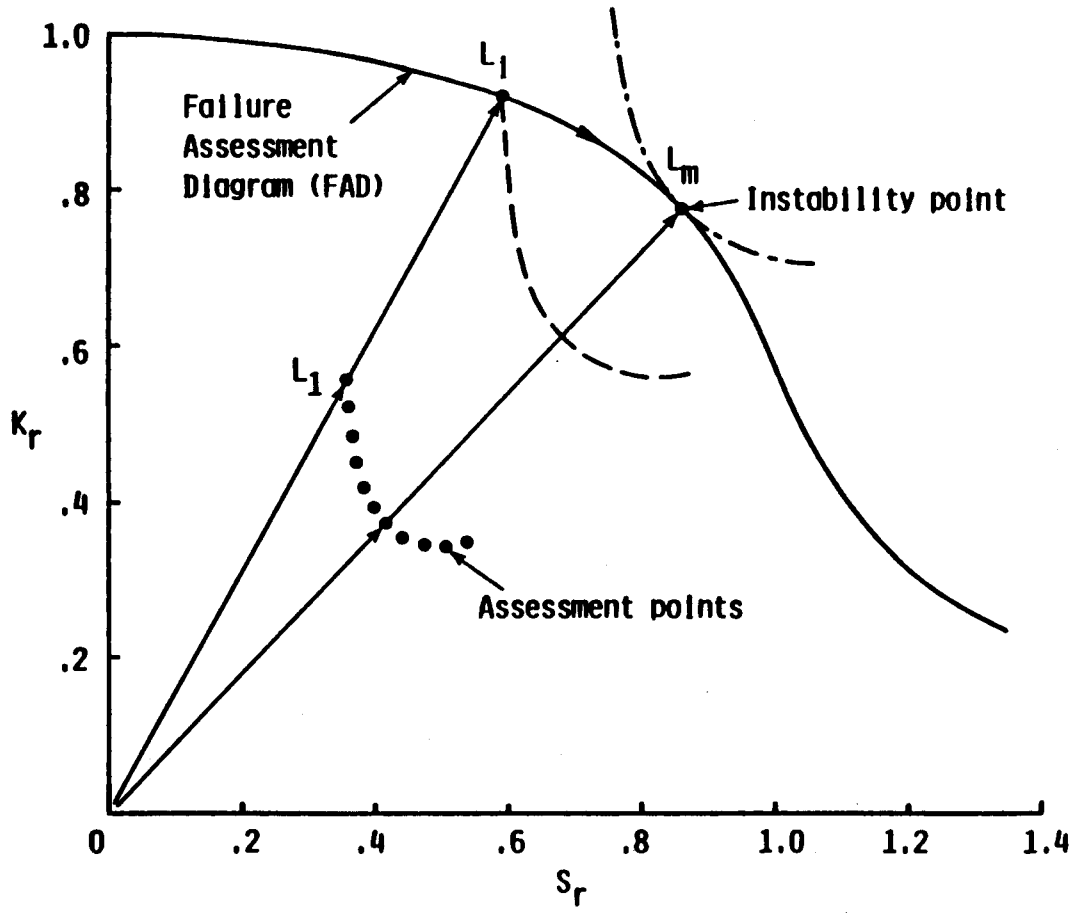

FIGURE 5. STRAIN-HARDENING FAILURE-ASSESSMENT DIAGRAM FOR A GIVEN MATERIAL

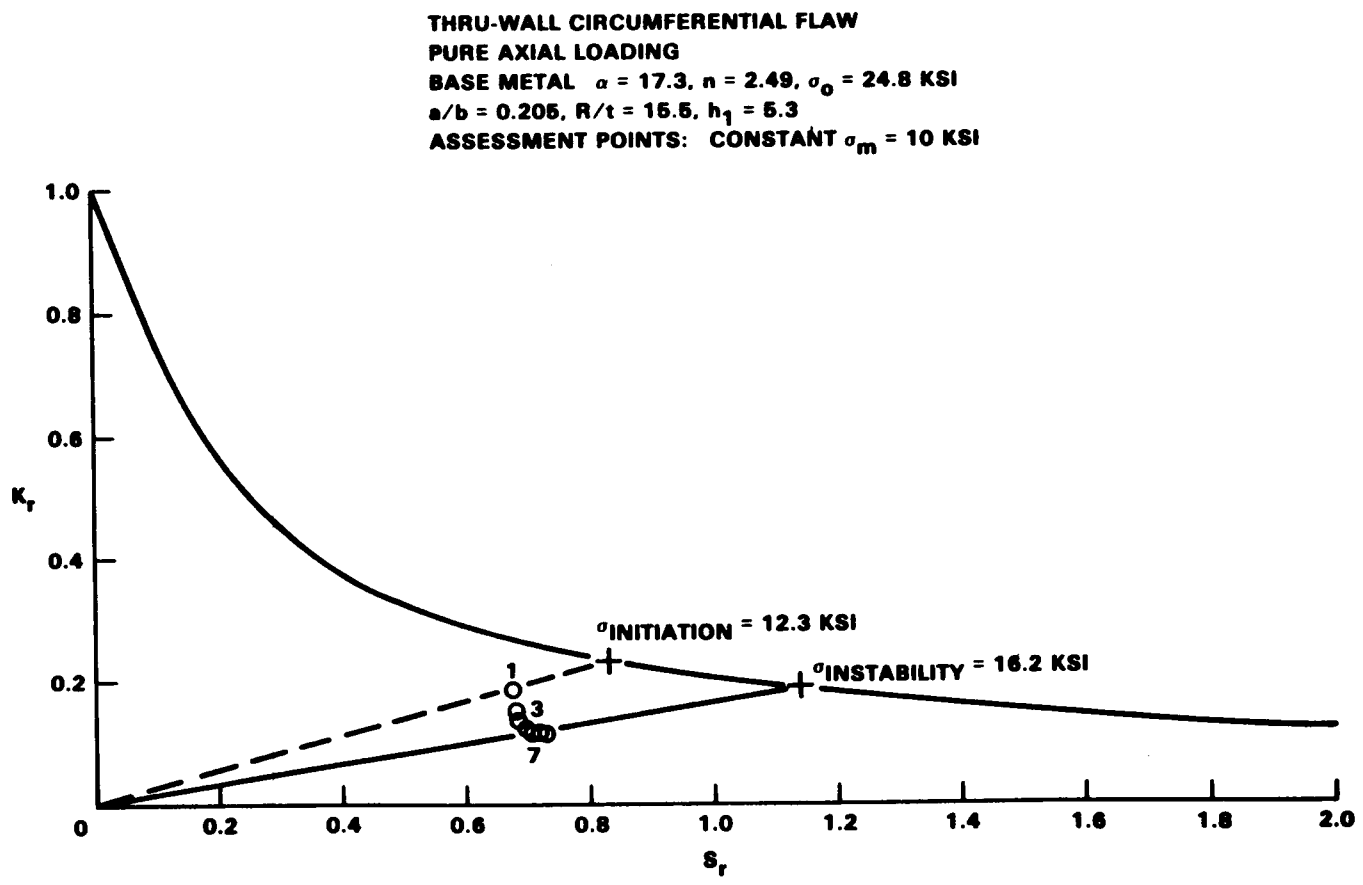

FIGURE 6. DPFAD AXIAL LOADING/BASE METAL

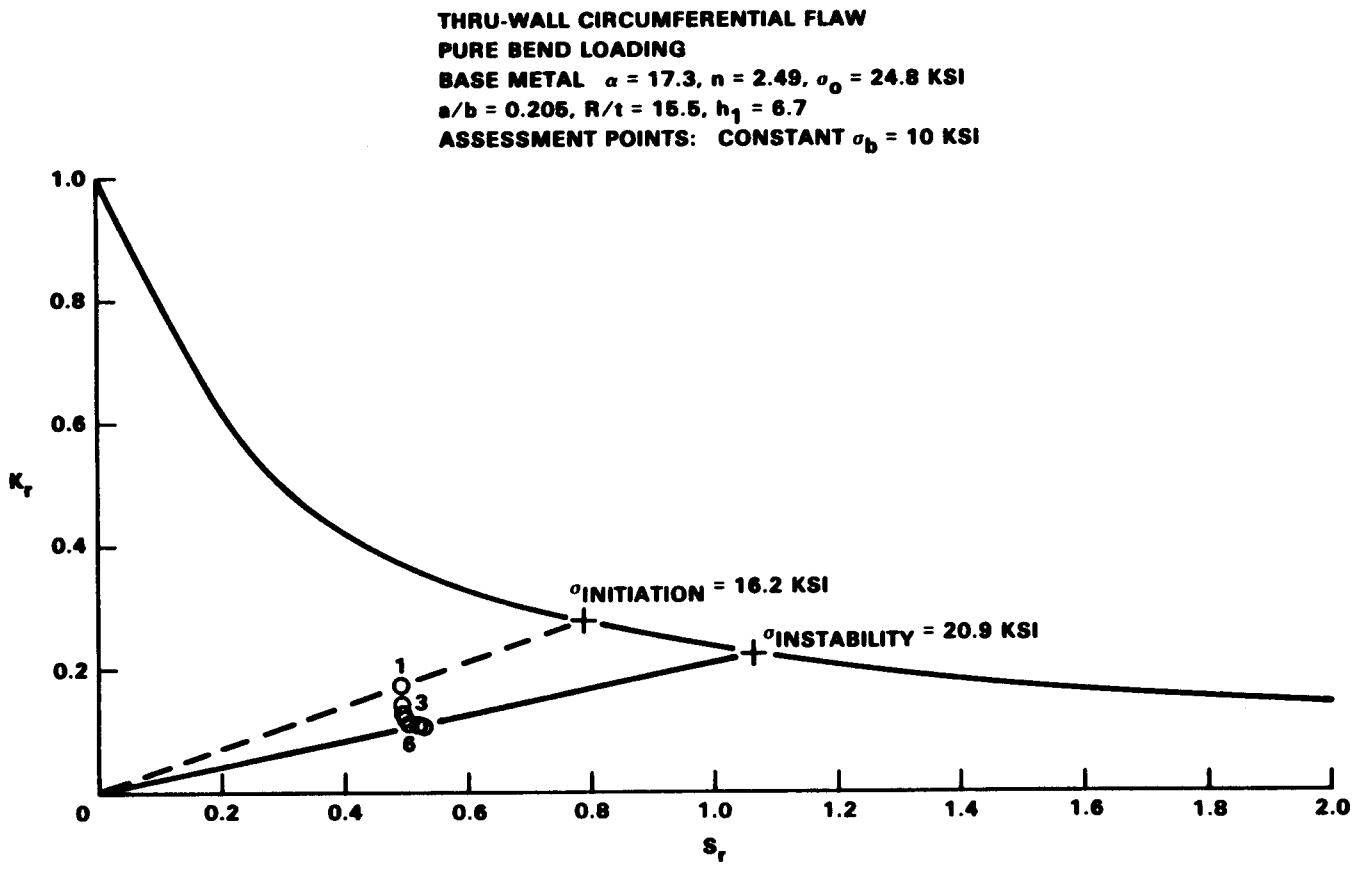

FIGURE 7. DPFAD BENDING LOAD/BASE METAL

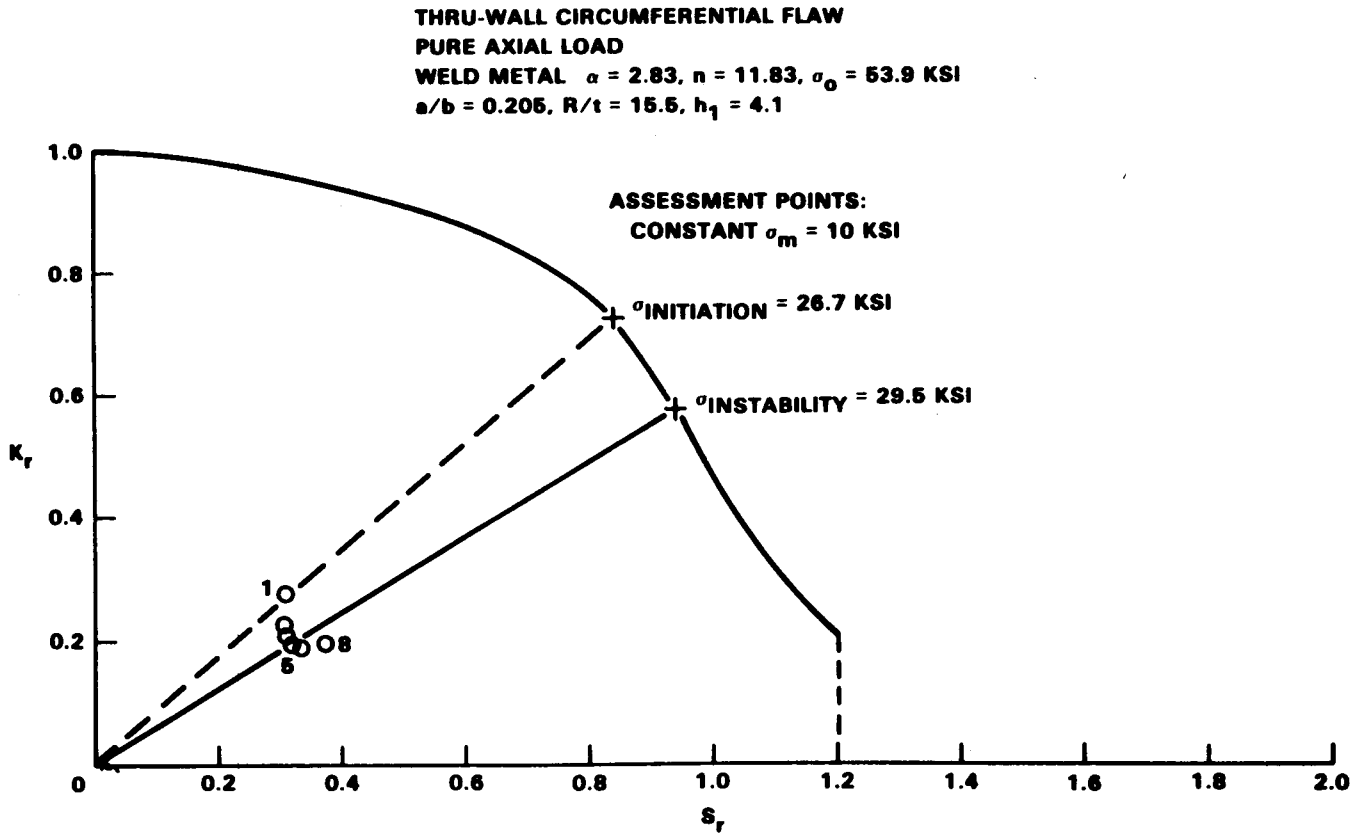

FIGURE 8. DPFAD AXIAL LOADING/WELD METAL

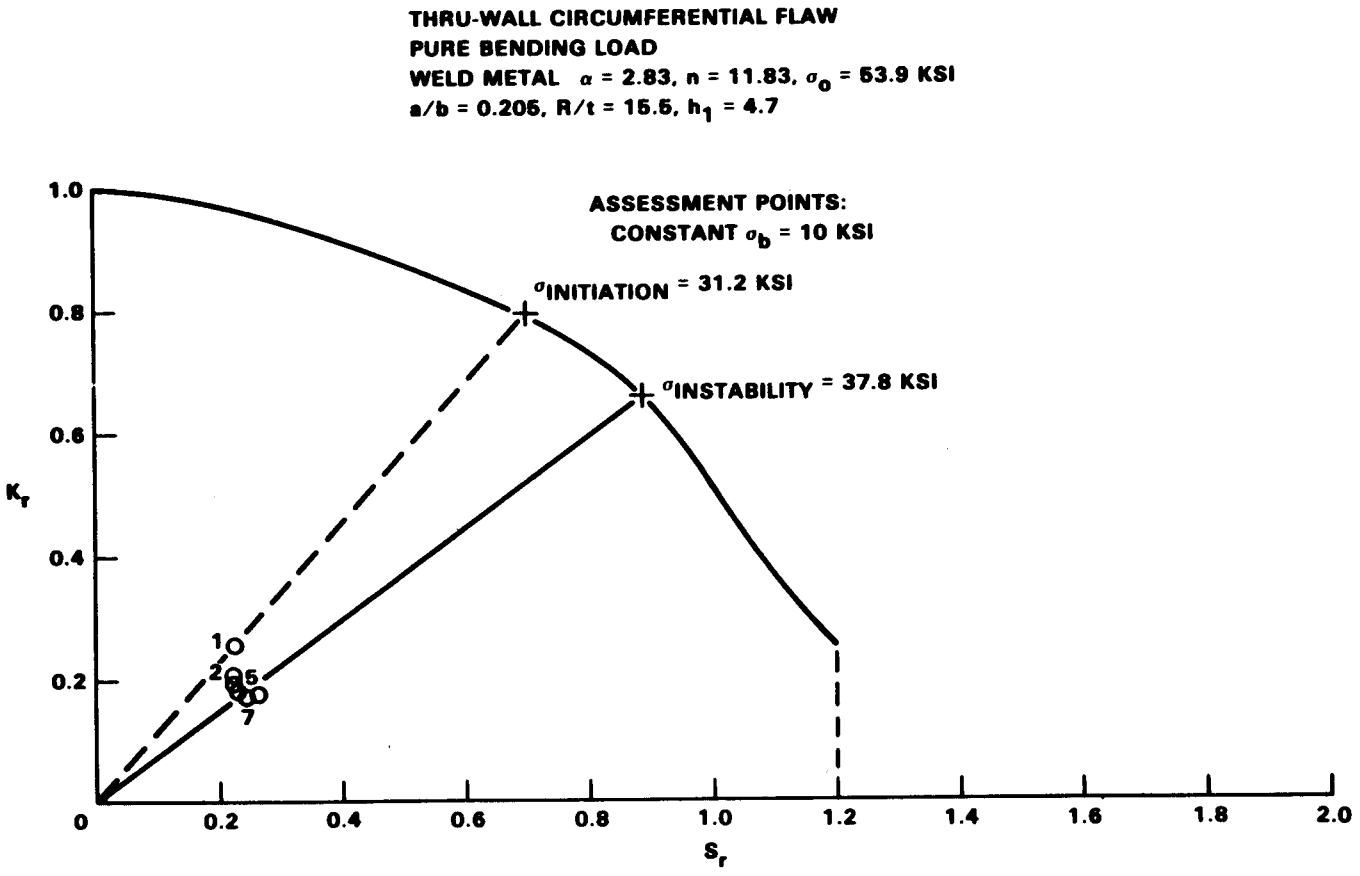

FIGURE 9. DPFAD BENDING LOAD/WELD METAL

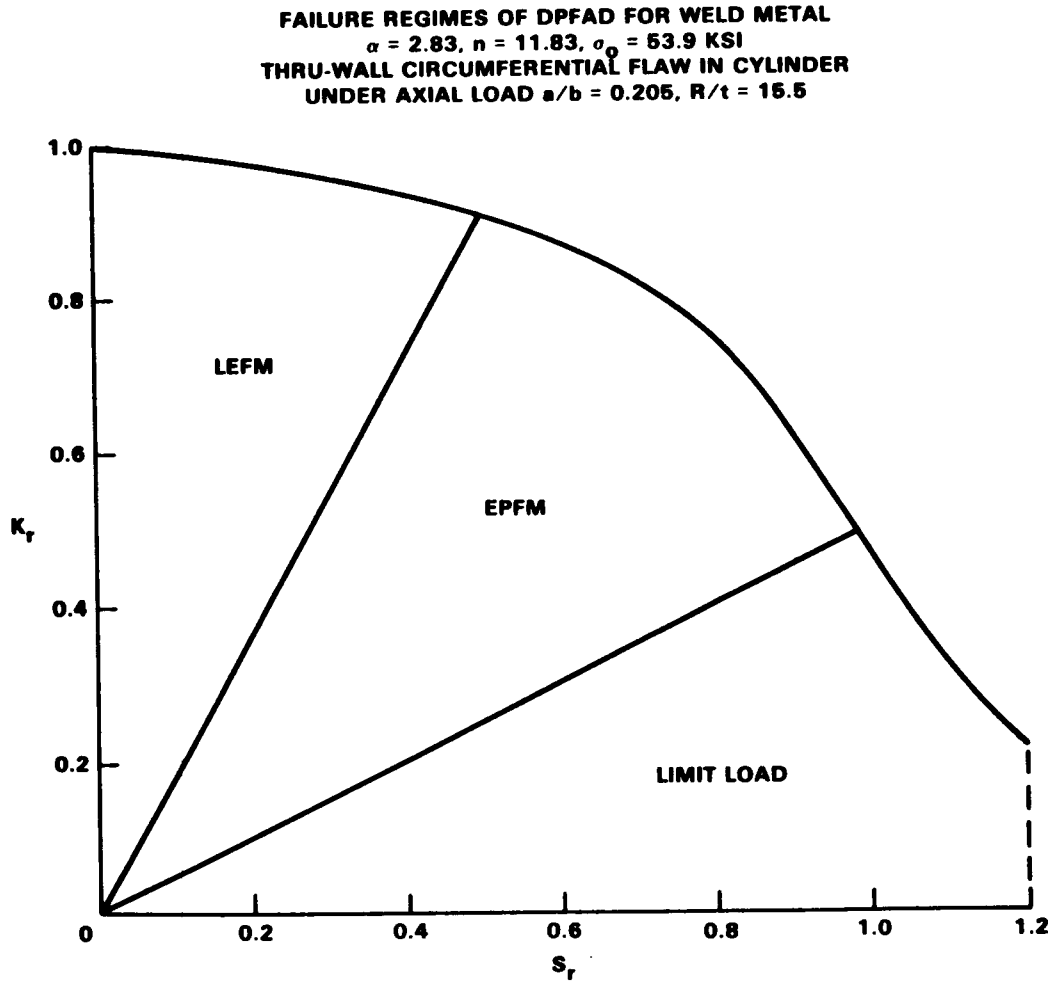

FIGURE 10. FAILURE REGIMES OF DPFAD/WELD METAL

TABLE 1

STRESS-STRAIN PROPERTIES TO BE USED IN THE WORKSHOP PROBLEM

	Base Material	Weldment
ε_o	$8.27\ 10^{-4}$	18.0×10^{-4}
σ_o	24.8 ksi	53.9 ksi
α	17.3	2.83
n	2.49	11.83

TABLE 2

THRU-WALL CIRCUMFERENTIAL FLAW
PURE AXIAL LOADING - σ_m = 10 ksi
BASE METAL

α = 17.3, n = 2.49, σ_o = 24.8 ksi
a/b = 0.205, R/t = 15.5, h_1 = 5.3

FAD S_r	S_r, K_r K_r	Pt	Δa (ins.)	J_R (in.-lb/in.^{2})	K_r'	S_r'	Safety Factor
0.2	0.57	1	0.025	4500	0.184	0.673	1.23
0.3	0.46						
0.4	0.38	2	0.10	7000	0.150	0.680	1.41
0.5	0.33						
0.6	0.29	3	0.13	8000	0.141	0.682	1.47
0.7	0.27						
0.8	0.24	4	0.21	10000	0.129	0.689	1.53
0.9	0.22						
1.0	0.21	5	0.31	12000	0.120	0.698	1.58
1.1	0.19						
1.2	0.18	6	0.39	13000	0.117	0.705	1.62
1.3	0.17						
1.4	0.16	7	0.50	14000	0.115	0.716	1.60
1.5	0.15						
1.6	0.147	8	0.67	15000	0.115	0.732	1.57
1.7	0.141						
1.8	0.135						
1.9	0.130		σ_i = 12.3 ksi		σ_{max} = 16.2 ksi		
2.0	0.125						

TABLE 3

THRU-WALL CIRCUMFERENTIAL FLAW
PURE BENDING LOAD - σ_b = 10ksi
BASE METAL

α = 17.3, n = 2.49, σ_o = 24.8 ksi
a/b = 0.205, R/t = 15.5, h_1 = 6.7

FAD S_r	S_r, K_r K_r	Pt	Δa (ins.)	J_R (in.-lb/in.^{2})	K_r'	S_r'	Safety Factor
0.1	0.796						
0.2	0.617						
0.3	0.501	1	0.025	4500	0.171	0.490	1.62
0.4	0.423						
0.5	0.367	2	0.10	7000	0.139	0.494	1.80
0.6	0.326						
0.7	0.294	3	0.13	8000	0.131	0.496	1.88
0.8	0.268						
0.9	0.247	4	0.21	10000	0.119	0.500	1.98
1.0	0.230						
1.1	0.215	5	0.31	12000	0.111	0.506	2.05
1.2	0.202						
1.3	0.191	6	0.39	13000	0.108	0.510	2.09
1.4	0.181						
1.5	0.172	7	0.50	14000	0.106	0.517	2.08
1.6	0.164						
1.7	0.157	8	0.67	15000	0.106	0.527	2.04
1.8	0.151						
1.9	0.145						
2.0	0.140		σ_i = 16.2 ksi		σ_{max} = 20.9 ksi		

TABLE 4

THRU-WALL CIRCUMFERENTICAL FLAW
PURE AXIAL LOADING - σ_m = 10 ksi
WELD METAL

α = 2.83, n = 11.83, σ_o = 53.9 ksi
a/b = 0.205, R/t = 15.5, h_1 = 4.1

FAD S_r	S_r, K_r K_r	Pt	Δa (ins.)	J_R (in.-lb/in.^{2})	K_r'	S_r'	Safety Factor
0.2	0.981	1	0.025	2000	0.276	0.310	2.67
0.4	0.936	2	0.050	3000	0.227	0.311	2.88
0.6	0.880	3	0.100	3600	0.209	0.313	2.92
0.8	0.771	4	0.150	4000	0.201	0.315	2.94
0.9	0.645	5	0.250	4500	0.193	0.319	2.95
1.0	0.478	6	0.400	5000	0.189	0.325	2.92
1.1	0.311	7	0.750	6000	0.185	0.340	2.89
1.2	0.213	8	1.400	7000	0.194	0.372	2.63

σ_i = 26.7 ksi

σ_{max} = 29.5 ksi

TABLE 5

THRU-WALL CIRCUMFERENTIAL FLAW
PURE BENDING LOAD - σ_b = 10 ksi
WELD METAL

α = 2.83, n = 11.83, σ_o = 53.9 ksi
a/b = 0.205, R/t = 15.5, h_1 = 4.7

FAD S_r	S_r, K_r K_r	Pt	Δa (ins.)	J_R (in.-lb/in.^{2})	K_r'	S_r'	Safety Factor
0.2	0.973	1	0.025	2000	0.256	0.225	3.12
0.4	0.910	2	0.050	3000	0.210	0.226	3.50
0.6	0.836	3	0.10	3600	0.194	0.227	3.66
0.8	0.739	4	0.150	4000	0.186	0.229	3.73
0.9	0.645	5	0.250	4500	0.179	0.231	3.78
1.0	0.509	6	0.400	5000	0.174	0.235	3.76
1.1	0.364	7	0.750	6000	0.170	0.245	3.69
1.2	0.247	8	1.40	7000	0.175	0.266	3.49

σ_i = 31.2 ksi

σ_{max} = 37.8 ksi

TABLE 6

BASE METAL RESULTS

$\sigma_i^{axial} = 12.3$ ksi ; $\sigma_i^{bend} = 16.2$ ksi

$P_m = 10$ ksi

$P_m + P_b' = 13.03$ ksi

$P_b' = 3.03$ ksi ⟶ $M_i = 286$ in-kips

$\sigma_{max}^{axial} = 16.2$ ksi ; $\sigma_{max}^{bend} = 20.9$ ksi

$P_m = 10$ ksi

$P_m + P_b' = 18.0$ ksi

$P_b' = 8.0$ ksi ⟶ $M_{max} = 755$ in-kips

$\Delta a_{instability} = 0.39\text{-}0.50$ inch

TABLE 7

WELD METAL RESULTS

$\sigma_i^{axial} = 26.7$ ksi ; $\sigma_i^{bend} = 31.2$ ksi

$P_m = 10$ ksi

$P_m + P_b' = 29.51$ ksi

$P_b' = 19.51$ ksi ⟶ $M_i = 1843$ in-kips

$\sigma_{max}^{axial} = 29.5$; $\sigma^{bend} = 37.8$ ksi

$P_m = 10$ ksi

$P_m + P_b' = 35.0$ ksi

$P_b' = 25.0$ ksi ⟶ $M_{max} = 2360$ in-kips

$\Delta a_{instability} = 0.25\text{-}0.40$ inch

DUCTILE PIPING FRACTURE MECHANICS

-by-

G. M. Wilkowski,* D. Broek+, M. Nakagaki,* and J. Pan,**

INTRODUCTION

The objective of this Workshop's calculational exercises falls within the scope of the "NRC Degraded Piping Program - Phase II", presently being conducted by Battelle. Since Battelle's approach to the workshop problem is governed and dictated by this program, a summary of the program is given below.

The NRC Degraded Piping Program - Phase II was initiated at Battelle in March, 1984. Its objective is to develop and experimentally validate ductile fracture analyses techniques for practical engineering applications to service cracks and to postulated cracks in nuclear piping of BWR as well as PWR systems. The program is for a 3-year duration. In the second year, an effort similar to this workshop is scheduled, but it will be based on an actual, not a hypothetical case; it will consist of a round-robin analysis of cracked piping experiments.

The efforts in the NRC Degraded Piping Program will move from the simple to the more complex. During the first year, simple loading cases and cracks in the base metal will be considered, while in the later stages cracked pipe removed from service will be tested and analyzed, complex crack shapes in welds under complex loading situations (including water hammer) and compliant loading will be considered.

Research during the first year will focus on the verification of J-estimation schemes for circumferential through-wall, surface, and complex

*Battelle, Columbus Laboratories
**University of Michigan
+FractuREsearch, Inc.

cracks in pipes in pure bending and pure axial tension. Evaluation of each crack geometry and loading condition involves coordinated efforts of material characterization, full-scale pipe fracture experiments, estimation scheme analyses, and selected finite element analyses.

Additional first year efforts include:

- Procurement of cracked pipe removed from nuclear power plants for pipe fracture experiments
- Assessment of specimen geometry effects on J-R curve for typical specimen sizes that can be machined from pipes
- Assessment of capability to account for large amount of crack growth on the basis of small specimen data
- Assessment of the effect of notch acuity on behavior of surface cracks in base metal, weld, and HAZ
- Preparation of compliant test system for up to 42-inch-diameter pipe
- Assessment of the weld-overlay repair method
- Evaluation and modification of J-estimation schemes for application to weld cracks in pipes
- Development of an international cooperative effort.

With respect to the last item, an International Piping Integrity Research Group (IPIRG) is currently being formed to evaluate additional fracture concerns (seismic loading, fracture of components, postfracture events such as leakage and thrust loads at LWR service conditions, fracture of piping in brittle-ductile transition region, etc.). This group will build upon the NRC Degraded Piping Program and have full access to all results.

Results of the first year's efforts may dictate a redirectioning of subsequent work, but present plans call for the following efforts in the second and third year:

- Evaluation of sustained load effects

- Evaluation of instability under compliant loading of surface cracked pipes and assessment of leakage

- Evaluation of instability under combined membrane and bending loads

- Evaluation of cracks in welds, HAZ

- Tests on cracked pipe removed from service

- Assessment of fracture under dynamic loads from water hammer

- Compilation of a handbook and computer code for ductile fracture analysis of piping and a data record book.

The pipe fracture case forming the subject of this workshop involves:

- Assessment of predictive J-estimation methods for a circumferentially cracked pipe in bending

- Similar assessment for pipe in tension

- Combination of above cases and assessment of combination

- Outline of approach to a weld crack in a pipe.

All of these are being or will be evaluated in the NRC program, but are not completed since the program was just initiated in March of this year. Consequently, the results and approaches presented by Battelle are tentative and were generated exclusively for the benefit of this workshop; without the benefit of many more test results, the appropriateness of the approach cannot yet be an issue here. However, the various solutions presented in this workshop will at least lead to a discussion of the many assumptions upon which this and other approaches are based.

It is worthwhile to note that the problem selected for this workshop represents a case that may be experimentally evaluated in the second year of the NRC program. At the next ASME PVP meeting, we will be inviting a similar round-robin effort on a different pipe and crack geometry, and will also present the absolute measure of the accuracy of the computations, namely, the experimental result.

PROBLEM DEFINITION AND METHOD OF ANALYSIS

The problem is defined in Figure 1. The toughness of the material given in terms of a J-R curve follows from Figure 2.

A solution is solicited on the basis of a J-estimation scheme. The proposed "absolute" measure of verification is a finite element solution, rather than an experimental result. A variety of J-estimation schemes have been proposed for the simple case of a circumferential through-the-thickness crack in a pipe; however, some of these have no other use than for the evaluation of J-R curves from an experimental result (they have no predictive capability).

The estimation schemes useful for predictive purposes have been used by the other participants in this workshop. Application of these schemes to the present problem poses the following difficulties:

(a) The evaluation of J for the case of a fixed axial tension in combination with an increasing bending moment cannot be done, at present, in accordance with an established procedure. Any combination procedure is based on assumptions and subject to doubt.

(b) Use of the G.E. estimation scheme, strictly speaking, is not possible because h-functions are presently not available for the value of $R/t = 16$ for the present problem. Values of the h-function available to us are for $R/t = 6$ only. In addition, they are for values of $n = 1$ and 5, so that an extrapolation would be necessary for the case of $n = 11.83$ for the weldment.

Given difficulty (a), and given the fact that this problem is to be addressed as part of a thorough 3-year program, Battelle does not consider it appropriate at this time to present the world with another or modified (but untried) J-estimation scheme. Such schemes will be established during the course of the NRC program. Thus, for the present purpose, Battelle has selected one of the existing schemes, namely, the G.E. scheme as the one exclusively developed for a material with a stress-strain behavior as assumed for the present problem.

In view of difficulties (a) and (b) above, additional assumptions are involved. Thus, the results have no value whatsoever for a judgment of the adequacy of the G.E. procedure.

In order to sustain some of the assumptions and judgment calls that were necessary to obtain a solution to the workshop problem, use will be made of the results of a sensitivity study conducted earlier for the benefit of the NRC program. As this sensitivity study is based on actual test data, a summary of its results will be presented first. Subsequently, the solution to the workshop problem will be discussed.

SENSITIVITY ANALYSIS

Results of tests on Type 304 stainless steel pipes in bending with circumferential through-the-thickness cracks are available for pipes with outside diameters of 2.375, 4.5, and 16 inches. These permit a comparison of various J-estimation schemes with respect to their sensitivity to pipe diameter. As the results of this comparison have some bearing on the workshop problem, they will be presented in this section. However, because the diameter effect is beyond the scope of this workshop, only a summary of the findings will be given. The essential details of the three tests are given in Table 1. Note that R/t for the three cases is not too far from 6.

The assumptions involved in using any of the estimation schemes will not be repeated. However, it is important to note that various stress-strain curve approximations were used in applying the G.E. procedure, as summarized in Table 2.

Results of some finite element analyses are available as well. For all cases, the following estimation schemes were used.

Experimental Eta-Factor Method

For this method is used only for calculating a J-R curve from experimental data. It cannot be used to predict loads or displacements given a J-R curve for a material. In this method J is estimated as*

$$J = J_e + J_p = \frac{1}{4Rt} C'(\theta) P^2 - \frac{F'(\theta)}{2Rt\, F(\theta)} \int_0^{\Delta_{cp}} P d\Delta_{cp}$$

where $C'(\theta)$ follows from experiments and the integral is obtained from the load-displacement curve from a pipe test. For this purpose, the calculated elastic displacements for the uncracked pipe were subtracted from the measured displacements, and it was assumed that the remaining displacement was due to the crack only.

G.E. Method

This method can be used to calculate a J-R curve, or to predict loads during crack growth. The definition of J is

$$J = J_e + J_p = F(a, \frac{R}{t}) \frac{M^2}{E} + \alpha\, \sigma_o\, \varepsilon_o\, c\, h(\frac{a}{b}, n, \frac{R}{t}) (\frac{M}{M_o})^{n+1}$$

where $C = R(\pi-\theta)$, $b = \pi R$, and F and h are tabulated results obtained by G.E. from finite element computations using for the linear elastic part

$$\varepsilon/\varepsilon_o = \sigma/\sigma_o$$

and for the nonlinear elastic part

$$\varepsilon/\varepsilon_o = \alpha(\sigma/\sigma_o)^n.$$

Note that values of h are available only for R/t = 6.

NUREG/CR-3464 Method

This method obtains J from a load-displacement curve estimated as an

interpolation between the linear elastic and fully plastic (limit-load) load-displacement lines (Figure 3). It uses a variable plastic zone corection factor to make this interpolation. The materials strain hardening is not included in this analysis. For further details see NRC report NUREG/CR-3464.

NRC-NRR Method

This method is a further extension of the NUREG/CR-3464 method accounting for strain hardening. J is obtained from the load-displacement diagram as estimated by the NUREG/CR-3464 method, but the diagram is modified to conform to

$$\frac{\phi_c}{\phi_o} = C(\theta) \left\{ \frac{M}{M_o} + \alpha \left(\frac{M}{M_o} \right)^n \right\}$$

where $C(\theta)$ is the compliance obtained by the NUREG/CR-3464 method. For further details of this method see NUREG 1061 Volume 3.

Results

The results are summarized in Table 3. Also shown in this table are results of finite element analyses. In all cases, the J-value at crack growth initiation was calculated. At the bottom of the table are the J_{Ic}-values[a] found from three-point-bend-bar specimens cut from the individual pipes.

Clearly, there is a considerable discrepancy between the values of J at initiation as obtained by various methods. Also these values are considerably different from J_{Ic}. Figures 4, 5 and 6 show how the various methods would have predicted the stress (or moment) at crack initiation if initiation had been assumed to occur at the measured J_{Ic}. These can be compared with the actual values at initiation.

The results of the finite element analysis in Table 3 show that finite element analysis cannot be used as an absolute standard against which to

(a) Strictly speaking, these values are not J_{Ic} values since they do not meet the ASTM thickness requirements.

compare the results of the other analyses, although the FEM results however are closer to the bend bar J_{IC} values than the estimation schemes. It might be argued that initiation in the pipe tests may not have taken place at the measured J_{IC}, because initiation in bend bar specimens may occur at a lower value of J than in the pipe. However, there is no reason to justify the assumption that initiation took place at the J-value calculated by finite elements until such would be borne out by a series of tests and analyses on the same pipe, but with different crack sizes and under different loading conditions.

Most important is that none of the methods seem to account properly for the effect of diameter. (Note that in all cases R/t was approximately equal to 6, so that h-functions for R/t = 6 were used for lack of an alternative.)

It appears from Table 3 that the moment at initiation and the maximum moment would be predicted within 5 percent using collapse analysis. Thus, it would seem that fc the purpose of the prediction of allowable bending moment or stress, the collapse analysis is still the most reliable.

Implications for Solution to Workshop Problem

The results of this sensitivity study indicate that J-estimation schemes in their present stage are not likely to produce reliable results, and that comparison of such results to a finite element analysis is not likely to resolve any issues. The additional complications of combined tension and bending and of an R/t = 16, for which as yet no h-functions are available, will not make comparisons any easier. As the NRC Degraded Piping Program will resolve many of these issues by providing actual test results, and revised or modified estimation schemes, Battelle has chosen to use the simplest possible solution (apart from collapse analysis). Solution of the second part of the problem, dealing with displacement control, requires many further assumptions, and therefore, only an outline of a solution is provided.

SOLUTION TO THE WORKSHOP PROBLEM

Assumptions

The solution chosen makes use of the G.E. estimation scheme. Therefore, all assumptions intrinsic to the G.E. scheme are implied in the present

solution. One of the dubious assumptions is that of power-law hardening material, but the problem statement prescribes this kind of material behavior.

All the equations underlying the analysis are compiled in Table 4. In order to obtain h_1 for R/t = 16, it was assumed that the ratio of the values of h_1 for R/t = 16 and R/t = 6 is the same as the ratio of the linear elastic F-function for these same R/t values

$$\frac{(h_1)_{16}}{(h_1)_6} = \frac{F_{16}}{F_6} .$$

The F-functions chosen for this calculation are those of Sanders. In order to account for the combined bending and tension, it was assumed that the combination leads to an equivalent bending moment given by

$$M_{eq} = M + \frac{R}{2} \frac{F_t}{F_b} P .$$

The problem can then be treated as one for pure bending.

The Load Control Problem

To facilitate comparisons with other solutions, some intermediate results are given in Table 5. The curve of J as a function of moment is given in Figure 7. This leads to a value of M_{eq} = 1,600,000 in-lb at crack growth initiation, the actual moment with an axial tension stress of 10 ksi is 560,000 in-lb.

Figure 8 shows the values of J during crack growth. Moments and crack size at instability and initiation are given in Table 6.

The Displacement Control Problem

If h_3 were available for combined loads to calculate Δ_c^p, it would be possible to evaluate

$$\phi_{tot} = \phi_{nc}^e + \phi_{nc}^p + \phi_c^e + \phi_c^p$$

Using a plot as in Figure 9, the stability problem could then be evaluated.

WELD CRACK

Scope

The last part of the workshop problem is a discussion of the approach that would be used if the crack was located in or at a circumferential weld, given the same configuration of crack and pipe as in the first part of the problem.

Resistance and stability of cracks in pipe girth welds are of major concern, because service cracks have occurred in welds. It is for this reason that the NRC Degraded Piping Program - Phase II is geared to arrive at a practical solution for the analysis of cracks in pipe girth welds. However, this 3-year program is structured to move from the simple to the complicated, and a solution for weld cracks is not yet in sight. Consequently, the discussion of the weld crack problem will pertain primarily to the approach Battelle will follow during the NRC Program. However, what are believed to be upper and lower bound solutions will be discussed as well.

Problem Definition

The simplest form to which the case of a weld crack can be idealized is shown in Figure 10. The specific difficulties involved are then

a. The existence of 2 bi-metal interfaces close to the crack tip.

b. The weld material having a different yield stress (considerably higher than Type 304 stainless steel) and different strain hardening properties than the base metal.

The use of J-estimation schemes that assume homogeneous material may well be the cause of significant discrepancies. At an elastic-plastic bi-metal interface, such as in a welded pipe, strain discontinuities may occur. In that case, the J-integral is not path independent when the contour crosses the interface. Thus, any relationship between near field and far field J (as required for estimation schemes) may become questionable.

Approach

The problem discussed in the previous section can be amended by defining J as (Figure 10)

$$J = J_{\Gamma_1} - J_{\Gamma_2} .$$

With this definition path independence is preserved, whether or not the contour crosses the interface.

Using this definition of J, Battelle will be analyzing test results obtained by DTNSRDC of various size CT specimens with weld cracks. The J-integral, as defined above, will be obtained from finite element analysis of a model properly simulating the different yield and strain hardening of base metal and weld. Conventional J-estimation schemes will be used as well to assess discrepancies.

Since finite element analysis permits easy calculation of other mechanical quantities as well, comparisons will be made also on the basis of the conventional J, Atluri's ΔT_p^* integral, and virtual crack extension methods.

After this analysis of CT specimens, a similar analysis will be performed of an experiment on a pipe with a weld crack, also performed at DTNSRDC.

Based on the results of these analyses, present J-estimation schemes will be modified to account for welds. Depending upon the results, two alternatives for modification are considered:

a. The use of correction factors as a function of geometrical and material parameters.

b. A J-estimation scheme that accounts for welds in an approximate way.

The work described above will be performed during the first year of the program. It will form the basis for the design of tests on pipes with weld cracks to be performed during the second year, to critically evaluate the parameters that have emerged as the most important. These tests will be used to verify and further refine the modified J-estimation schemes.

It should be kept in mind that the objective of the NRC Program is to arrive at practical engineering solutions to pipe crack problems. Thus, the procedure to arrive at modified J-estimation schemes is in concert with NRC's objective. It should also be kept in mind that the real problem of a crack in a weld is a complicated one and would have to be idealized a great deal in all "rigorous" modeling (Figure 11).

Upper and Lower Bound Solutions

At present, the problem of the weld crack could be addressed when it is assumed that J-estimation schemes for homogeneous materials apply. In that case, what are believed to be upper and lower bound solutions can be obtained as follows:

a. Assume the entire pipe to have the properties (yield, strain hardening, and toughness) of the weld metal (lower bound).

b. Assume the entire pipe to have the properties (yield and strain hardening) of the base metal but the toughness of the weld metal (upper bound).

With these assumptions, J and the bending moment at crack initiation and instability could be calculated using the G.E. estimation scheme, provided h_1 for $n = 11.83$ (the value specified for the weld in this problem) were available. If one would simply extrapolate the h-function from $n = 5$ to $n = 16$ (a dangerous procedure), one would arrive at a negative h_1. Therefore, a numerical solution was not attempted.

DISCUSSION AND CONCLUSION

Apart from the assumptions implicit in the G.E. estimation scheme used here, assumptions had to be made with regard to the combination of tension and bending, and with regard to the h-functions for $R/t = 16$. Assumptions for the combination of tension and bending are necessary for all estimation schemes. It is to be anticipated then that largely different solutions with regard to J-values will emerge. Although, this may be of theoretical interest, it is of limited practical value. The true practical test is whether bending moments

at crack initiation and displacements at instability are predicted with reasonable accuracy.

Considering the developments to be made in the course of the NRC Degraded Piping Program, the problem presented to this workshop was perhaps a little premature. The lack of an absolute measure against which to compare the results, in the form of a test result, further complicates the judgment of the results. As shown by the sensitivity study presented here, a finite element analysis lacks the quality of an absolute measure. In view of this, the solution to the workshop problem presented here is considered of value only in that it shows what was already known; namely, that further development of estimation schemes for practical application is necessary. The actual solution obtained is based on assumptions to which Battelle does not necessarily subscribe, but which had to be made for lack of proven alternatives in order to obtain a solution at all at this stage in time. Although assumptions will always be necessary, better and more reliable methods will be developed and experimentally verified in the course of the NRC Program.

	Base Metal	Weld
ϵ_o =	8.274×10^{-4}	18.04×10^{-4}
σ_o =	24.8 ksi	53.9 ksi
α =	17.3	2.83
n =	2.49	11.83

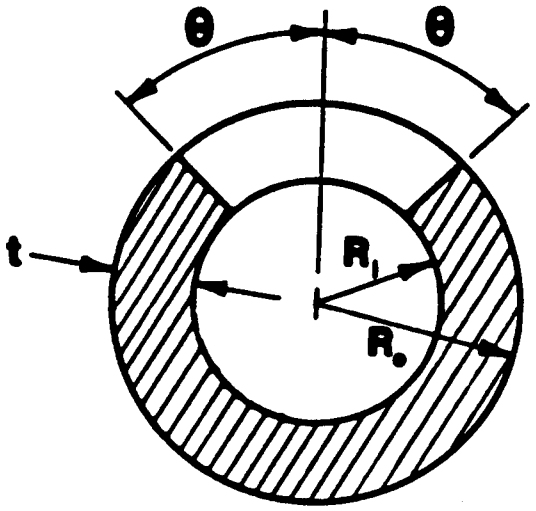

θ = 0.645 radian
R_i = 7.5 inches
R_o = 8.0 inches
t = 0.5 inch

Constant axial stress 10 ksi plus pure bending

FIGURE 1. CRACKED PIPE GEOMETRY

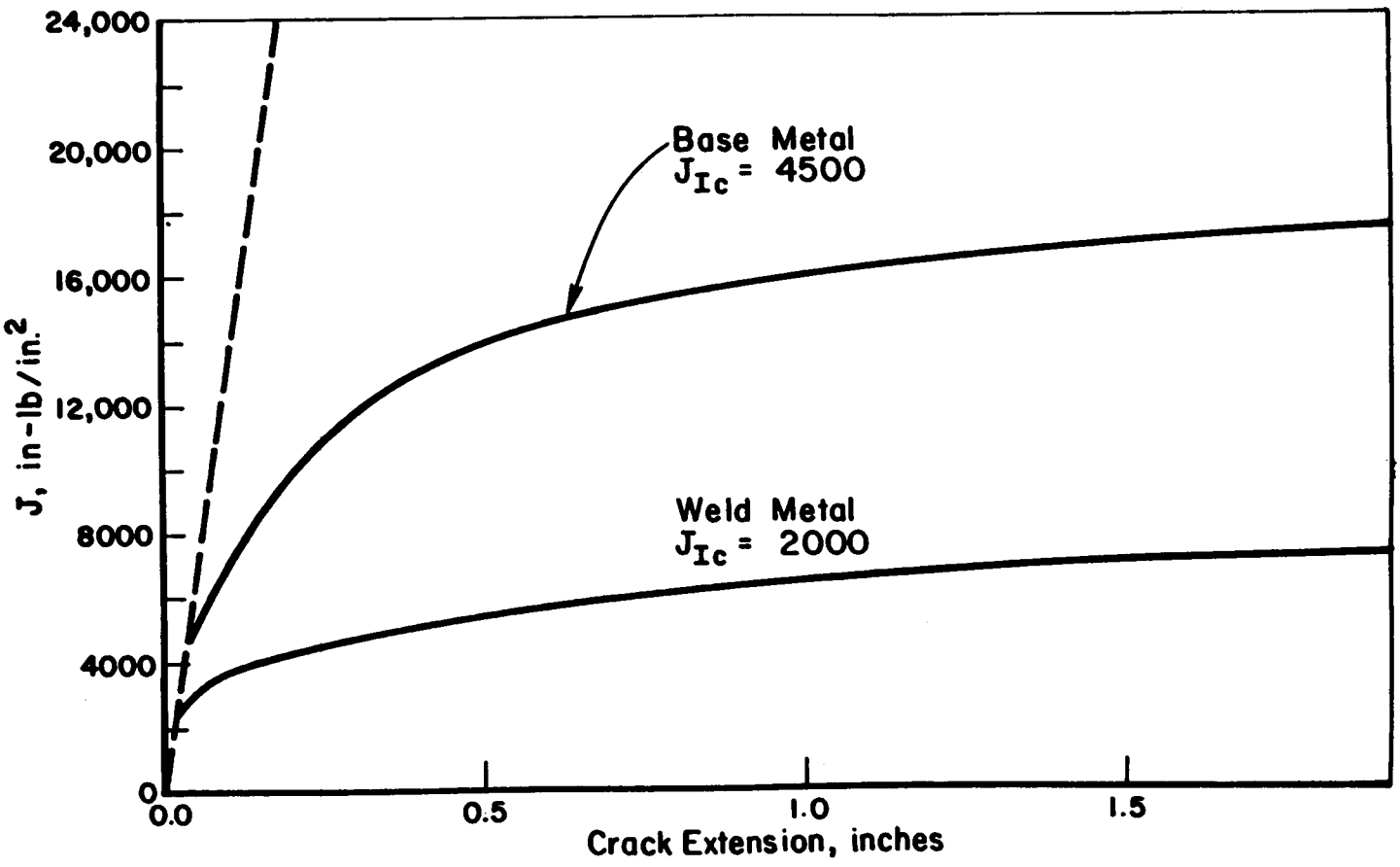

FIGURE 2. J-INTEGRAL RESISTANCE CURVES

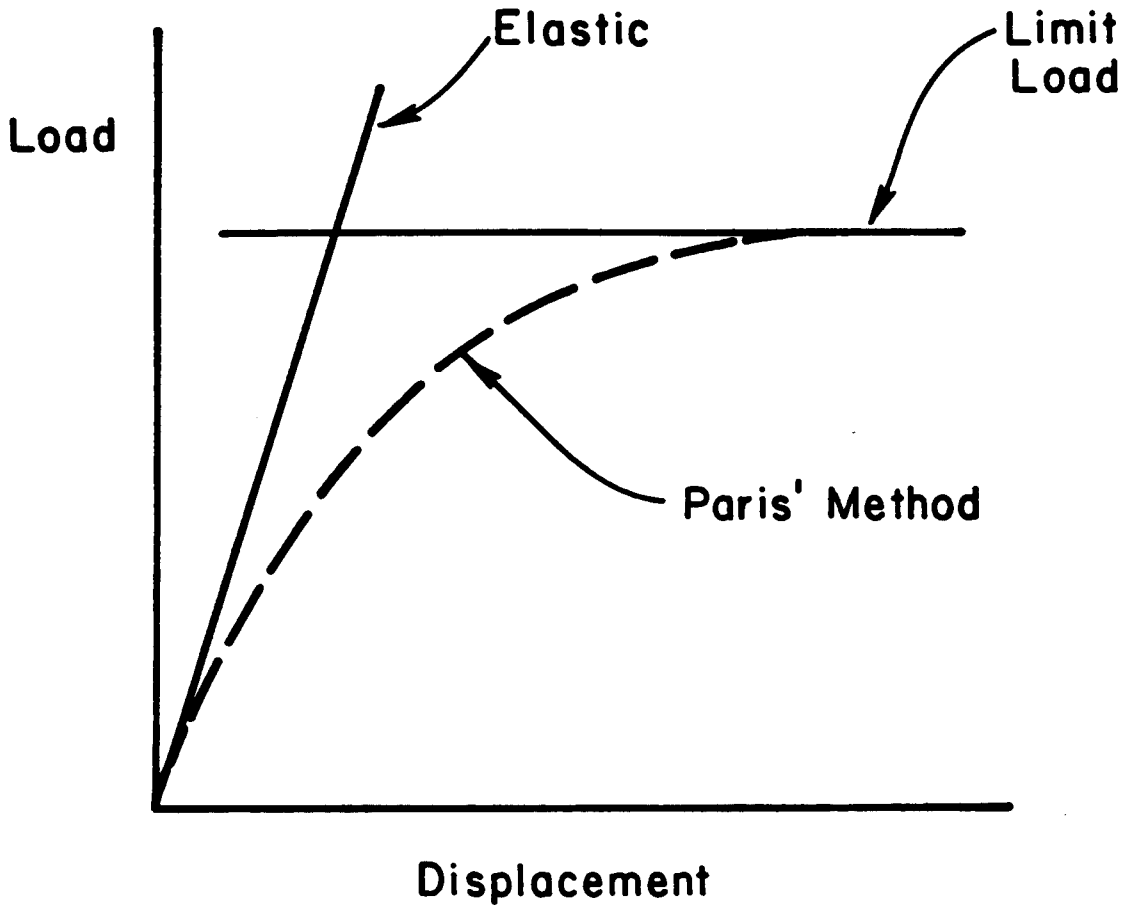

FIGURE 3. NUREG/CR-3464 METHOD

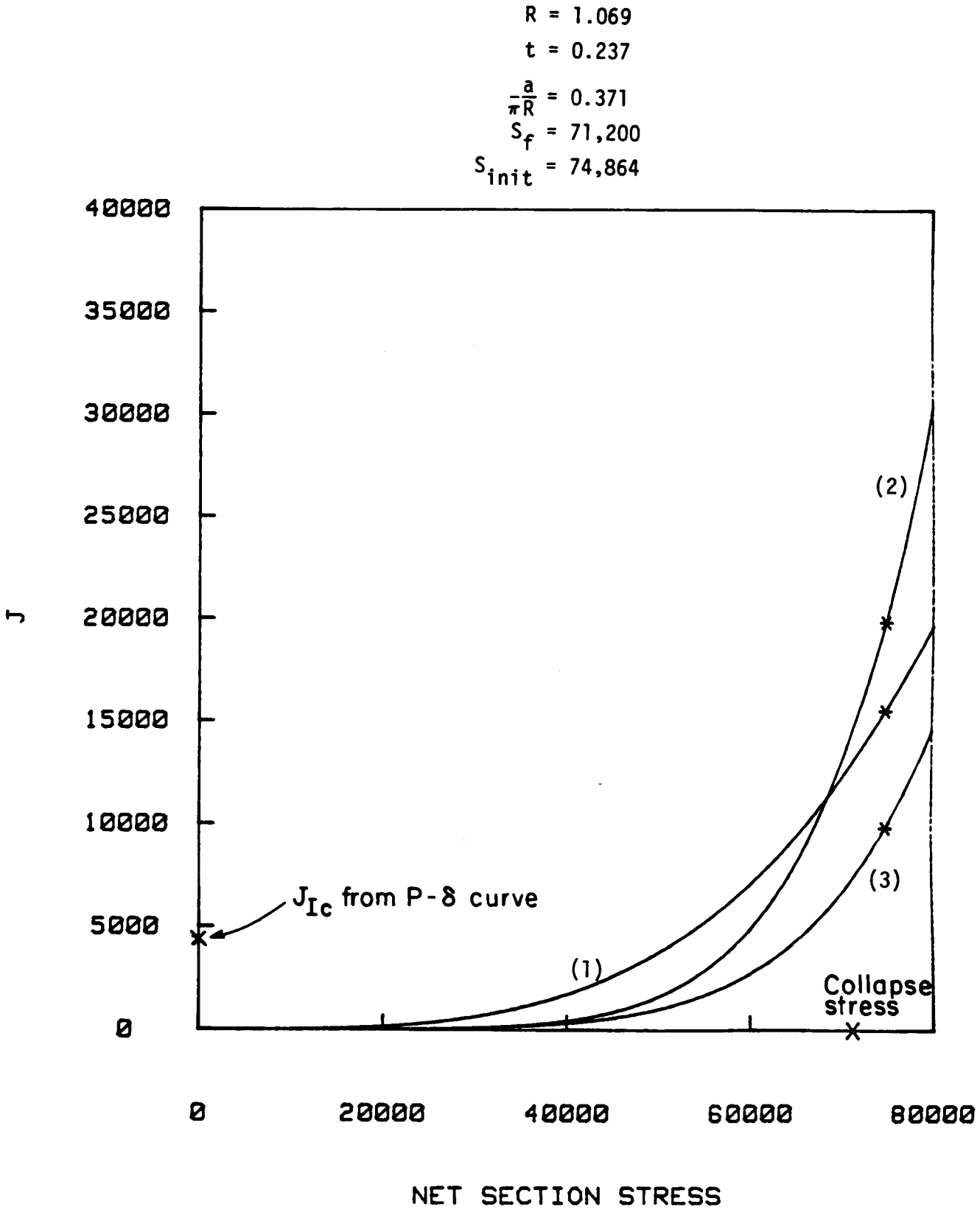

FIGURE 4. EXPERIMENT 7T, G.E. METHOD
(1,2 AND 3 REFER TO RAMBERG-OSGOOD
EQUATIONS IN TABLE 2)

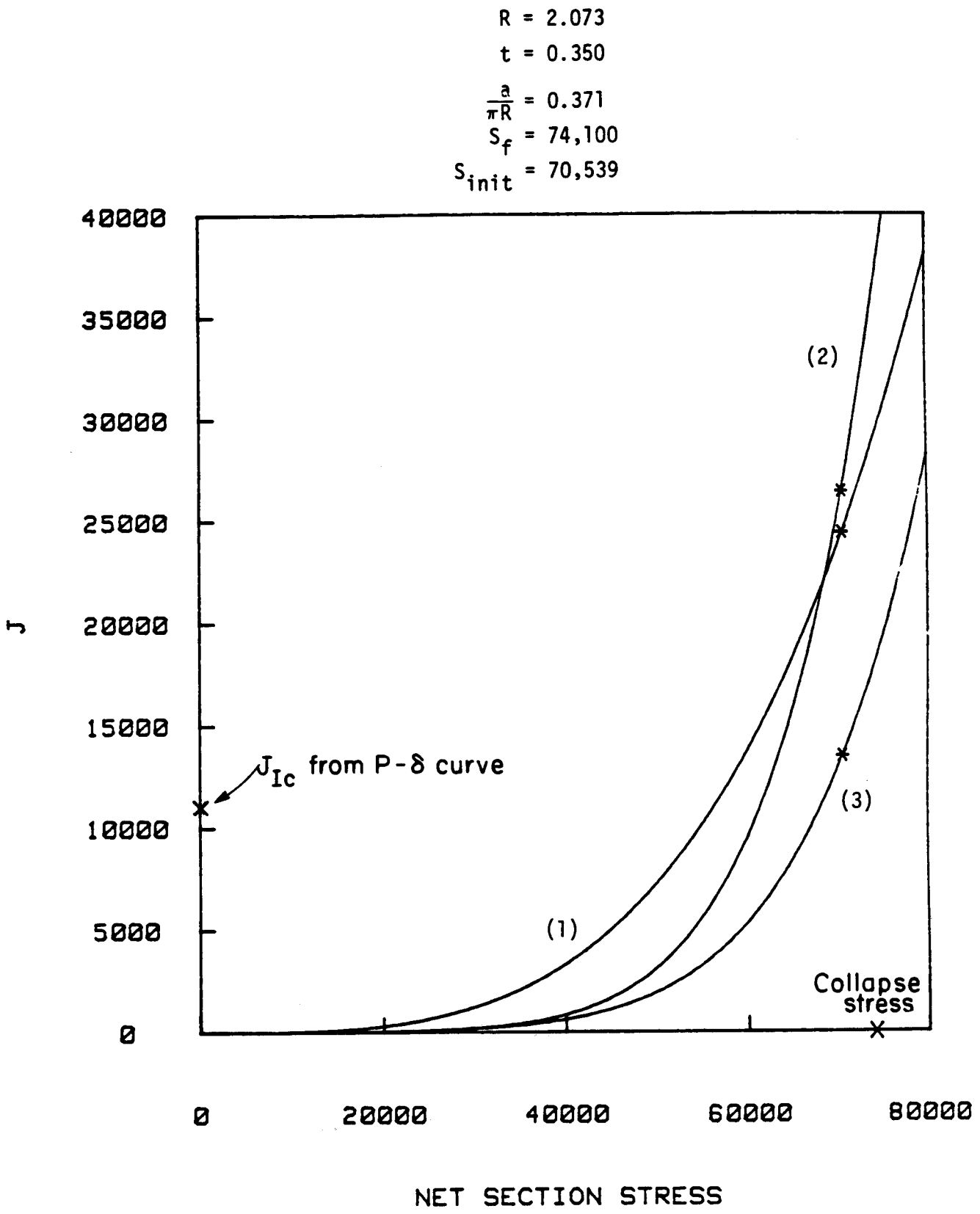

FIGURE 5. EXPERIMENT 1T, G.E. METHOD
(1,2 AND 3 REFER TO RAMBERG-OSGOOD
EQUATIONS IN TABLE 2)

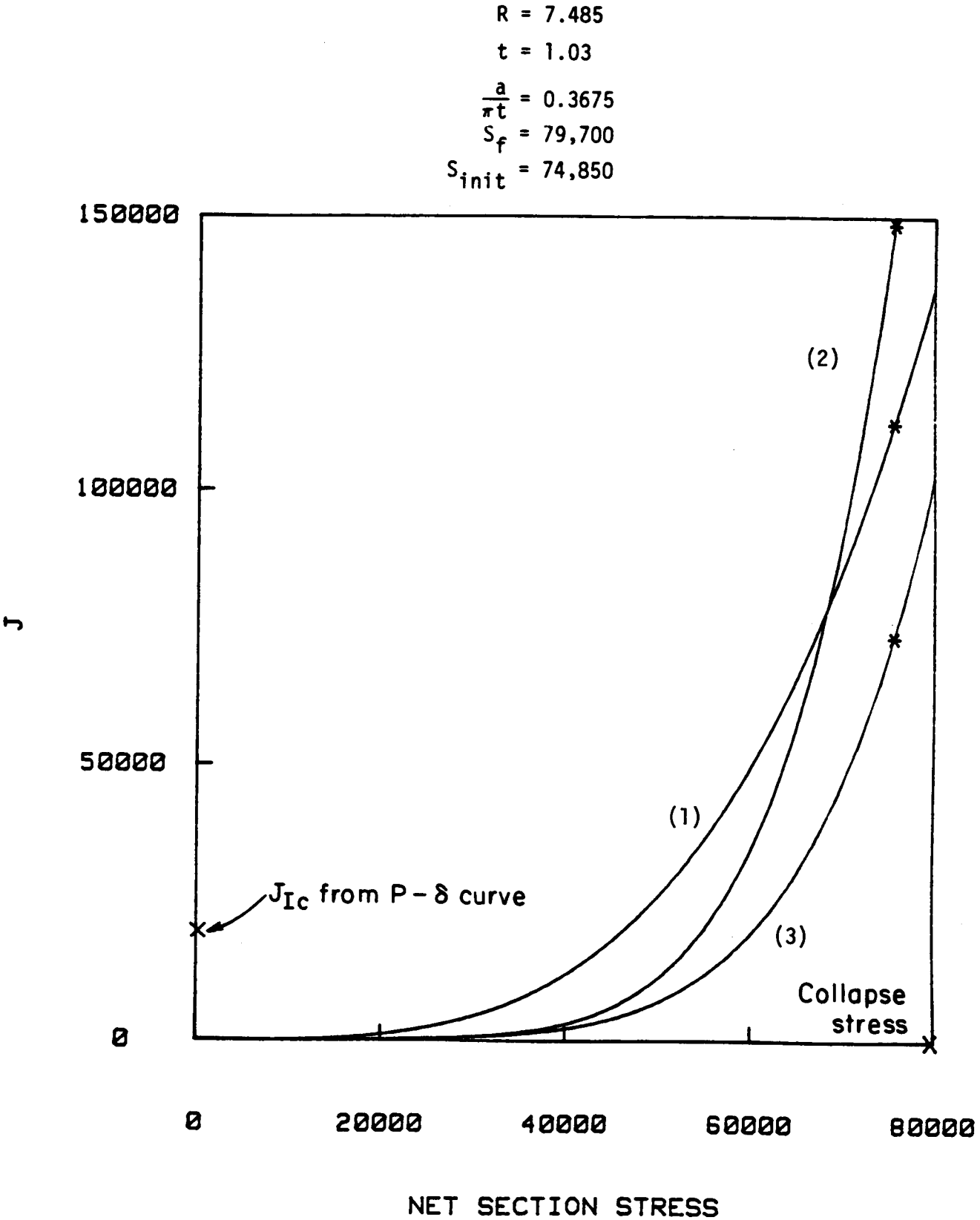

FIGURE 6. EXPERIMENT 8T, G.E. METHOD
(1,2, AND 3 REFER TO RAMBERG-OSGOOD
EQUATIONS IN TABLE 2)

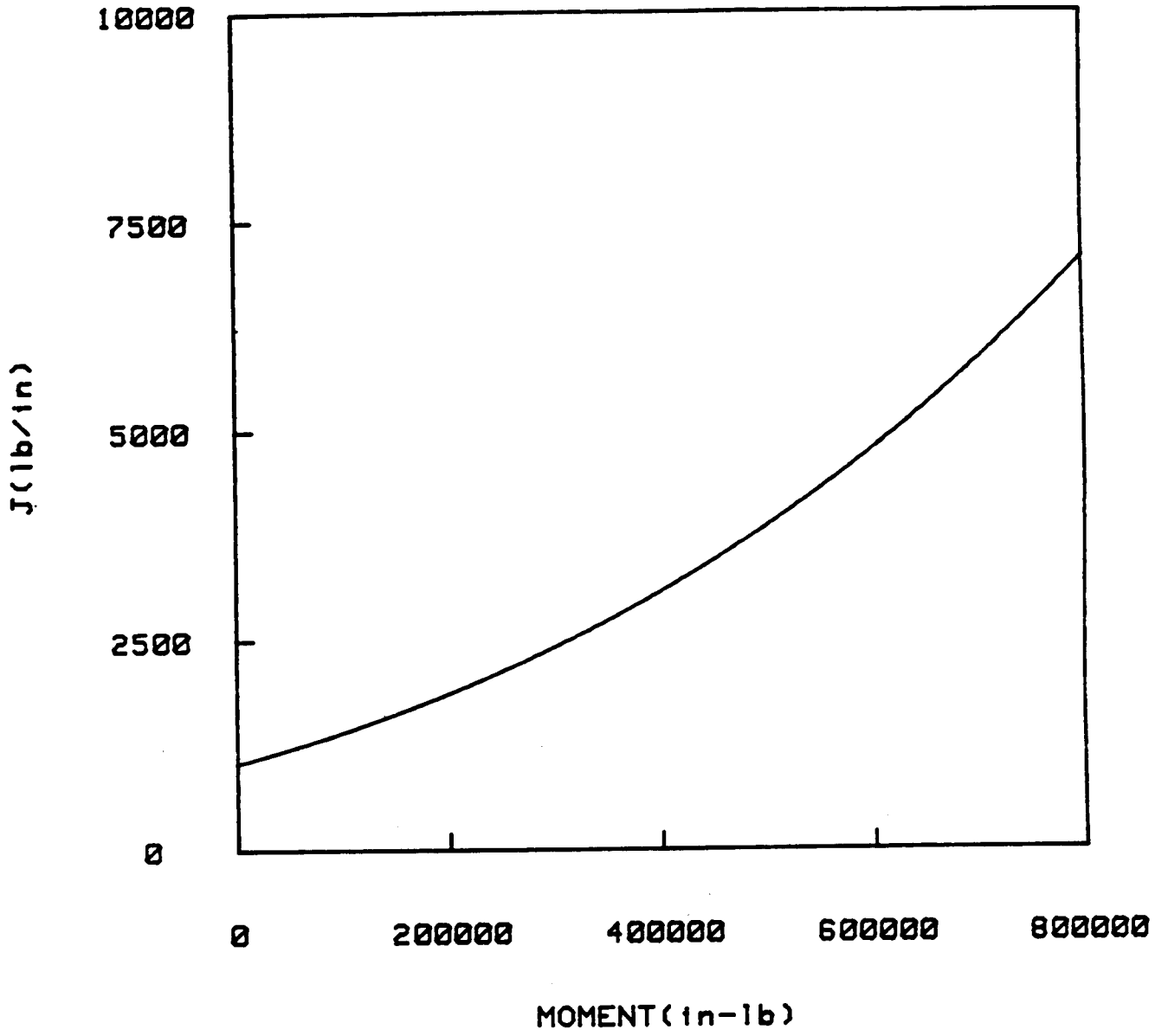

FIGURE 7. J AS A FUNCTION OF M WITHOUT CRACK GROWTH FOR CRACK IN BASE METAL

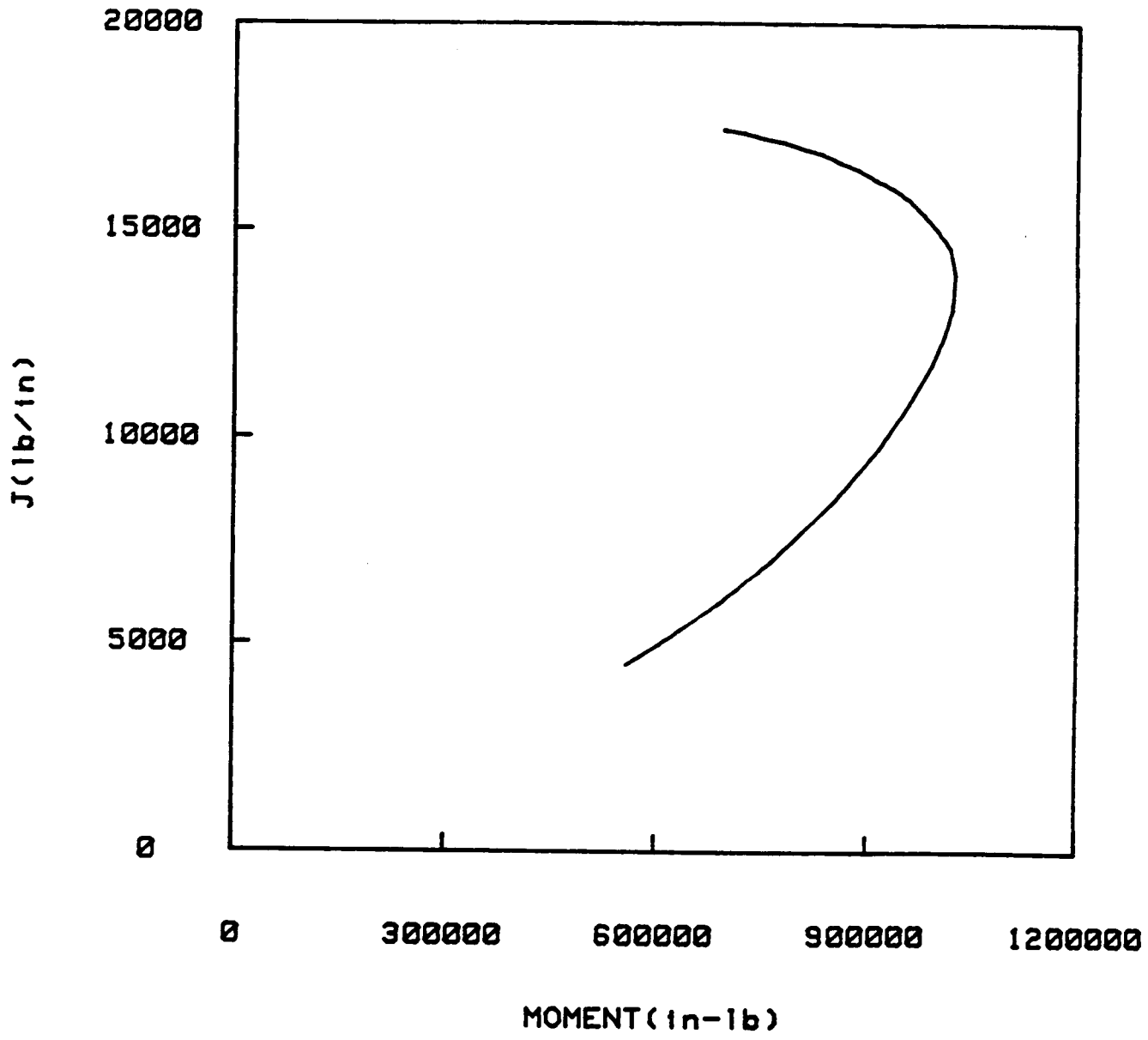

FIGURE 8. J AS A FUNCTION OF M DURING CRACK GROWTH FOR CRACK IN BASE METAL

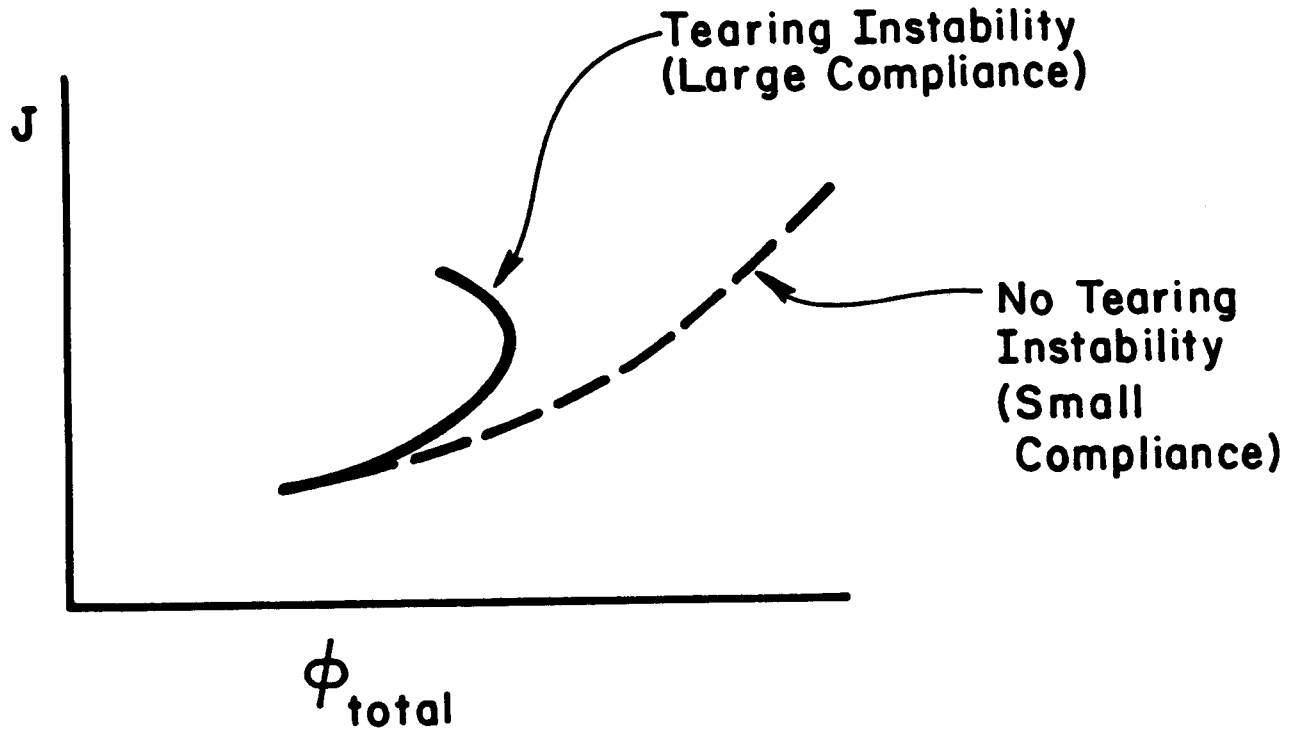

FIGURE 9. INSTABILITY IN DISPLACEMENT CONTROL

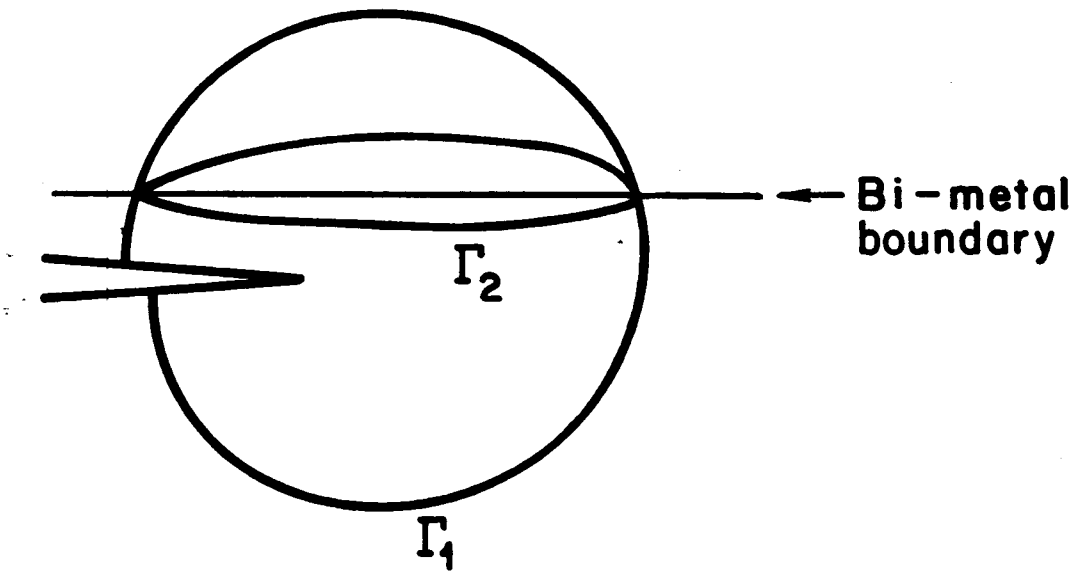

FIGURE 10. INTEGRATION PATHS FOR J TO ADDRESS THE WELD PROBLEM

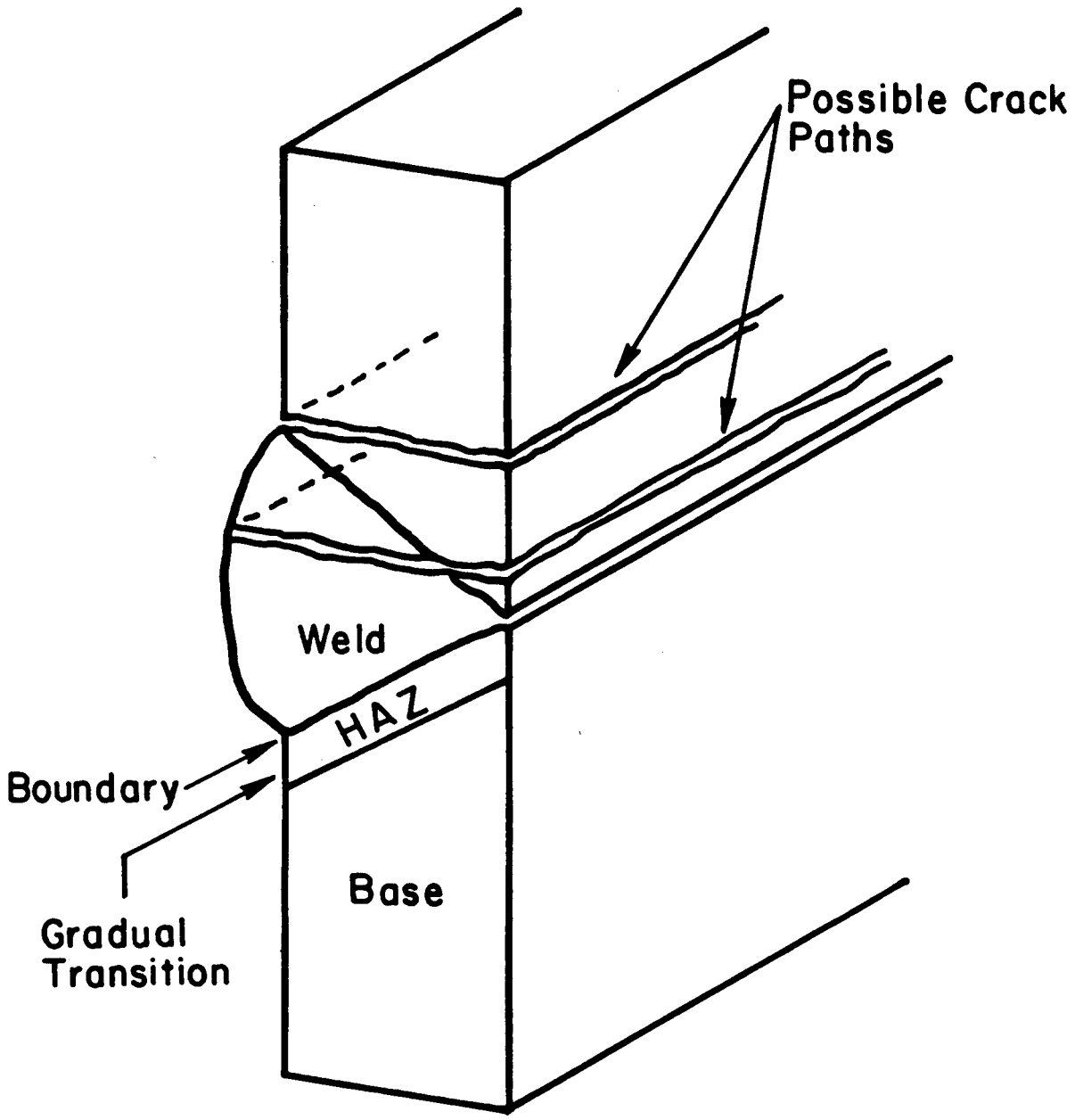

FIGURE 11. WELD CRACKS

TABLE 1. EXPERIMENTAL DATA FOR TYPE 304 STAINLESS STEEL PIPES IN BENDING WITH THROUGH-WALL CIRCUMFERENTIAL CRACKS)

	Exp 7T	Exp 1T	Exp 8T
Outer diameter (D_o), inch	2.375	4.500	16.000
R (mean radius), inch	1.069	2.073	7.485
t (wall thickness), inch	0.237	0.354	1.030
R/t	4.51	5.85	7.26
$\frac{2a}{\pi D_o}$	0.371	0.371	0.3675
θ (half crack angle), degrees	66.78	66.78	66.15
Net section stress (a) at initiation, psi	74,864	70,537	75,604
Net section stress at maximum load, psi	75,823	71,775	78,811
Flow stress (b) from tensile tests, psi	71,200	74,100	79,700

(a) Net section stress = $M/\{2R_g^2\, t[2\sin(\beta/4) - \sin(\theta)]\}$
where $\beta = 2(\pi-\theta)$.

(b) Flow stress = $1.15(\sigma_y+\sigma_u)/2$.

TABLE 2. STAINLESS STEEL RAMBERG-OSGOOD PROPERTIES

G.E. Method

1. δ-ε Curve

   $n = 5.42$
   $\alpha = 1.69$
   $\sigma_o = 30 \times 10^3$ psi
   $E = 30 \times 10^6$ psi

2. True σ-ε Curve[a]

   $n = 2.57$
   $\alpha = 11.94$
   $\sigma_o = 44.3 \times 10^3$ psi
   $E = 26.8 \times 10^6$ PSI

3. Engineering σ-ε Curve[a]

   $n = 5.0$
   $\alpha = 4.22$
   $\sigma_o = 44.3 \times 10^3$ psi
   $E = 26.8 \times 10^6$ psi

NUREG/CR-3464 Method

$n = 5.02$
$\alpha = 8.50$ (4.5 in. diameter pipe)
$\alpha = 1.70$ (16 in. diameter pipe)
$\sigma_o = 38.9 \times 10^3$ psi
$E = 28 \times 10^6$ psi

(a) For strains greater than 0.04.

TABLE 3. RESULTS OF COMPARISON OF J-ESTIMATION METHODS

	Exp 7T	Exp 1T	Exp 8T
Outer diameter, inch	2.375	4.500	16.00
J at initiation load (J estimation scheme based on η factor using P-δ curves), in-lb/in^2	4,200	10,300	20,000
J at initiation load G. E. estimation scheme using several n and α for stainless steel), in-lb/in^2	10,000 to 20,000	14,000 to 26,000	20,600 to 150,000
J at initiation load NUREG/CR-3464), in-lb/in^2	---	1,650	7,700
J at initiation load (NRC-NRR's method), in-lb/in^2	--- to 64,000	3,800 to ---	16,000 to 12,500
Finite element analysis (on pipe geometry), in-lb/in^2	---	6,700	---
J at initiation (from laboratory bend bar specimens), in-lb/in^2	2,856	4,000 to 6,000	12,400
	3,435		12,390
	2,577		14,100
Average	2,956		13,000

TABLE 4. EQUATIONS USED

Tension

$$J_t = f_1^t(a_e, \frac{R}{t})\,\frac{P^2}{E} + \alpha\,\sigma_o\,\varepsilon_o\,C(\frac{a}{b})\,h_1^t\,(\frac{a}{b}, n, \frac{R}{t})\,(\frac{P}{P_o})^{n+1}$$

$$f_1^t(\frac{a}{b}, \frac{R}{t}) = \frac{a\,F_t^2(\frac{a}{b}, \frac{R}{t})}{4\,\pi R^2 t^2}\;;\; P_o = 2\,\sigma_o\,Rt\,(\pi-\theta - 2\sin^{-1}(\tfrac{1}{2}\sin\theta))$$

$$K_t = \sigma^\infty \sqrt{\pi a}\,F_t(\frac{a}{b}, \frac{R}{t})$$

$$\sigma^\infty = \frac{P}{2\pi Rt}$$

Bending

$$J_b = f_1^b(a_e, \frac{R}{t})\,\frac{M^2}{E} + \alpha\,\sigma_o\,\varepsilon_o\,C\,h_1^b\,(\frac{a}{b}, n, \frac{R}{t})\,(\frac{M}{M_o})^{n+1}$$

$$f_1^b\,(\frac{a}{b}, \frac{R}{t}) = \pi\,\alpha(\frac{R}{I})^2\,F_b^2\,(\frac{a}{b}, \frac{R}{t})\;;\; M_o = 4\,\sigma_o R^2 t\,(\cos\tfrac{\theta}{2} - \tfrac{1}{2}\sin\theta)$$

$$K_b = \sigma\sqrt{\pi a}\,F_b\,(\frac{a}{b}, \frac{R}{t})$$

$$\sigma = \frac{MR}{I}$$

with
$a = R\,\theta$
$b = \pi R$
$c = b-a$

TABLE 5. INTERMEDIATE RESULTS AT INITIATION FOR CRACK IN BASE METAL

$F_t = 1.554$

$K_t = 61,538$

$J_e = 126$

$h_{1t} = 3.72$

$J_p = 1,305$

$F_b = 1.41$

$h_{1b} = 1.12$

$M_o = 1,929,000$

$$K_{eq} = \frac{M_{eq}}{\pi R^2 t} \sqrt{\pi a}\, F_b = 61,588$$

$J_e = 126$

$J_p = 888$

For M = 577,433 $K_{eq} = 95,838$ $J_e = 306$ $J_p = 4,167$

TABLE 6. SUMMARY OF RESULTS: INSTABILITY AT MAXIMUM LOAD FOR CRACK IN BASE METAL

$J_{mat} \rightarrow J(M_{eq}) \rightarrow J(M, P)$	
At Crack Initiation	At Maximum Load
J_{mat} (lb/in) 4494	13,947
Δa (in)	0.5
M_{eq} (in-lb) 1,601,865	2,080,078
M (in-lb) 559,862	1,025,032

A J-INTEGRAL ANALYSIS OF A CIRCUMFERENTIALLY CRACKED PIPE SUBJECTED TO BENDING LOADS

- by -

R. Packeiser, W. Brocks, D. Aurich*

BASIS OF THE APPROACH

For the calculation of the J-integral (applied values) in the presence of large scale yielding the modified Dugdale solution has been used[1].

$$J = \beta \cdot G \cdot \frac{8}{\pi^2} \left(\frac{\sigma_K}{\sigma}\right)^2 \cdot \ln \sec \left(\frac{\pi}{2} \cdot \frac{\sigma}{\sigma_K}\right) \qquad (1)$$

where

$$\left.\begin{aligned} G &= \frac{K^2}{E} \\ \beta &= 1.2 \end{aligned}\right\} \text{ plane stress (thin wall pipe)}$$

For a pipe, which is subjected to axial force and bending moment at the same time, the stress intensity factor is obtained by superposition of the tension and bending factors[2]:

$$K = K_t + K_b \qquad (2)$$

with

$$K_t = \sigma_t \sqrt{\pi \cdot R \cdot \theta} \cdot F_t(\theta) \qquad (3)$$

$$K_b = \sigma_b \sqrt{\pi \cdot R \cdot \theta} \cdot F_b(\theta) \qquad (4)$$

The functions $F_t(\theta)$ and $F_b(\theta)$ are given by the approximate formulas[2] for

*Bundesanstalt Fur Materialprufung, Berlin

$R/t = 10$ and $0 < \theta < 100^0$

$$F_t = 1 + 7.5(\frac{\theta}{\pi})^{3/2} - 15(\frac{\theta}{\pi})^{5/2} + 33(\frac{\theta}{\pi})^{7/2} \quad (5)$$

$$F_b = 1 + 6.8(\frac{\theta}{\pi})^{3/2} - 13.6(\frac{\theta}{\pi})^{5/2} + 20(\frac{\theta}{\pi})^{7/2} \quad (6)$$

For the presented problems these factors should overestimate F and therefore be conservative.

The nominal stress due to bending is defined by

$$\sigma_b = \frac{M}{\pi \cdot R^2 \cdot t} \quad (7)$$

The limit bending moment is given by[3]

$$M_p = 4 \cdot \sigma_f \cdot R^2 \cdot t \, (\cos \frac{\theta}{2} - \frac{1}{2} \cdot \sin \theta) \quad (8)$$

and

$$\frac{\sigma}{\sigma_F} = \frac{M}{M_p} \quad (9)$$

CALCULATIONS

The flow stress (303 MPa) was chosen as the arithmetic mean of the engineering yield stress (171 MPa) and the engineering ultimate stress 435 MPa). For the estimation of the engineering ultimate stress the engineering stress strain curve was calculated from the true stress strain curve (Figure 1). The value of initiation toughness J_i was defined in two different ways:

1. Curve fitting and extrapolation to zero crack extension:

   $J_i = 537$ N/mm

2. $J_i = J_{Ic} = 788$ N/mm

The applied J-value as a function of bending moment (Figure 2) was calculated by using Equations 1 to 4. The applied bending moments at crack

initiation and at load controlled instability (Table 1) were then obtained by using the crack driving force diagram technique (Figure 3). The predicted bending moment ratio at instability is $M_{max}/M_p = 0.99$, so that the pipe will fail, when the collapse moment has nearly been reached.

REFERENCES

1. Developments in Fracture Mechanics, edited by G.G. Chell, Applied Science Publishers Ltd. 1979 (London).

2. Tada, N., In: "The Application of Fracture Proof Design Methods Using Tearing Instability Theory to Nuclear Piping Postulation Circumferential Through Wall Cracks" NUREG/OR-3454, Sect. II-1, p. 71/81.

3. Tada, H., F. Paris, Zn: "The Application of Fracture Proof Design Methods Using Tearing Instability Theory to Nuclear Piping Postulation Circumferential Through Wall Cracks" NUREG/OR-3461, Sect. II-2, p. 82/136.

M_i $\Delta a = 0$ kNm	M_i $J_i = J_{Ic}$ kNm	M_{max} kNm	$\frac{M_{max}}{M_p}$	$\Delta\theta$ rad
310	347	374	0.99	0.025

TABLE 1. BENDING MOMENTS AT INITIATION AND INSTABILITY

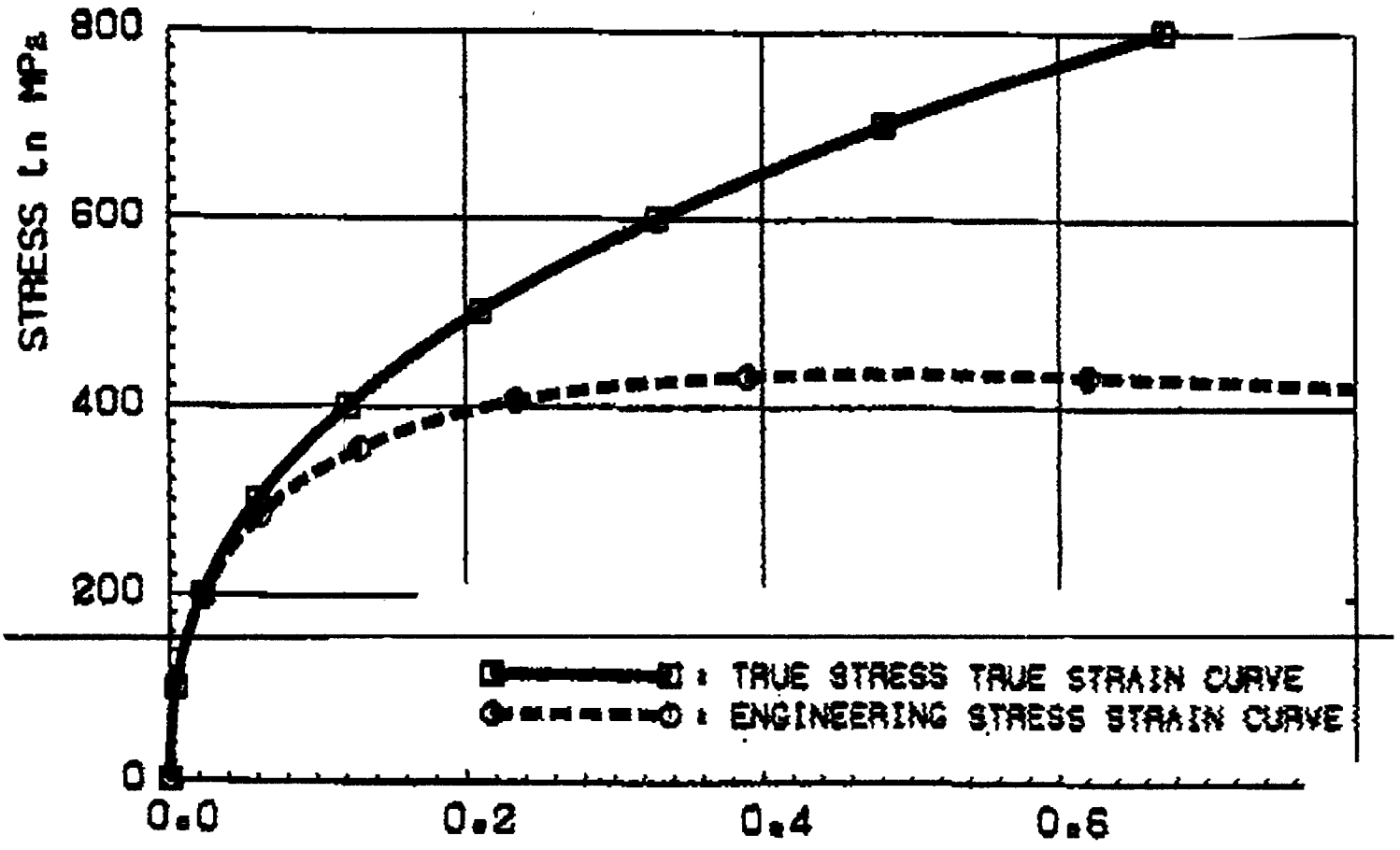

FIGURE 1. STRESS-STRAIN CURVES

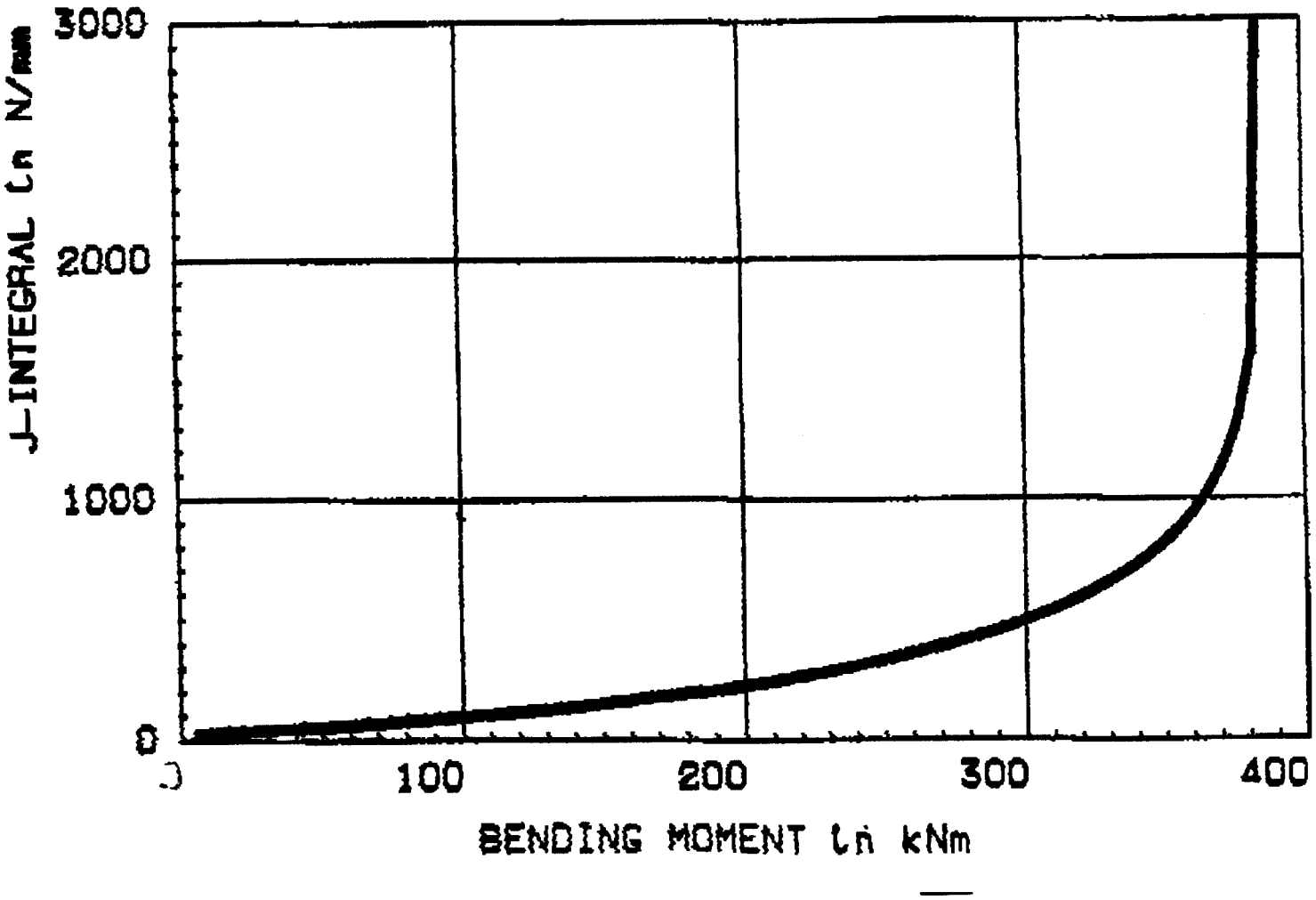

FIGURE 2. J-INTEGRAL VS BENDING MOMENT

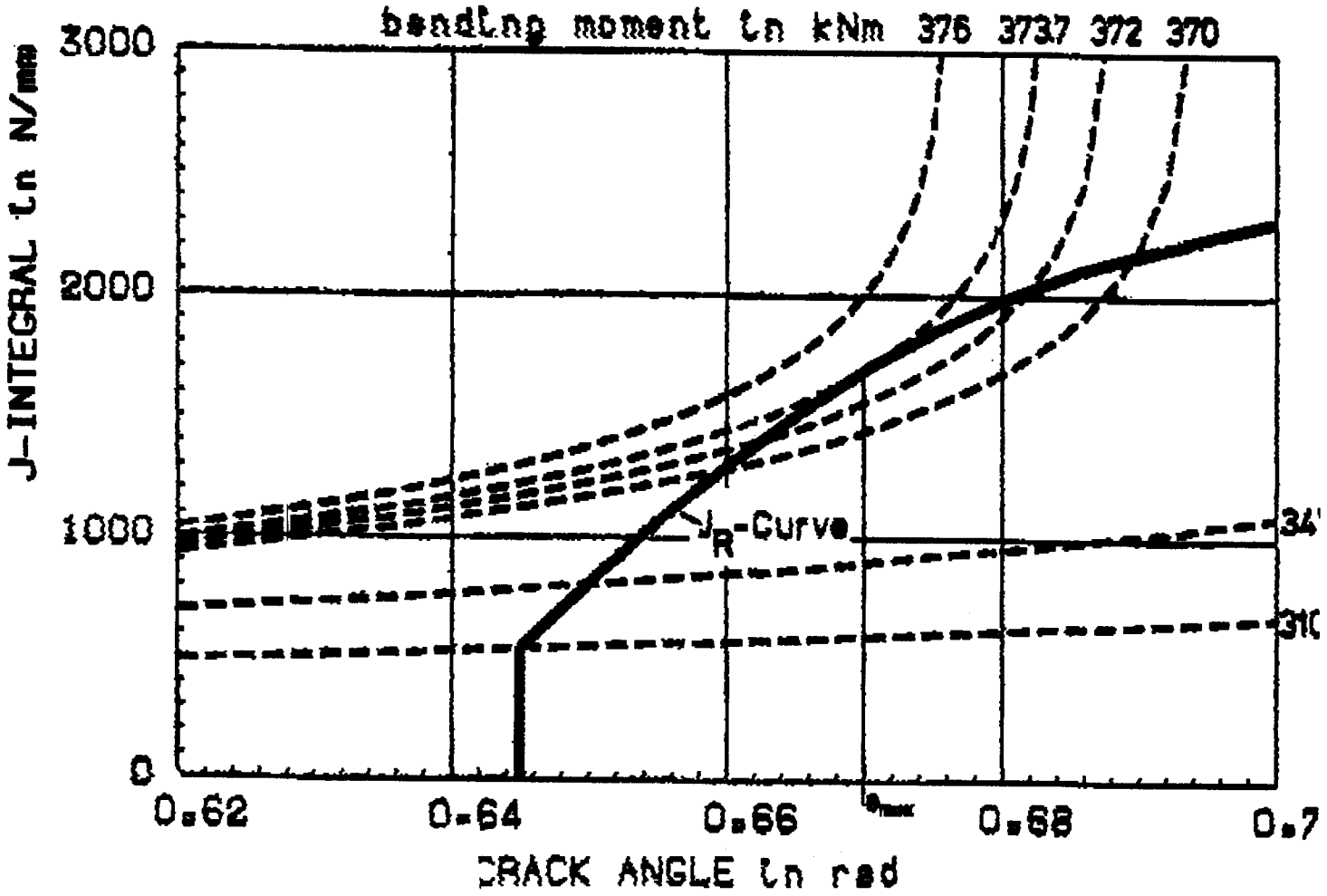

FIGURE 3. CRACK DRIVING FORCE DIAGRAM

CLOSED FORM EXPRESSIONS FOR FRACTURE MECHANICS ANALYSIS OF CRACKED PIPES

-by -

Akram Zahoor*

ABSTRACT

Closed form stress intensity factor (K_I) expressions are presented for cracks in pipes subjected to a variety of loading conditions. The loadings considered are: i) axial tension, (ii) remotely applied bending moment, and (iii) internal pressure. Expressions are presented for circumferential and axial cracks, and include both part-through and throughcrack geometries. The closed form K_I expressions are valid for pipe radius to wall thickness ratio between 5 and 20. In addition, J and T expressions suitable for tearing instability analysis are presented for circumferential through cracks under combined tension and bending. This latter expression is valid for contained yielding applications.

INTRODUCTION

Accurate prediction of the behavior of cracked pipes requires that the pipe geometry be properly incorporated in any fracture mechanics analysis. Very often the predictive analyses make use of fracture mechanics solutions that are valid only for pipe radius to wall thickness ratio (R/t) of 10. While such a solution may be considered reasonable for applications where R/t < 10, non-conservative predictions result if it is applied for cracked pipes having R/t appreciably greater than 10.

Closed form stress intensity factor K_I expressions are developed for cracked pipes that include the pipe geometry effects using the recent work from Refs. 1 and 2. The closed form expressions are presented for: (1) circumferential through crack in a pipe under a) tension and b) bending, (2) full circumference internal part-through crack in a pipe under axial tension,

*NOVETECH Corp.

(3) circumferential through crack in a pipe subjected to internal pressure, and (4) long axial internal part through crack in a pipe subjected to internal pressure. With the exception of the through crack under pressure loading case, all expressions are valid for pipe R/t between 5 and 20.

CIRCUMFERENTIAL THROUGH CRACK

K_I expressions for this crack geometry were developed from the work in Ref. 1. Let R and t be the pipe mean radius and wall thickness. Defining a quantity A that depends only on the pipe geometry,

$$A = \{0.125(R/t) - 0.25\}^{0.25} \quad \text{for } 5 \leq R/t \leq 10$$

and

$$A = \{0.4(R/t) - 3.0\}^{0.25} \quad \text{for } 10 < R/t \leq 20.$$

With this definition, the K_I for remotely applied axial load, P, may be expressed by

$$K_I = \sigma_t \sqrt{\pi R\theta}\, F_t(R/t, \theta/\pi)$$

where

$\sigma_t = P/2\pi Rt$

$R\theta$ = crack half-length

$F_t = 1 + A\,\{5.3303(\theta/\pi)^{1.5} + 18.773(\theta/\pi)^{4.24}\}$.

Similarly, K_I for remotely applied bending moment, M, may be expressed by

$$K_I = \sigma_b \sqrt{\pi R\theta}\, F_b(R/t, \theta/\pi)$$

where

$$\sigma_b = M/\pi R^2 t,$$

$$F_b = 1 + A\{4.5967(\theta/\pi)^{1.5} + 2.6422(\theta/\pi)^{4.24}\}.$$

The above expressions are recommended for use between $0 < \theta/\pi < 0.55$ K_I for the tension and bending cases are slightly conservative than the solutions in Ref. 1. These expressions have better than 2 percent accuracy for expressions for R/t = 10 as compared to those in Ref. 1. The stress intensity factor expression for R/t close to 5 give slightly conservative values (up to 4%) as compared to those in Ref. 1. The results for R/t between 15 and 20 are estimated to be conservative by as much as 10 percent for large crack lengths.

FULL CIRCUMFERENCE INTERNAL PART-THROUGH CRACK

The closed form expression for this crack geometry and remotely applied axial load was developed from the solutions based on finite element analyses that are reported in Ref. 2. The K_I may be conveniently expressed as

$$K_I = \sigma_t \sqrt{\pi a}\, F(R_i/t, a/t)$$

where

a = crack depth,

t = pipe wall thickness,

R_1 = pipe inner radius,

P = Axial load,

$\sigma_t = P/2\pi Rt$,

$F = 1.1 + A\{1.948(a/t)^{1.5} + 0.3342(a/t)^{4.2}\}$.

In the above, A is given by the same expression as for the circumferential through crack where now R/t is replaced by Ri/t. The above expression gives K_I values having better than 2 percent accuracy.

CIRCUMFERENTIAL THROUGH CRACK, INTERNAL PRESSURE

The K_I solution for the circumferential through crack in a pipe subjected to internal pressure was taken from Ref. 3 and curve fitted for convenience.

$$K_I = \sigma_m \sqrt{\pi R\theta}\ F_m(\lambda)$$

where

$\lambda = \theta\ R/t$

$F_m = 1 + 0.1501\lambda^{3/2}$ for $\lambda \leq 2$

$F_m = 0.8875 + 0.2625\lambda$ for $2 \leq \lambda \leq 5$

θ = crack half-angle

R = pipe mean radius

t = pipe wall thickness.

σ_m is the membrane stress in the axial direction. The pressure loading K_I expression is estimated to have better than 1 percent accuracy for $R/t = 10$.

LONG AXIAL PART-THROUGH CRACK

The finite element based K_I solutions for internal part-through crack in a pipe subjected to internal pressure are given in Ref. 2. These solutions are available for $a/t = 0.125$, 0.25, 0.5, and 0.75, and $R_i/t = 5$, 10, and 20, where a, R_i, and t are the crack depth, pipe inner radius and wall thickness, respectively. A simple closed form K_I expression, developed from these results, may be given by

$$K_I = \frac{2pR_o^2}{R_o 2 - R_i 2} \cdot \sqrt{\pi a} \cdot F(a/t, R_i/t)$$

where

$$A = \{0.125(R_i/t) - 0.25\}^{0.25} \text{ for } 5 \leq R_i/t \leq 10,$$

$$A = \{0.2(R_i/t) - 1.0\}^{0.25} \text{ for } 10 < R_i/t \leq 20,$$

$$F = 1.1 + A\{4.951(a/t)^2 + 1.092(a/t)^4\}$$

R_o = pipe outer radius

P = internal pressure

The above expression is accurate within ± 3 percent for R_i/t between 5 and 20 and a/t between 0 and 0.75; slightly conservative results are obtained for R_i/t near 20.

APPLIED TEARING MODULUS FOR CIRCUMFERENTIAL THROUGH-WALL CRACKS UNDER COMBINED TENSION AND BENDING

The total stress intensity factor for combined tension and bending is given by

$$K_I \text{ (total)} = K_I\text{(tension)} + K_I\text{(bending)}$$

Under linear elastic conditions, the J integral is related to K_I by

$$J = K_I^2/E'.$$

Using the formulas given in Section 2, the applied J may be expressed as {4}.

$$\frac{JE'}{\sigma_b^2 \pi^2 R} = (\theta/\pi)\{F_b + (\sigma_t/\sigma_b)F_t\}^2$$

Next, the applied tearing modulus expressions are summarized for load control and displacement controlled loadings {4,5}.

Applied T for Load Controlled Loading, LEFM Solution

$$J/T = \left(\frac{\sigma_f^2}{E}\right) \pi R\,(\theta/\pi)\ \frac{1+(\sigma_b/\sigma_t)\cdot(F_b/F_t)}{1+F_3/F_t+(\sigma_b/\sigma_t)\cdot(F_b/F_t)\cdot(1+F_4/F_b)}$$

where

$$F_3 = 2A\,[7.9955(\theta/\pi)^{1.5} + 79.598(\theta/\pi)^{4.24}]$$

$$F_4 = 2A\,[6.8951(\theta/\pi)^{1.5} + 11.203(\theta/\pi)^{4.24}]$$

Applied T for Displacement Controlled Loading, Predominantly Bend Loading, LEFM Solution

$$T = -\frac{2M^2(1-\nu^2)}{\pi R^4 t^2 \sigma_f^2} \cdot (\theta/\pi)F_b \frac{(H_1' + H_2'PR/2M)\ (F_b + F_b'PR/2M)}{\left(H_1 + \frac{L}{(1-\nu^2)R}\right)}$$

$$+ \frac{JE}{R\theta\sigma_f^2}\ 1 + \frac{2(\theta/\pi)\cdot(F_b'+F_t'PR/2M)}{F_b+F_tPR/2M}$$

where

$$F_t' = A\,[7.9955(\theta/\pi)^{0.5} + 79.598(\theta/\pi)^{3.24}]$$

$$F_b' = A\,[6/8951(\theta/\pi)^{0.5} + 11.203(\theta/\pi)^{3.24}]$$

$$H_1 = 19.739(\theta/\pi)^2 + 103.7A(\theta/\pi)^{3.5} + 166.83A^2(\theta/\pi)^5 + 33.433A(\theta/\pi)^{6.24} + 123.90A^2(\theta/\pi)^{7.74} + 26.298A^2(\theta/\pi)^{10.48}$$

$$H_1' = 39.478(\theta/\pi) + 362.95A(\theta/\pi)^{2.5} + 834.15A^2(\theta/\pi)^4 + 208.62A(\theta/\pi)^{5.24} + 958.99A^2(\theta/\pi)^{6.74} + 275.6A^2(\theta/\pi)^{9.48}$$

$$H_2' = 39.478(\theta/\pi) + 391.9A(\theta/\pi)^{2.5}\ 967.3A^2(\theta/\pi)^4 + 845.46A(\theta/\pi)^{5.24} + 3962.73A^2(\theta/\pi)^{6.74} + 1958.2A^2(\theta/\pi)^{9.48}$$

APPLICATION TO SMALL SCALE YIELDING

Replace θ by θ_{eff} as defined below

$$\theta_{eff}/\pi = \theta/\pi + (\sigma_b/\sigma_f)^2 \cdot (JE'/\beta\pi^2 R\sigma_b^2)$$

$\beta = 2$ for plane stress

$\beta = 6$ for plane strain

Let

$$T_p = T \text{ computed using } \theta = \theta_{eff}$$

The applied tearing modulus for small scale yielding is then calculated from

$$T = T_p/(1-T_p/\beta\pi)$$

By the nature of approximation, small scale yielding solutions are valid as long as T_p is less than $\beta\pi$.

REFERENCES

1. Sanders, J.L., Jr., "Circumferential Through-Crack in a Cylindrical Shell Under Combined Bending and Tension," ASME J. of Applied Mechanics, Vol. 50, No. 1, 1983, p. 221.

2. Kumar, V., German, M.D., and Shih, C.F., "An Engineering Approach for Elastic Plastic Fracture Analysis," EPRI Report NP-1931, July 1981.

3. Rooke, D.P., Cartwright, J.C., "Compendium of Stress Intensity Factors," Her Majesty's Stationary Office, London, 1976.

4. Zahoor, A., Progress Reports on EPRI RP 2457-1, "Flaw Evaluation in Ferritic Piping," by Impell Corporation, 1983-84.

5. Zahoor, A., and Kanninen, M.F., "A Plastic Fracture Mechanics Prediction of Fracture Instability in a Circumferentially Cracked Pipe in Bending - Part I: J-Integral Analysis," ASME J. of Pressure Vessel Technology, November 1981, pp 352-358.

ACKNOWLEDGEMENT

The work presented herein was supported by the Electric Power Research Institute on Project RP 2457-1, "Flaw Evaluation in Ferritic Piping". The author wishes to thank Dr. Douglas M. Norris for support and encouragement on this project.

ELASTIC-PLASTIC FINITE ELEMENT ANALYSES OF CIRCUMFERENTIALLY CRACKED PIPE GEOMETRIES

- by -

J.W. Cardinal, E.Z. Polch, P.K. Nair, and M.F. Kanninen*

INTRODUCTION

Detailed elastic-plastic finite element fracture mechanics analyses were conducted for the evaluation of the workshop problem. The purpose of these analyses was to provide reasonable benchmark solutions to help assess the various approximate elastic-plastic analyses presented at the CSNI meeting. Calculations were performed to analyze (1) the monolithic base metal pipe, and (2) the welded pipe treated as a composite of base metal and weldment. In the latter, each constituent was assigned distinct mechanical and fracture properties. In both solutions applied J values were calculated for a constant axial load and increasing values of applied bending moment. The material J-resistance curves were used to initiate and grow the initial crack in a stable manner with fracture instability occurring under load control.

PROBLEM DEFINITION

The workshop problem consists of a 16-inch diameter stainless steel pipe containing a circumferential through-wall crack. The pipe is subjected to a constant axial stress of 10 ksi combined with monotonically increasing values of applied bending moment. The pipe section has a length of 70 feet and a circumferential crack geometry as shown in Figure 1. For the analysis of the case when the crack is located in the weld, the weld is assumed to be equal in width to the thickness of the pipe.

*Southwest Research Institute, San Antonio, Texas

The objectives of the analyses were to obtain the applied J values as a function of increasing bending moment and to determine the bending moments at crack initiation and at instability. The analyses were also to provide data on the pipe rotations as a function of bending load and the extent of crack growth at load-controlled instability.

The material stress-strain curves used in the analyses, shown in Figure 2, are for Type 304 stainless steel at an operating temperature of 550°F. The curve fit of the experimental data generated by Milne [1] was used to model the material behavior of the stainless steel monolithic pipe. True stress-true strain data for the base metal and weldment were also obtained from raw data supplied directly by McCabe [2]. McCabe's data were provided in the form of load versus diameter reduction. These data were transformed to true stress-true strain by converting the measured diametral strains to longitudinal strains. From Figure 2, it can be seen that the McCabe data and the curve fit Milne data for the base metal agree reasonably well. Hence, to facilitate comparisons between the two solutions, the welded pipe analysis employed the Milne base metal curve and the McCabe weldment data.

The input parameters used in the analyses are summarized in Table 1. Values for J_{Ic} were obtained from the material crack growth J-integral resistance curves given in Figure 3.

TABLE 1. ANALYSIS INPUT PARAMETERS

BASE METAL:	
Young's Modulus,	E = 31,250 ksi (Milne data)
Yield Stress,	σ_y = 25.0 ksi (Milne data)
Poisson's ratio,	ν = 0.3
Critical J value,	J_{Ic} = 4,500 in-lb/in (Figure 3)
WELDMENT:	
Young's Modulus	E = 29,940 ksi (McCabe data)
Yield Stress,	σ_y = 53.9 ksi (McCabe data)
Poisson's ratio,	ν = 0.3
Critical J value,	J_{Ic} = 2,000 in-lb/in (Figure 3)

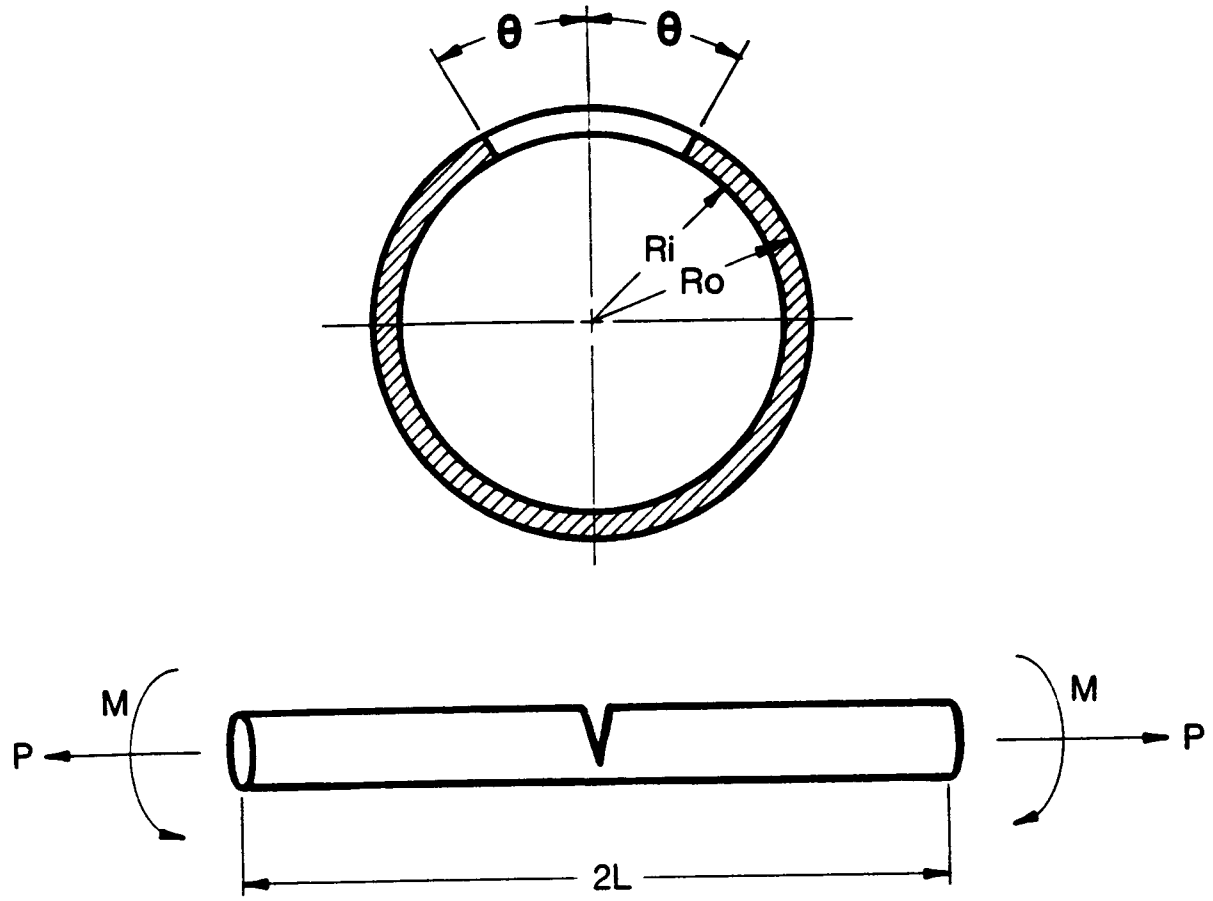

θ = 0.645 rad
Ri = 7.5 inches
Ro = 8.0 inches
L = 35 feet

FIGURE 1. CRACKED PIPE GEOMETRY AND LOADING

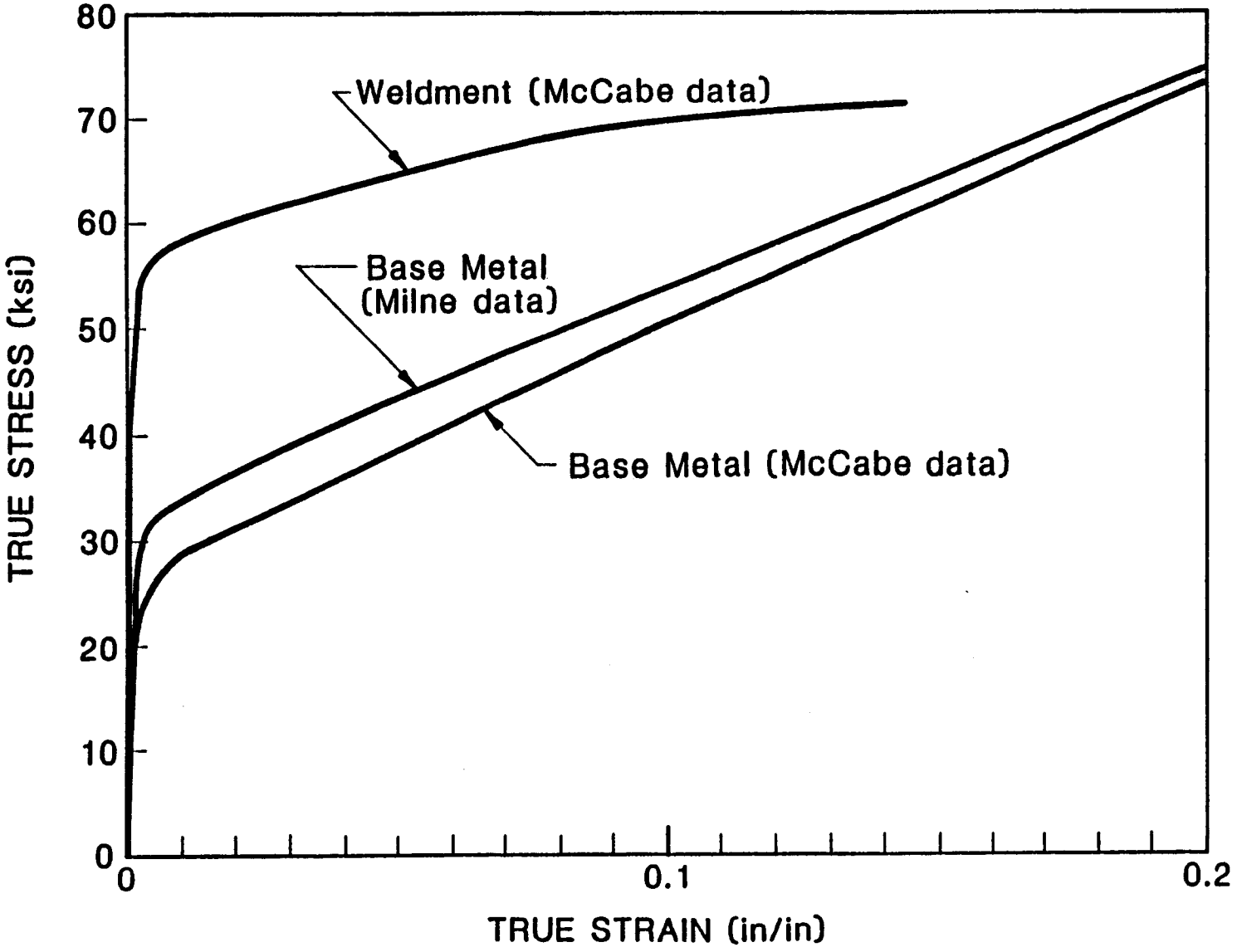

FIGURE 2. TYPE 304 STAINLESS STEEL AND WELDMEMT STRESS-STRAIN CURVES AT 550°F

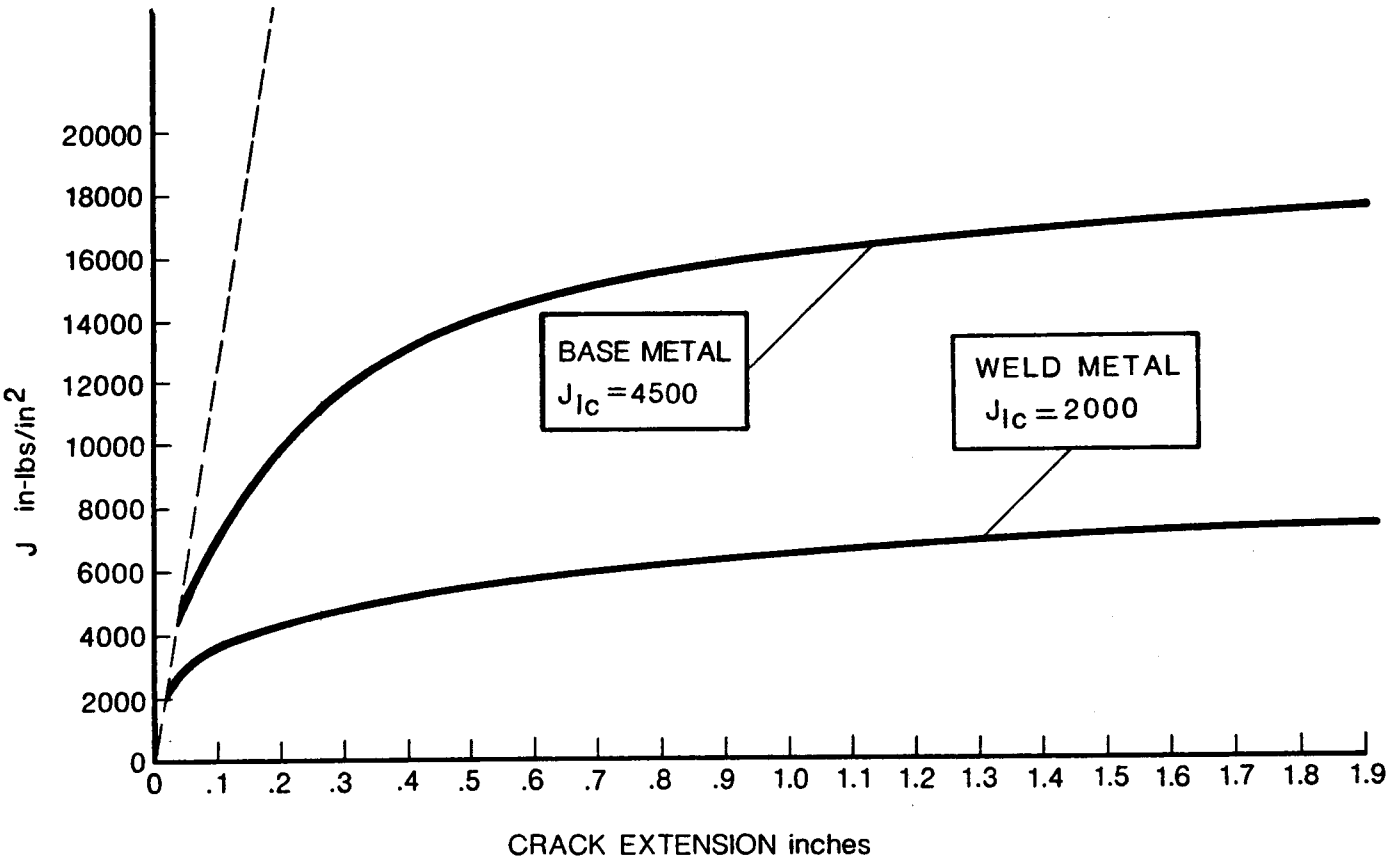

FIGURE 3. MATERIAL J-RESISTANCE CURVES

ANALYSIS PROCEDURE

The analyses were performed using an SwRI in-house finite element code: a modified version of ADINA [3] capable of calculating elastic and elastic-plastic energy release rates. Implementation of the energy release rate calculations into the ADINA code generally followed the virtual crack extension methodology originally introduced by Hellen [4,6] and Parks [5,7,8]. An analytical expression for the energy release rate more suitable for numerical analysis of general 3-dimensional crack configurations was subsequently derived by de Lorenzi [9] and is used in the SwRI version of the ADINA code.

Since the virtual crack extension method assumes small displacements and small strains, the ADINA calculations consider material nonlinearities only. Geometrical nonlinearities are not accounted for in the model behavior. The experimental stress-strain data for the base metal and the weldment were incorporated into the analyses using elastic-plastic material models with isotropic hardening. The von Mises yield criterion and flow rule were used.

The solution of the system of nonlinear equations is performed in ADINA using a modified Newton-Raphson method. However, it was necessary to manually implement a scheme similar to a full Newton-Raphson method subsequent to crack extension to account for unloading in the wake of the crack. This was done by manually specifying a number of stiffness reformations prior to each equilibrium iteration.

The pipe was modeled using eight-noded, isoparametric, three-dimensional solid elements with a 2x2x2 order of integration. One element was used through the thickness of the pipe.

In the analyses, the applied bending moment was increased until J_{Ic} was reached. Crack growth was then modeled by forcing the applied load and crack length to be such that the calculated J value matched the J resistance value for that amount of crack extension. This was accomplished by releasing the crack tip node under constant load, using a gradual reduction in force until the crack extended the length of one element. After this extension, the load was increased until the calculated J value reached the corresponding material value. This dictated a further increment of crack extension. This procedure was repeated until the applied J in the constant-load crack extension portion of the computation equalled or exceeded the material J resistance level for the longer crack. The crack length prior to the extension at which this occurred was taken as the load-controlled instability point.

Prior to the development of a detailed model of the cracked pipe, a coarse grid pipe model using the full symmetric half length of the pipe (420 inches) was studied. This coarse grid model contained 378 elements, each of which subtended a circumferential arc of the pipe ranging from 18 to 30 degrees. The objective was to determine the influence of the crack on the compliance of the pipe. Specifically, the minimum axial distance from the crack plane where plane sections remained plane under bending load was determined. For the coarse grid model given in Figure 4, it was found that linear bending deformations in the pipe were reasonably exhibited at a distance of 40 inches from the crack plane. For the development of the detailed cracked pipe model, a pipe with a symmetric half-length of 80 inches was chosen. This choice assured that the bending and axial loads applied remote to the crack would induce the proper bending deformation in the pipe.

Figure 5 presents the detailed finite element model of the pipe used in the solution of the workshop problem. This model contains 495 eight-noded solid elements and a total of 3085 active degrees of freedom. Modeling details near the crack tip are illustrated in the enlarged views of the model shown in Figures 6 and 7. For the welded pipe analysis, material properties corresponding to the McCabe weldment data are used for the elements extending around the pipe circumference within 0.5 inches of the crack plane. Elements at the crack tip and along the circumferential crack growth path have dimensions of 0.1 in. x 0.1 in. x 0.5 in., where the 0.5 inch dimension corresponds to the pipe wall thickness. At an axial distance of 3 inches from the crack tip, the geometry of the pipe is discretized such that each element subtends a circumferential arc of 10 degrees. Figure 5 shows the gradual transition in element size along the length of the pipe as the distance from the crack plane increases.

The J-integral was calculated by considering the contributions to the energy released by a virtual crack extension of all elements within a zone having a dimension of 12 inches in all directions from the crack tip. Thus, when interpreting the J results, it must be kept in mind that plastically deformed regions may exist outside of this zone. The choice of 12 inches for use in this problem was arrived at by preliminary test calculations, considerations of the pipe geometry, and acknowledgement of the fact that, outside this region, plastic strains were three to four orders of magnitude below those contained within this "radius of influence."

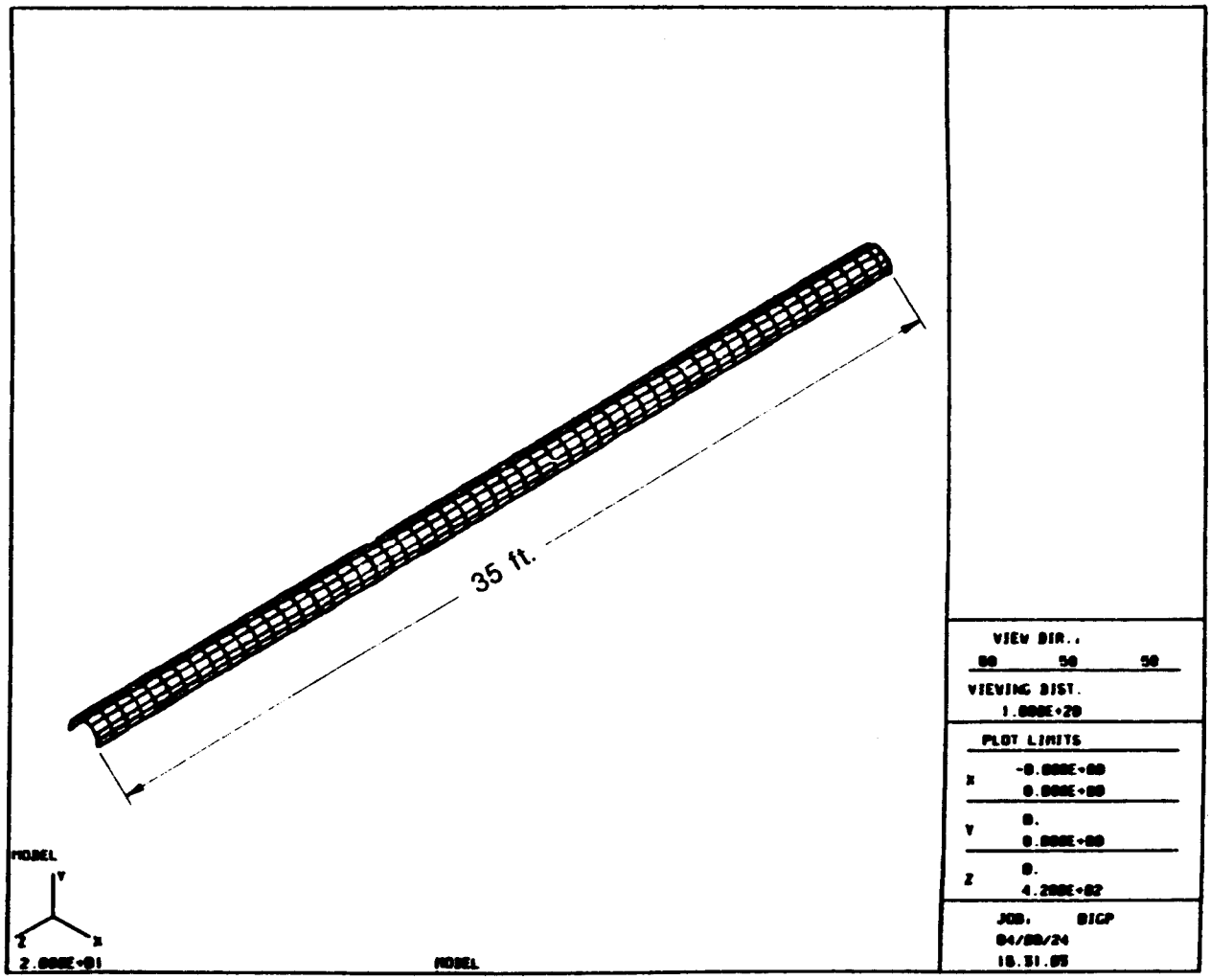

FIGURE 4. COARSE GRID FINITE ELEMENT MODEL OF CRACKED PIPE (L = 420 INCHES)

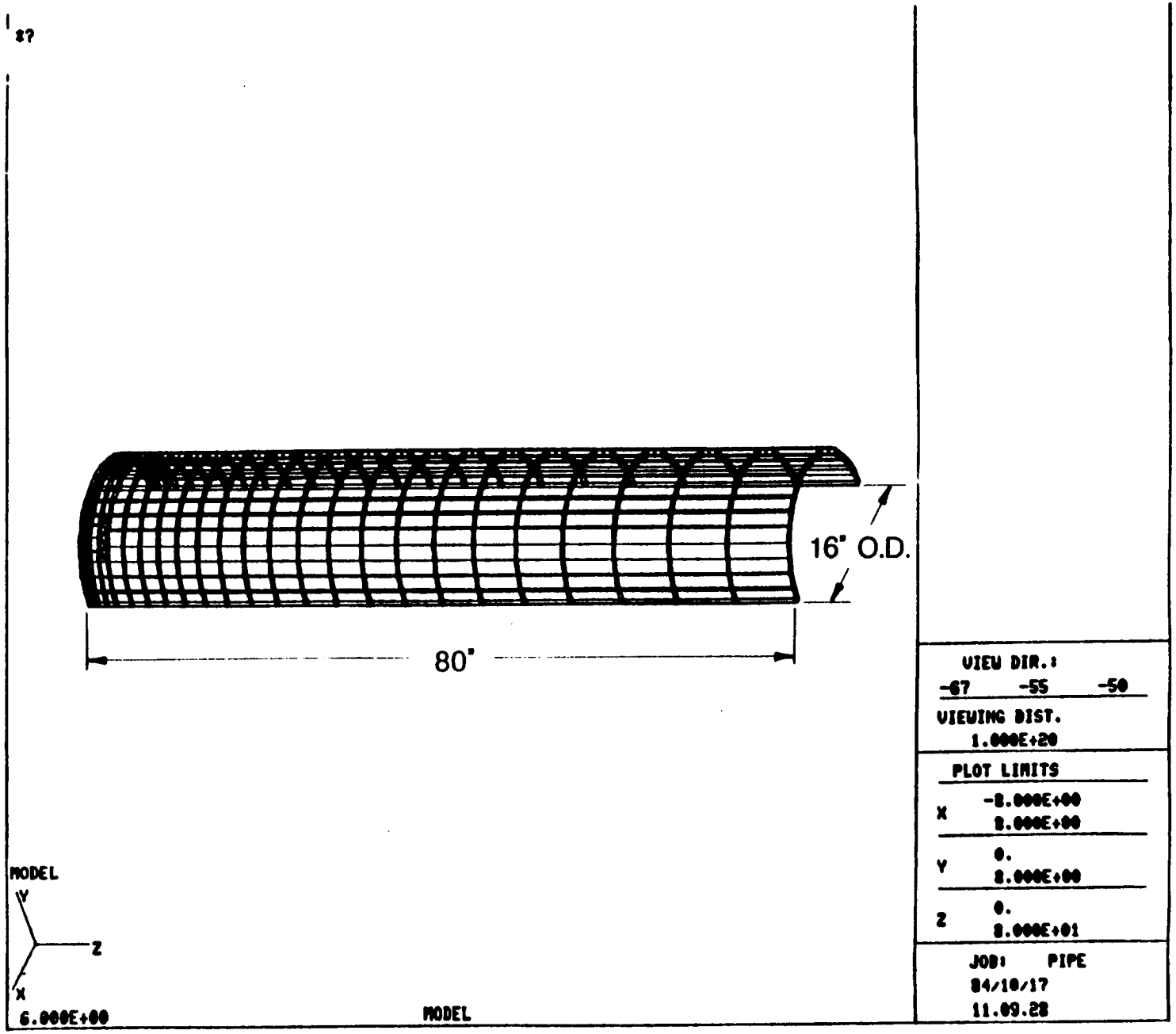

FIGURE 5. DETAILED FINITE ELEMENT MODEL OF THE CRACKED PIPE (L = 80 IN.)

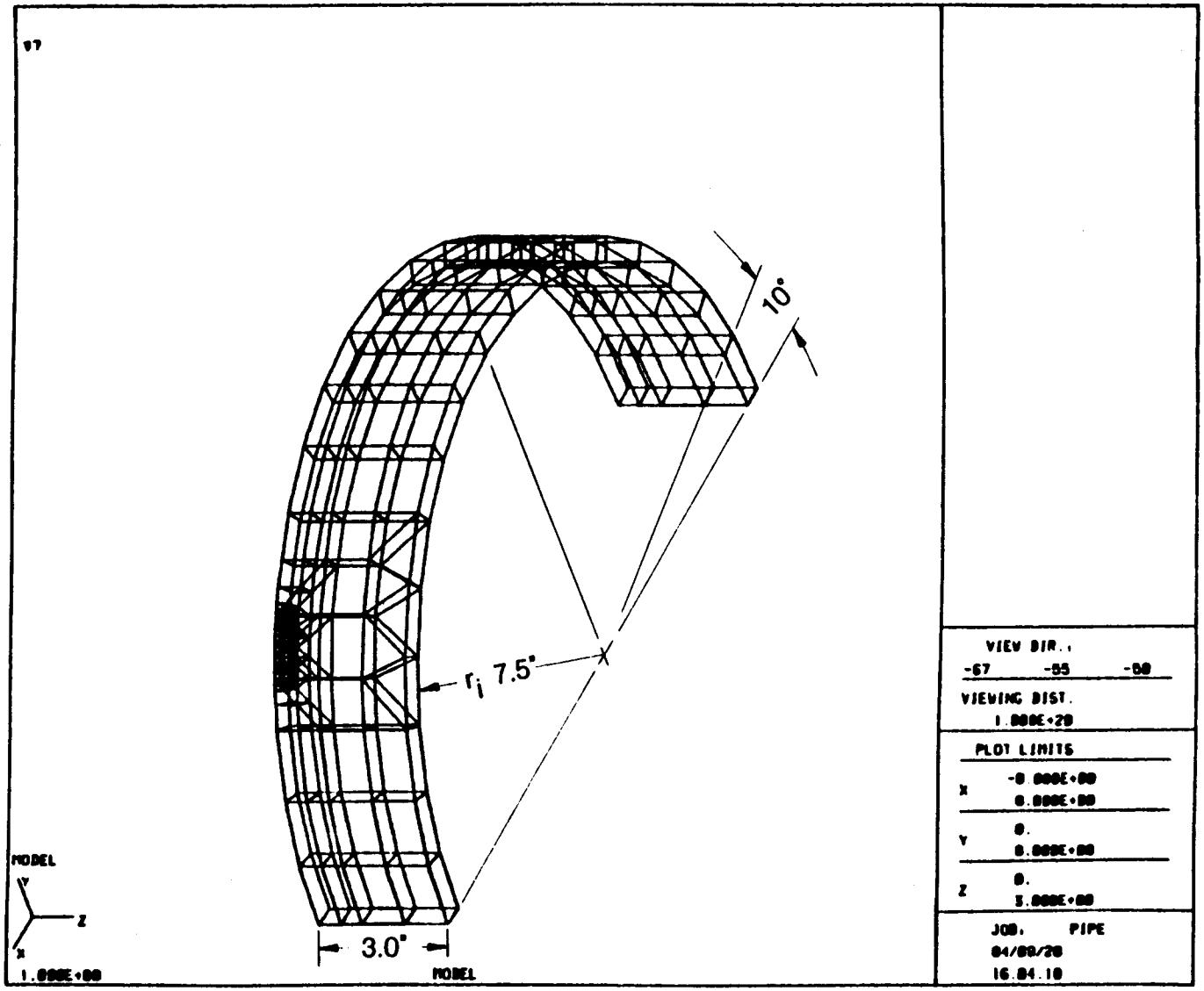

FIGURE 6. ENLARGEMENT OF DETAILED MODEL

COMPUTATIONAL RESULTS

For each analysis, the loads were applied to the model as remote axial and monotonically increasing bending stress distributions; i.e., the model was analyzed under load control. Since the problems were to be analyzed under a constant axial load of 10 ksi, this load component was applied first and thereafter remained unchanged as the bending moment was gradually increased. Table 2 summarizes the results obtained for the monolithic and welded pipe elastic-plastic finite element fracture analyses.

The results given in Table 2 show that crack initiation was calculated to occur at an applied bending moment of 2013 in-kips for the monolithic pipe and at 1578 in-kips for the welded pipe. The corresponding plastic zone distributions for each case at the respective crack initiation loads are given in Figures 8 and 9. Here the cylindrical pipe geometry is mapped into a rectangular plane surface for ease of viewing the plotted plastic zone areas. It can be seen that in each figure there is an extensive zone that has yielded in bending in the area remote from the crack tip. The presence of a compressive yield zone, indicated by the cross-hatched area, can also be seen in the monolithic pipe.

TABLE 2. SUMMARY OF ELASTIC-PLASTIC FINITE ELEMENT FRACTURE ANALYSIS RESULTS

	Monolithic Pipe Analysis	Welded Pipe Analysis
Initiation Moment (in-kips)	2013	1578
Rotation^{+} at Initiation (degrees)	0.46	0.26
Amount of Stable Crack Growth (in)	0.3	0.1
Instability Moment (in-kips)	2535	2013
Rotation^{+} at Instability (degrees)	1.02	0.41
Instability J (in-lb/in^2)	11792	3733

$^{+}$Note: Pipe rotation is calculated using the length of the detailed finite element model (80.0 inches).

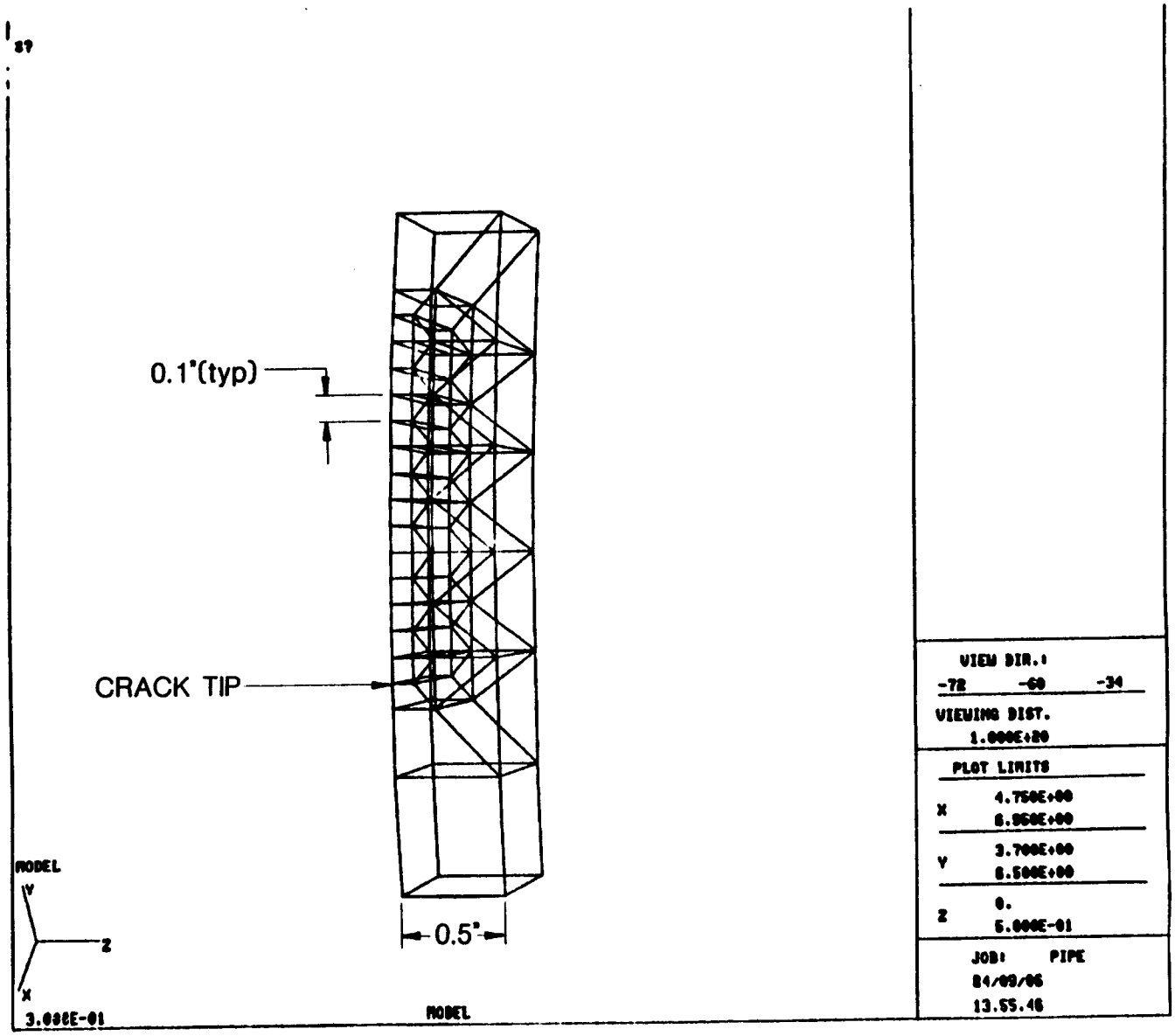

FIGURE 7. DETAILED MODEL AHEAD OF CRACK

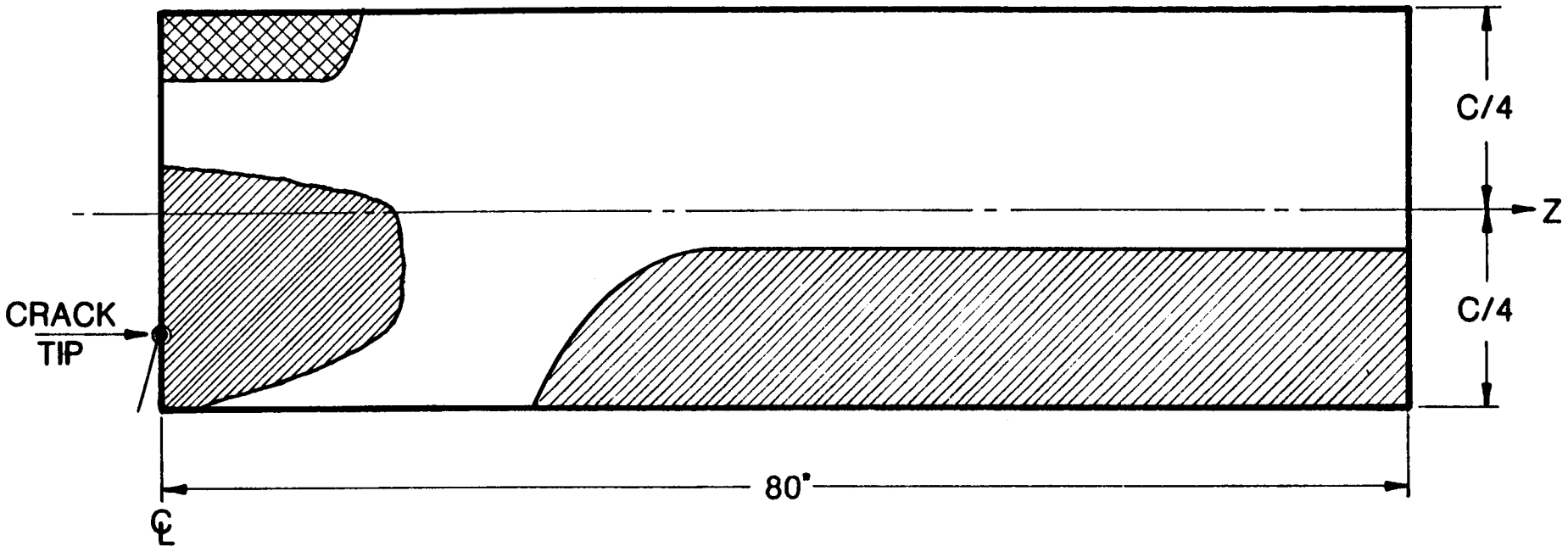

FIGURE 8. MONOLITHIC PIPE PLASTIC ZONE AT M = 2013 IN.-KIPS (INITIATION)

$J = 4500 \text{ in-lb/in}^2$

$\sigma_a = 10 \text{ ksi}$
$\sigma_b = 22 \text{ ksi}$
$\sigma_{max} = 32 \text{ ksi}$

$M = 2013 \text{ in-kips}$
INITIATION

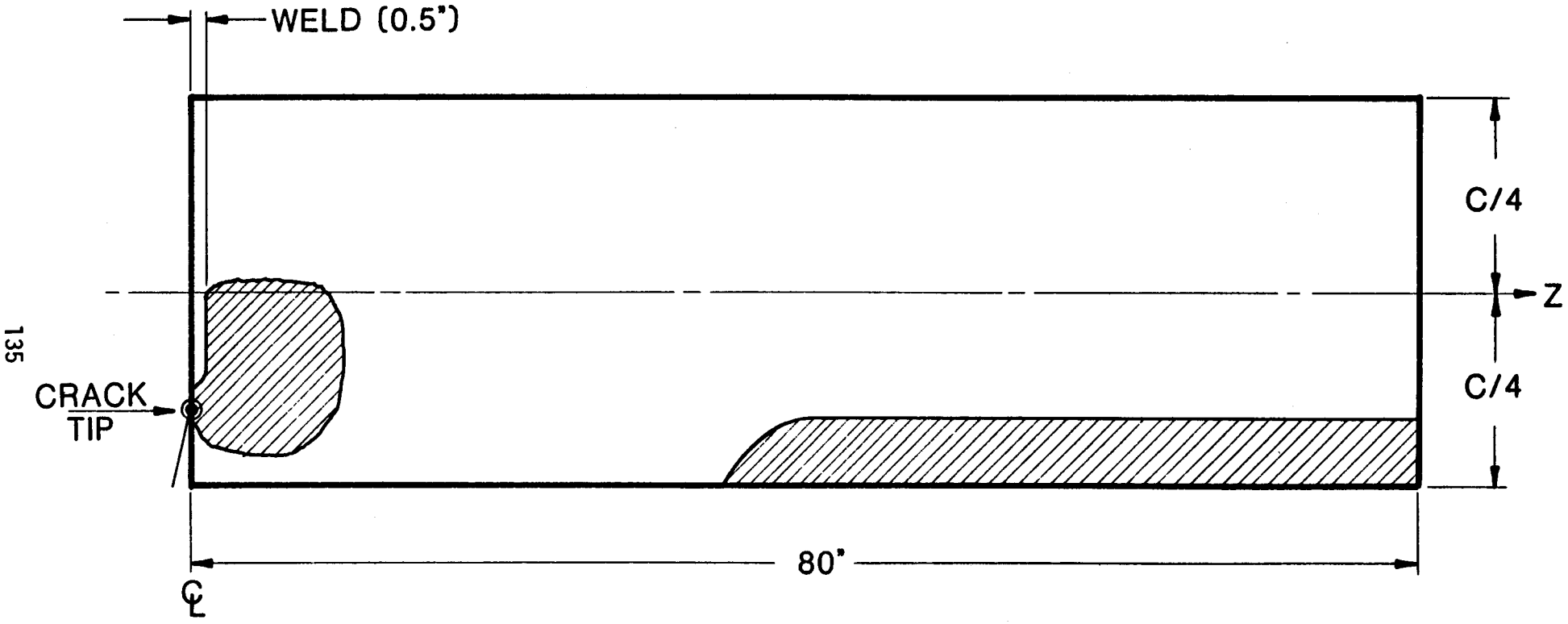

FIGURE 9. WELDED PIPE PLASTIC ZONE AT M = 1578 IN.-KIPS (INITIATION)

$J = 2000$ in-lb/in^2

$\sigma_a = 10.0$ksi
$\sigma_b = 17.25$ksi
$\sigma_{max} = 27.25$ksi

M = 1578in-kips
INITIATION

Once the initiation point was reached, the crack was extended 0.1 inch (the length of an element) under constant load. After crack extension for a length of 0.1 inch was complete, the bending moment was gradually increased until the magnitude of the calculated J required additional crack extension. This pattern of load increase, followed by crack extension under constant load, was repeated until the slope of the applied J curve at constant load was equal to or exceeded that of the material J-resistance curve. At this point, instability has occurred. This procedure is illustrated in Figure 10.

The applied J curves for each analysis are contrasted with the material J-resistance curves in Figure 10. In this figure, the vertical line segments result from increasing the applied bending moment while line segments representing crack growth occur under constant load. At instability, (indicated by the square symbols in the figure), it is seen that crack extension at constant load causes the slope of the applied J curve to be equal to that of the material J-resistance curve. Thus, instability has been reached since any further load increase would keep the applied J curve above the J-resistance curve.

Instability was calculated to take place at an applied bending moment of 2535 in-kips for the monolithic pipe and at 2013 in-kips for the welded pipe. Plastic zone distributions for each case at the respective instability loads are given in Figures 11 and 12. Net section plasticity has been achieved along the crack plane at the monolithic pipe instability condition. A small compressive zone appears at instability for the welded pipe and the yielded zones are much less widespread. In fact, by comparing Figures 8 and 12, it can be seen that, if the weldment area is neglected, the initiation plasticity distribution for the monolithic pipe corresponds almost exactly to the plastic zones present at instability for the welded pipe. This is not a suprising result since the bending moments for each of these conditions, by coincidence, are just equal (see Table 2). Similarly, Figures 9 and 12 indicate that only a very small area of weldment near the crack tip deforms plastically.

Applied J values plotted as a function of bending moment are given in Figures 13 and 14 for the monolithic and welded pipes, respectively. These figures show that the monolithic pipe can withstand an applied J value three times that of the welded pipe prior to reaching instability. The bending moment capacity of the monolithic pipe is calculated to be 25% greater than that of the welded pipe. Moment-rotation curves for each case are shown in Figures 15 and 16 indicating that the monolithic pipe rotates approximately 2.5 times as much as the welded pipe prior to instability.

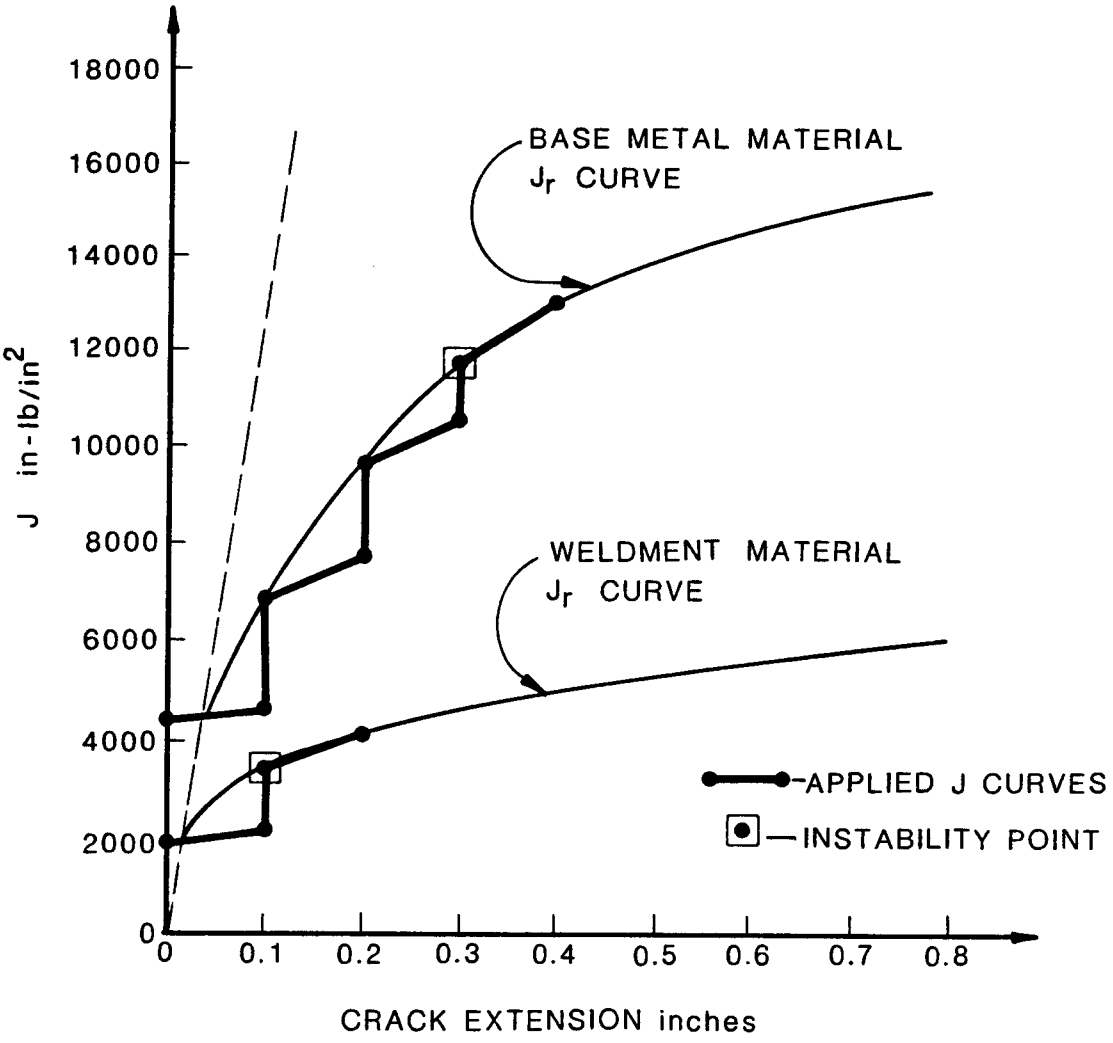

FIGURE 10. APPLIED J CURVES COMPARED WITH MATERIAL J-RESISTANCE CURVES FOR THE MONOLITHIC AND WELDED CRACKED PIPE ANALYSES

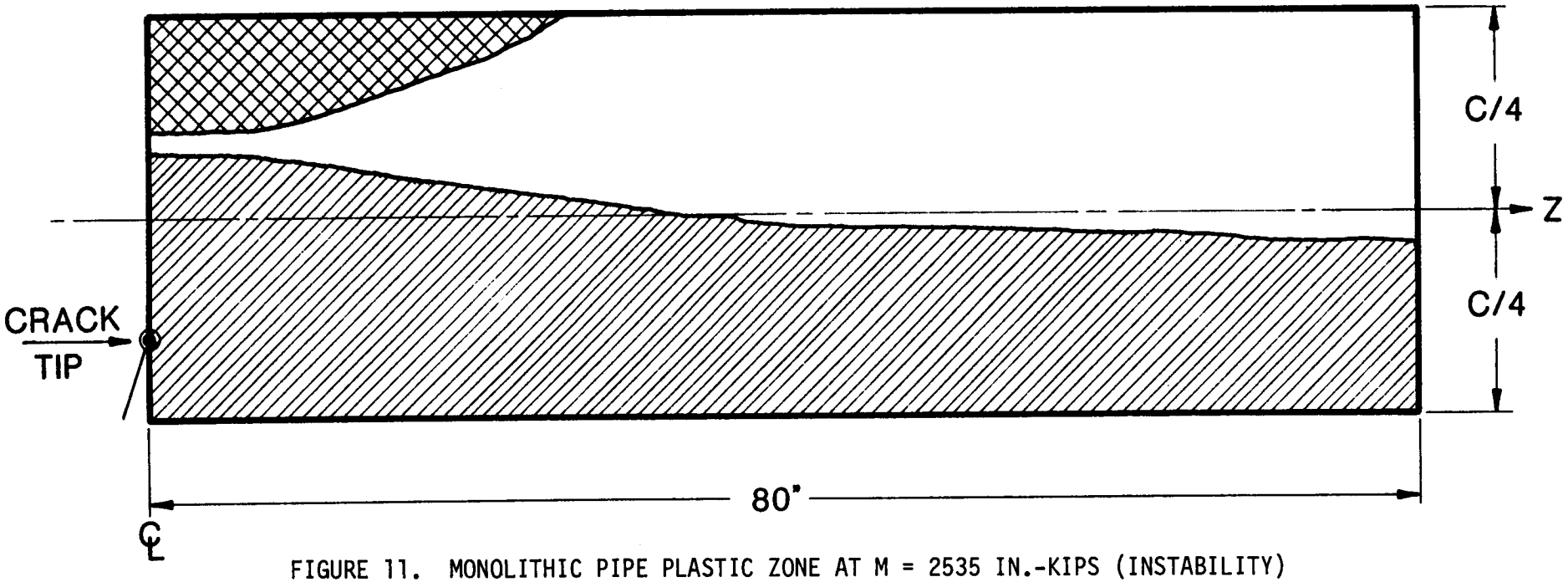

FIGURE 11. MONOLITHIC PIPE PLASTIC ZONE AT M = 2535 IN.-KIPS (INSTABILITY)

$J = 11792 \text{ in-lb/in}^2$

$\sigma_a = 10.0 \text{ ksi}$
$\sigma_b = 27.7 \text{ ksi}$
$\sigma_{max} = 37.7 \text{ ksi}$

$M = 2535 \text{ in-kips}$
INSTABILITY

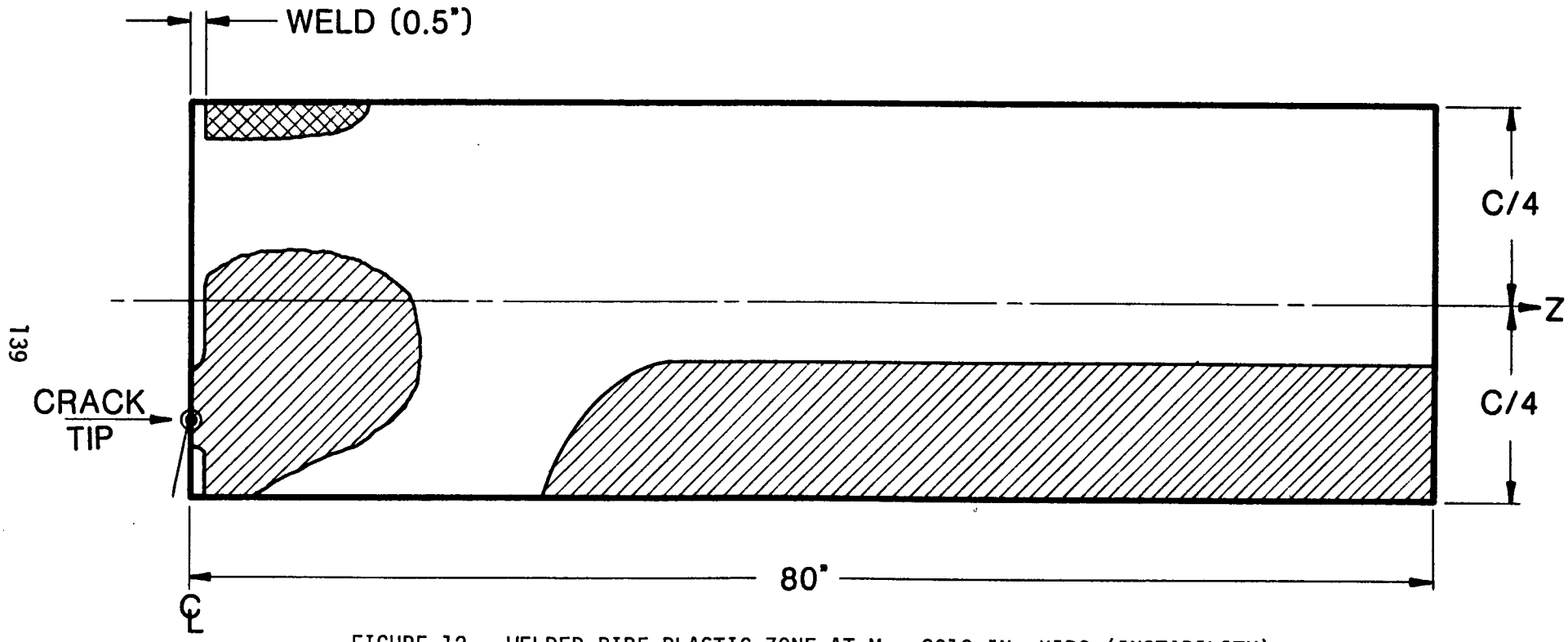

FIGURE 12. WELDED PIPE PLASTIC ZONE AT M = 2013 IN.-KIPS (INSTABILITY)

$J = 3733$ in-lb/in^2

$\sigma_a = 10$ksi
$\sigma_b = 22$ksi
$\sigma_{max} = 32$ksi

M = 2013in-kips
INSTABILITY

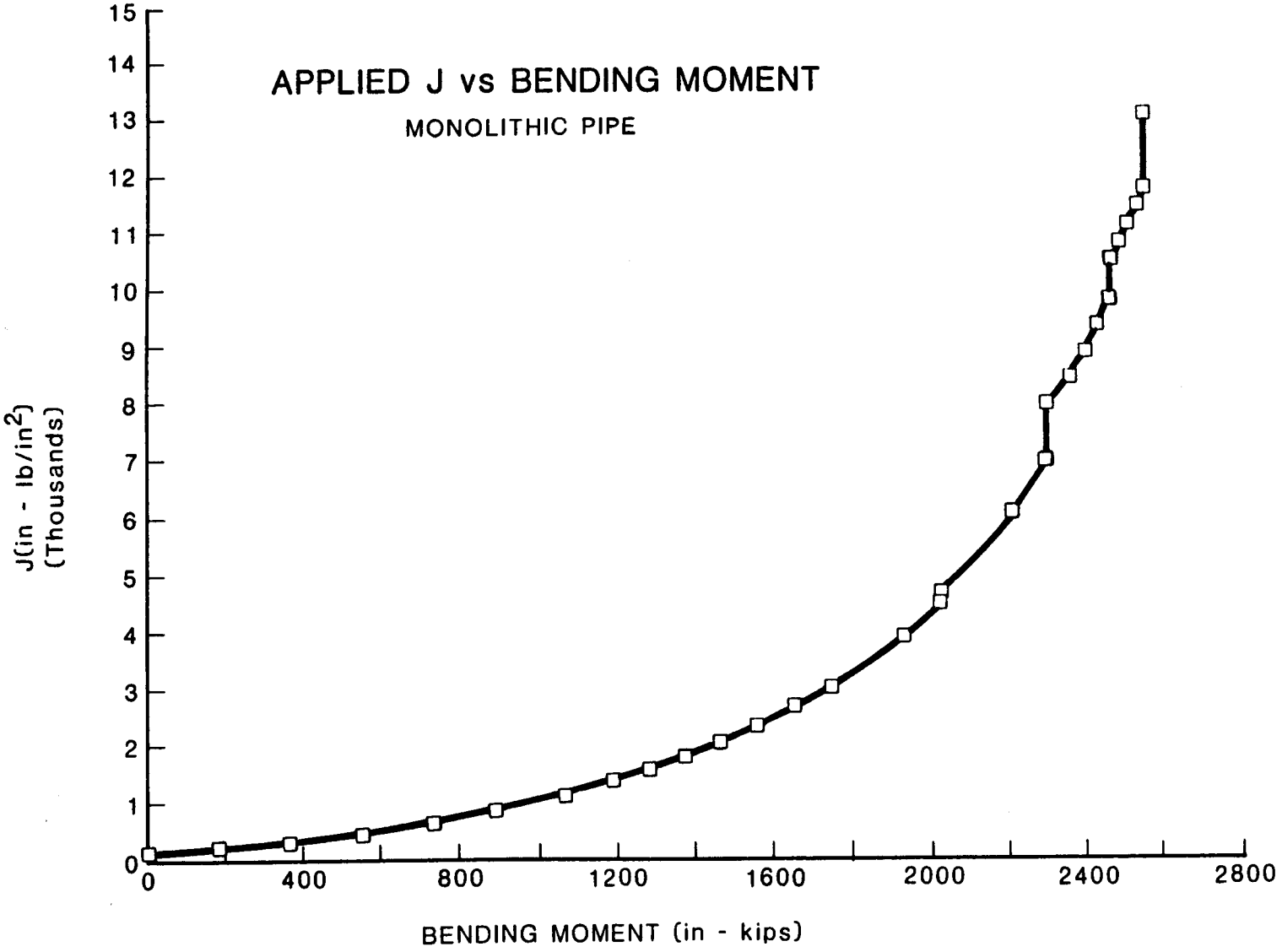

FIGURE 13. APPLIED J VS BENDING MOMENT FOR THE MONOLITHIC CRACKED PIPE

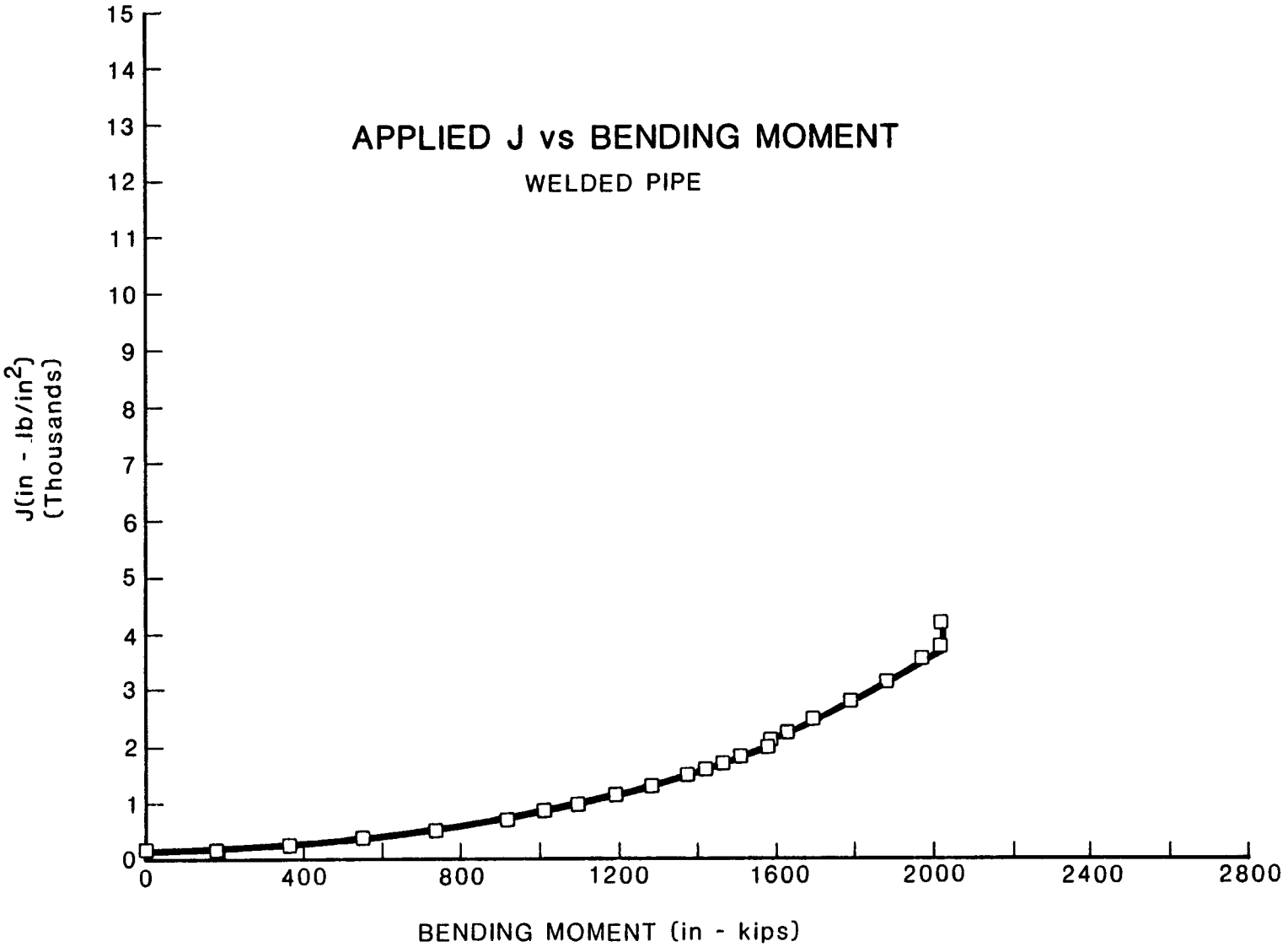

FIGURE 14. APPLIED J VS BENDING MOMENT FOR THE WELDED CRACKED PIPE

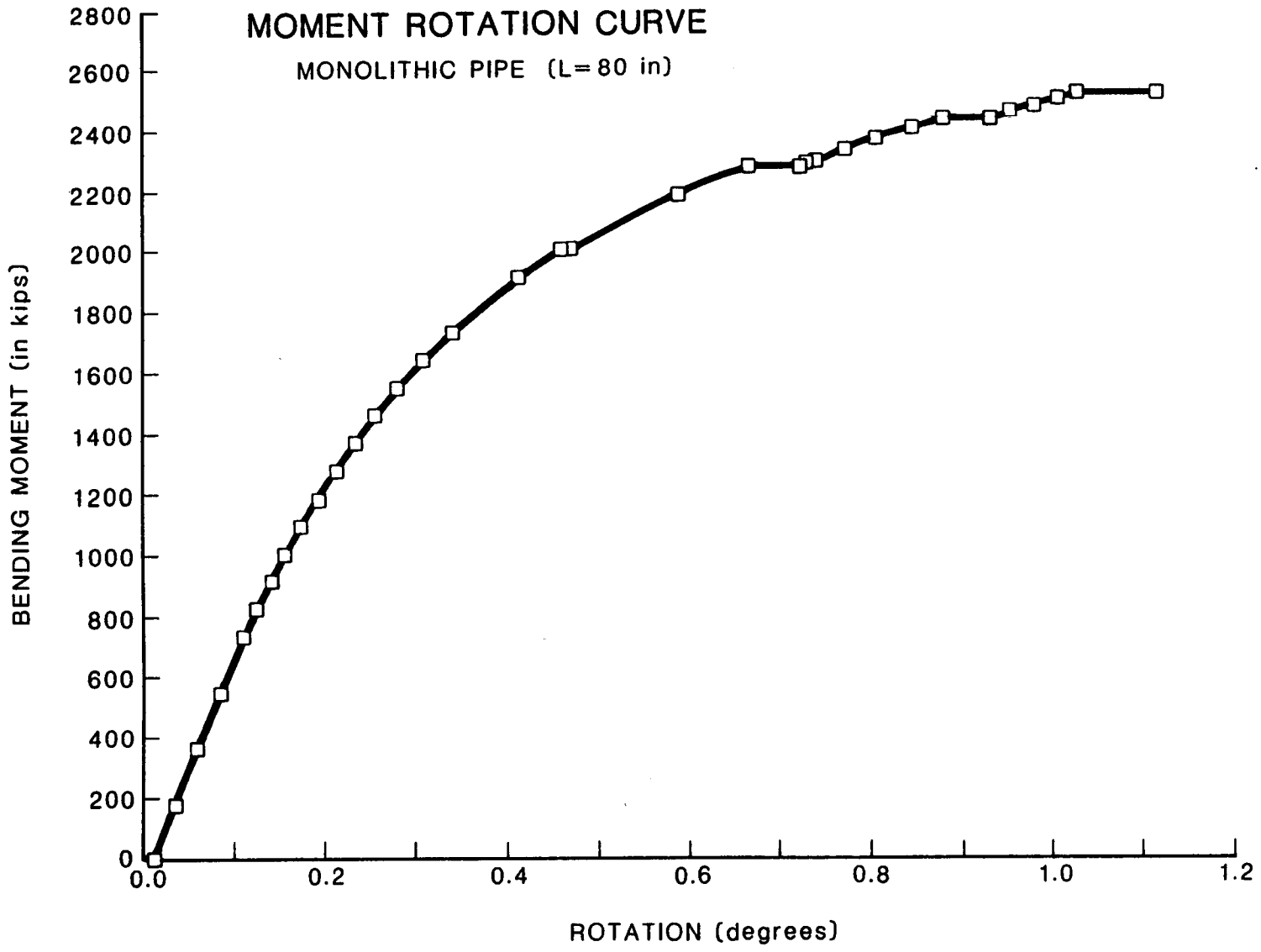

FIGURE 15. M-θ CURVE FOR THE MONOLITHIC CRACKED PIPE

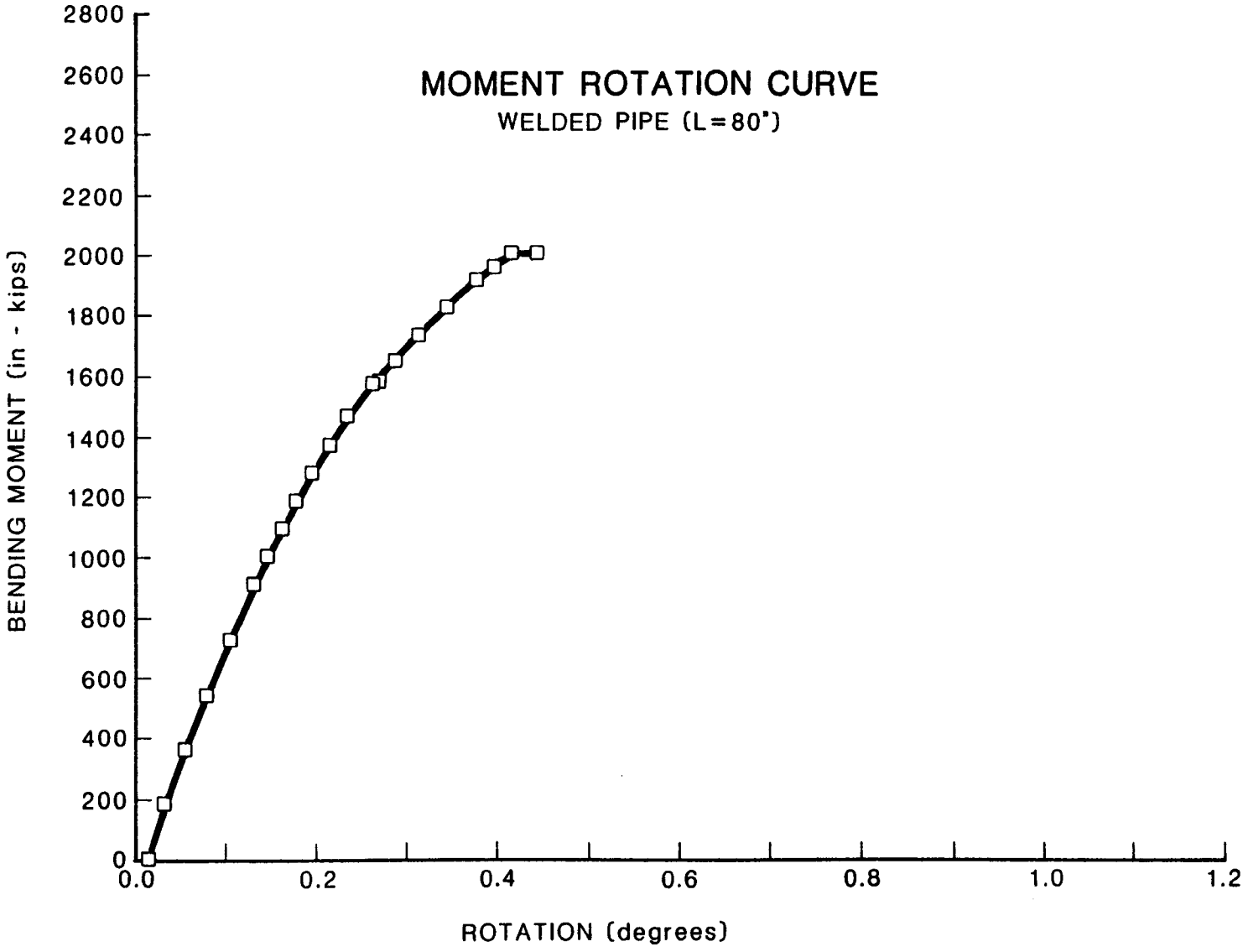

FIGURE 16. M-θ CURVE FOR THE WELDED CRACKED PIPE

DISCUSSIONS AND RECOMMENDATIONS

The computational results indicate that the extent of stable crack growth at fracture instability is 0.1 inches for the welded pipe and 0.3 inches for the monolithic pipe. The accuracy of these values is of course influenced by the mesh size ahead of the crack. A model containing a finer mesh ahead of the crack tip would provide a more precise calculation for the amount of stable crack extension and, hence, for the instability load.

As discussed in the preceding, the incremental crack extensions in this analysis were performed under constant load. This, in conjunction with the mesh size, results in the stair-step nature of the applied J curves shown in Figure 10. Ideally, the crack should be extended as the load is increased (or displacement, if displacement-control is used), such that the material J-resistance curve is followed exactly. This could be accomplished by first performing a trial analysis for crack extension assuming growth under constant load or displacement, then correcting this by increasing the load appropriately to remain on the material J-resistance curve. This "predictor-corrector" procedure should be used in future computations of this kind.

An implicit assumption in the analysis of the welded pipe is that the crack growth behavior of this composite structure is entirely controlled by the weldment material J-resistance curve. Although the crack is located in the weld, the "radius of influence" used to calculate J in the analysis extends well out into the base metal of the pipe. It could be argued that, since such a large volume of base metal is used in the calculation of J, a "hybrid material J-resistance" curve should be used to model the composite effect of both materials in this analysis. Such a curve would be more properly obtained from "generation phase" calculations performed on welded test specimens - see for example, reference [10]. In this type of calculation, a finite element model of a welded test specimen would be forced to respond to the exact experimental load and crack length history, thereby obtaining a "material" J-resistance curve for a welded member. This should be done in subsequent computations.

ACKNOWLEDGEMENT

This research was performed as part of the Oak Ridge National Laboratory Heavy Section Steel Technology Program under ORNL Contract No. 37X97036C. The authors would like to express their appreciation to Dr. Claud Pugh of ORNL together with Jack Strosnider, Charles Serpan and Milton Vagins of the U.S. Nuclear Regulatory Commission for giving them the opportunity to perform this work.

REFERENCES

1. Letter from I. Milne (CERL) to M. F. Kanninen (SwRI), May 29, 1984.

2. Letter from D.E. McCabe (Westinghouse) to M.F. Kanninen (SwRI), June 25, 1984.

3. ADINA - A Finite Element Program for Automatic Dynamic Incremental Nonlinear Analysis. USER'S MANUAL, September 1981. ADINA Engineering Report AE 81-1.

4. T.K. Hellen, "The Finite Element Calculations of Stress Intensity Factors Using Energy Techniques," 2nd International Conference on Structural Mechanics in Reactor Technology (SMiRT), Paper G5/3, Berlin, Germany, 1973.

5. D.M. Parks, "A Stiffness Derivative Finite Technique for Determination of Crack-Tip Stress Intensity Factors," Int. J. Fract., Vol. 10, No. 4, December 1974, p. 487.

6. T.K. Hellen, "On the method of Virtual Crack Extensions," International Journal for Numerical Methods in Engineering, Vol. 9, 1975, p. 187.

7. D.M. Parks, "The Virtual Crack Extension Method for Nonlinear Material Behavior," Computer Methods in Applied Mechanics and Engineering, Vol. 12, 1977, p. 353.

8. D.M. Parks, "Virtual Crack Extension: A general Finite Element Technique for J-Integral Evaluation," Proc. First International Conference on Numerical Methods in Fracture Mechanics, Swansea, England, 1978, p. 464.

9. de Lorenzi, H. G., "On the Energy Release Rate and the J.Integral for 3-D Crack Configurations," International Journal of Fracture, 19 (1982) 183-193.

10. M. F. Kanninen and C. H. Popelar, Advanced Fracture Mechanics, Oxford Press, New York (1985).

APPENDIX A. WORKSHOP PROBLEM
DUCTILE PIPING FRACTURE MECHANICS WORKSHOP
SOUTHWEST RESEARCH INSTITUTE, SAN ANTONIO, TEXAS

JUNE 21 and 22, 1984

WORKSHOP PROBLEM DESCRIPTION

The problem to be solved is that of a large diameter pipe containing a simple through-wall crack as shown in Figure 1. The pipe is subjected to a constant axial stress of 10 ksi. The pipe is made of a power law hardening material assumed to have a true-stress, true-strain curve of the following form:

$$\frac{\varepsilon}{\varepsilon_o} = \frac{\sigma}{\sigma_o} + \alpha\left(\frac{\sigma}{\sigma_o}\right)^n$$

This stress strain curve is for wrought Type 304 stainless steel at 550°F. Specific values for the material constants are given in Table 1.

The first problem is to calculate the applied J value as a function of bending moment up to the limit moment of the pipe. (Limit Moment ≈ 3300 in-Kips, based on a flow stress of 53 ksi.) The second part of the problem is to use the base metal J-integral resistance curve shown in Figure 2 to predict the applied bending moments at crack initiation and at load controlled instability. In addition, an optional exercise would be to assume that the pipe is connected at each end to large rigid masses and that the pipe ends are subject to unlimited monotonically increasing rotation. It should be assumed that the applied axial load of 10 ksi does not vary either as a result of crack growth or of the end rotation. The problem would be to calculate the end rotation ϕ_i at the initiation of circumferential crack growth, the end rotation ϕ_f at crack growth instability, and the extent of stable crack extension $(\Delta\theta)_f$ at instability. For the purpose of this optional exercise, the pipe should be assumed to have a total length of 70 feet.

Elastic-plastic finite element analyses of these problems, both load controlled and displacement controlled, will be performed to provide benchmark solutions. As such a procedure is readily adapted to consider the complications arising when the crack is located in a weld, benchmark solutions for this more complicated problem will also be obtained. This problem is of interest since stainless steel weld material has been shown to have lower

ductile fracture toughness than wrought stainless steel base metal. For this analysis the stress strain curve will be assumed to have the same form as in Equation 1, but with different values of the constants -- see Table 1.

The J-integral resistance curve that is to be assumed for the weld material is shown in Figure 2. The weld should be assumed to be equal in width to the thickness of the pipe. Although it is not expected that participants in the workshop would solve this more complicated weld problem, a discussion of the approach they would use in dealing with the cracked weld problem would be of interest. The results of the finite element analyses of the problem both with and without the weld will be presented toward the end of the workshop.

It should be recognized that this exercise is not intended to be competitive. Instead, the objective is to have the workshop participants be led to a complete and thorough understanding of the various J estimation methods that are available to attack problems such as this. Accordingly, any assumptions, approximations and simplifications that are deemed necessary to solve this problem are acceptable. The only requirement is that they be made clear to the workshop participants.

TABLE 1

STRESS-STRAIN PROPERTIES TO BE USED IN THE WORKSHOP PROBLEM

	Base Material	Weldment
ε_o	8.27 x 10-4	18.0 x 10-4
σ_o	24.8 ksi	53.9 ksi
α	17.3	2.83
n	2.49	11.83

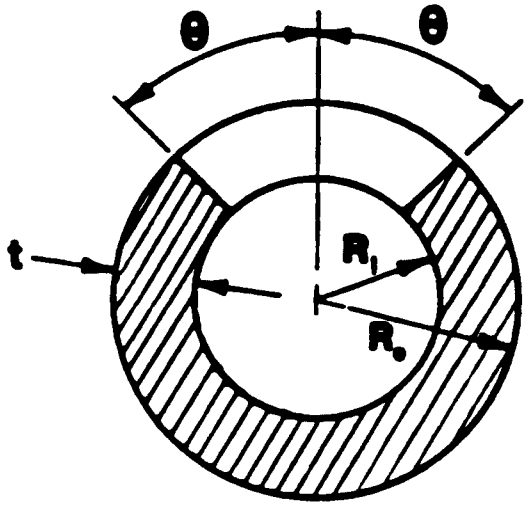

θ = 0.645 radians
R_i = 7.5 inches
R_o = 8.0 inches
t = 0.5 inches

FIGURE 1: CRACKED PIPE GEOMETRY

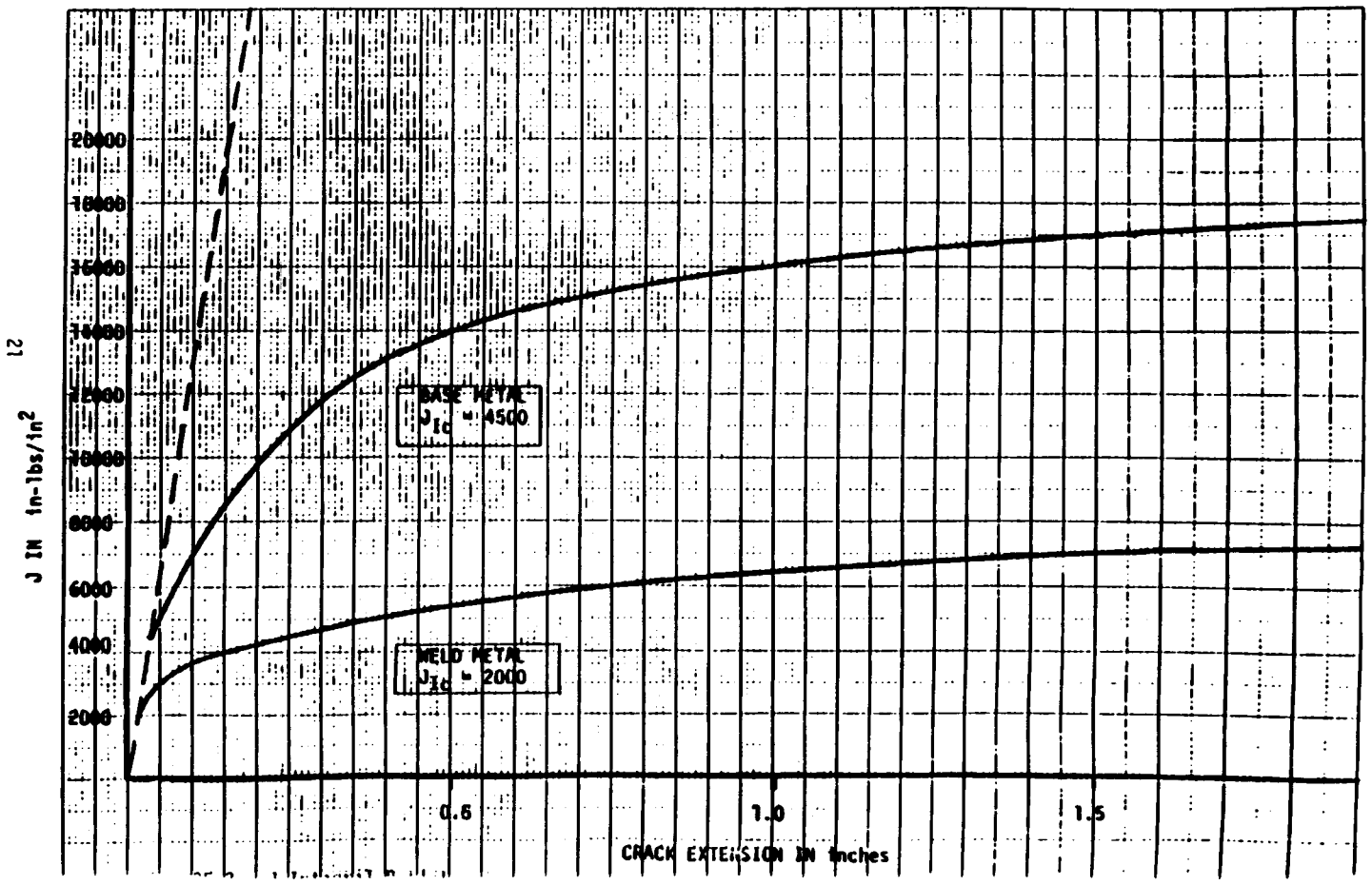

FIGURE 2: J-INTEGRAL RESISTANCE CURVES

APPENDIX B. PIECEWISE LINEAR STRESS-STRAIN CURVE PROPOSED BY MILNE

Following a discussion between M.F. Kanninen and Ian Milne of the UK Central Electricity Generating Board on 16 May 1984, it was agreed that a more appropriate representation of the stress-strain curve for Type 304 stainless steel would be appropriate and that this form could be used in the workshop problem. The true stress-true strain values selected by Milne for a piecewise linear representation are as follows:

True Stress (ksi)	True Strain
25.0	0.0008
28.5	0.0015
31.09	0.003
32.16	0.005
34.37	0.0109
36.72	0.0198
39.14	0.0296
44.27	0.0526
52.8	0.0953
60.42	0.131
112.5	0.405

Milne notes that these data correspond to engineering data with a proof stress of 31 ksi, an ultimate stress of 75 ksi, and a flow stress of 53 ksi. This representation is compared with the power representation (see Appendix A) in Figure 1 of the report.

APPENDIX C. WORKSHOP AGENDA

Thursday, 21 June 1984

9:00 a.m. - Introduction (M. F. Kanninen)

9:15 a.m. - Objectives of the Workshop (J. Strosnider)

9:30 a.m. - Presentation of Workshop Problem Solution by the U.K. Central Electricity Generating Board (R. Ainsworth)

10:30 a.m. - Coffee Break

11:00 a.m. - Presentation of Background for the Solution of the Workshop Problem by the General Electric Company (V. Kumar)

12:00 noon - Presentation of Workshop Problem Solution by the Electric Power Research Institute (D. Norris)

12:45 p.m. - Lunch

2:00 p.m. - Presentation of Elastic-Plastic Fracture Mechanics Applications to Nuclear Plant Piping (Asao Okamoto)

3:00 p.m. - Presentation of Workshop Problem Solution by the Babcock and Wilcox Company (J. Bloom)

4:00 p.m. - Contributed Solutions to the Workshop Problem and General Discussion

5:30 p.m. - Adjourn

Friday, 22 June 1984

9:00 a.m. - Presentation of Workshop Solution by Battelle's Columbus Laboratories (G. Wilkowski, J. Pan, D. Broek)

10:15 a.m. - Presentation of Elastic-Plastic Finite Element Solution by Southwest Research Institute (J. Ahmad)

11:15 a.m. - Coffee Break

11:45 a.m. - Presentation of Workshop Problem Solution by the Fracture Proof Design Corporation (K. C. Cotter)

12:45 p.m. - Lunch

2:00 p.m. - Presentation of Workshop Problem Solution by Structural Integrity Associates (P. Riccardella)

2:30 p.m. - General Discussion

3:30 p.m. - Adjourn

APPENDIX D. PARTICIPANT LIST

Jalees Ahmad
Battelle Columbus Laboratories
505 King Avenue
Columbus, Ohio 43201 (614)-424-4559

R.A. Ainsworth
CENTRAL ELECRICITY GENERATING BOARD
Berkeley Nuclear Laboratories
Berkeley, Gloucestershire GL13 9PB
ENGLAND (0453) 810451

Warren Bamford
WESTINGHOUSE NUCLEAR CENTER
P.O. BOX 355
Pittsburgh, Pennsylvania 15235 (412) 374-5541

B. R. Bass
OAK RIDGE NATIONAL LABORATORY
P.O. Box Y
Oak Ridge, Tennessee 37830 (615) 574-88718

Suren Bhandari
NOVATOME
RN 186
Le Plessis Robinson
F - 92357 FRANCE (331) 537-6047

Joseph M. Bloom
BABCOCK & WILCOX R&D
Box 828
Alliance, Ohio 44601 (216) 821-9110, ext. 229

Walter Bradley
TEXAS A&M UNIVERSITY
Mechanical Engineering
College Station, Texas 77843 (409) 845-1259

David Broek
FRACTURESEARCH INC.
123 Meadow Drive SW
Pataskala, Ohio 43062 (614) 927-6828

Gary Burnell
TEXAS A&M UNIVERSITY
College Station, Texas 77840 (609) 845-2471

Janet P. Buckingham
SOUTHWEST RESEARCH INSTITUTE
P.O. Drawer 28510
San Antonio, Texas 78284 (512) 684-5111, ext. 2407

Joseph W. Cardinal
SOUTHWEST RESEARCH INSTITUTE
P.O. Drawer 28510
San Antonio, Texas 78284 (512) 684-5111, ext. 3323

Jean-Louis Cheissoux
CEA
CEN de Cadarache
Saint-Paul-lez-Durance Tlx CEACA No. 440678 F
F 13115 FRANCE Tel (42)253328

L.R. Cornwell
TEXAS A&M UNIVERSITY
Department of Mechanical Engineering
College Station, Texas 77840 (409) 845-5243

K. H. Cotter
FRACTURE PROOF DESIGN CORPORATION
77 Maryland Plaza Tlx 469259
St. Louis, Missouri 63108 Tel (314) 361-6200

Claude Faidy
E.D.F.
CEDEX 08
Paris la Defense
F 92080 FRANCE (1) 7754151

B. R. Ganta
COMBUSTION ENGINEERING, INC.
1000 Prospect Hill Road
Windsor, Connecticut 06070 (203) 688-1911, ext. 3869

Bob Gates
CENTRAL ELECTRICITY GENERATING BOARD
Bedminster Down, Bridgwater Road
Bristol ENGLAND 0272 678260

Marge German
GENERAL ELECTRIC COMPANY
1 River Road
Schenectady, New York 12305 (518) 385-5970

Allen Hiser
MATERIALS ENGINEERING ASSOC.
9700B Martin Luther King, Jr., Hwy.
Lanham, Maryland 20770 (301) 577-9490

D. G. Hooten
NATIONAL NUCLEAR CORPORATION
Warrington Road
Risley, Warrington
Cheshire ENGLAND Warrington 51291

Joseph Jansky
BTB
Rilkestrasse 5
7250 Leonberg
Federal Republic of Germany (07152) 21008

M. F. Kanninen
SOUTHWEST RESEARCH INSTITUTE
P.O. Drawer 28510
San Antonio, Texas 78284 (512) 684-5111, ext. 3248

Rauli Pellervo Keskinen
FINNISH CENTRE FOR RADIATION AND NUCLEAR SAFETY
P.O. Box 268
SF - 00101 Helsinki
FINLAND Tlx 122 691 STUK

Virendra Kumar
GENERAL ELECTRIC CO., R&D CENTER
1 River Road, Bldg K-1, Rm 3A23
Schenectady, New York 12301 (518) 385-0d812

John Landes
The University of Tennessee
310 Perkins Hall
Knoxville, TN 37996 (615) 974-7670

B.D. Liaw
U.S. NUCLEAR REGULATORY COMMISSION
Mail Stop 7E-23
Washington, DC 20555 (301) 492-3233

Pietro P. Milella
ENEA
Via V. Brancati 48
Rome 00144 ITALY (396) 8528-2171

Prasad K. Nair
SOUTHWEST RESEARCH INSTITUTE
P.O. Drawer 28510
San Antonio, Texas 78284 (512) 684-5111, ext. 3248

Douglas M. Norris
ELECTRIC POWER RESEARCH INSTITUTE
3412 Hillview Avenue
P.O. Box 10412
Palo Alto, CA 94304 (415) 855-2791

Asao Okamoto
ELECTRIC POWER RESEARCH INSTITUTE
3412 Hillview Avenue
P.O. Box 10412
Palo Alto, CA 94043 (415) 969-5397

Jwo Pan
Univ. of Michigan
2250 G.G. Brown
Ann Arbor, MI 48109
(313) 764-9404

Victoria Papaspyropoulos
Battelle Columbus Laboratories
505 King Avenue
Columbus, Ohio 43261
(614) 424-4630

Andre Pellissier Tanon
FRAMATONE
TourFiat, Cedex 16
Paris - La Defense
F 9284 FRANCE 1-796-0468
1-796-0468

Carl H. Popelar
OHIO STATE UNIVERSITY
155 W. Woodruff Avenue
Columbus, Ohio 43210
(614) 422-7369

Claud E. Pugh
OAK RIDGE NATIONAL LABORATORY
Building 9204-1, MS6
P.O. Box Y
Oak Ridge, Tennessee 37831
(615) 574-0717

David Quinones
SCIENCE APPLICATIONS, INC.
2450 Washington Avenue, s240
San Leandro, California
(415) 351-7807

Pete Riccardella
STRUCTURAL INTEGRITY ASSOCIATES
3150 Almaden Expy, s226
San Jose, California 95120
(408) 978-8200

Rauno Rintamaa
TECHNICAL RESEARCH CENTRE OF FINLAND
Metalliraiehenkuja 6
SF-02150 Espoo Tlx 122972 vttha sf
FINLAND

Alfredo Squilloni
CISE
Via Reggio Emilia, 39
Segrate (Milano) 20090
ITALY
Tlx 311643 CISE I
02-21672413

Jack Strosnider
U.S. NUCLEAR REGULATORY COMMISSION
475 Allendale Rd.
King of Prussia, PA 19406
(215) 337-5198

Brian Tomkins
U.K. ATOMIC ENERGY AUTHORITY
Risley
Warrington ENGLAND 925-31244

Gery Wilkowski
BATTELLE COLUMBUS LABORATORIES
505 King Avenue
Columbus, Ohio 43201 (614) 424-4680

Kenneth K. Yoon
BABCOCK & WILCOX
P.O. Box 1260
Lynchburg, Virginia 24505 (804) 385-3280

Akram Zahoor
NOVETECH Corp.
5 Choke Cherry Rd., Suite 120
Rockville, Md. 20850 (301) 330-1919

NRC FORM 335 (2-84) NRCM 1102, 3201, 3202

U.S. NUCLEAR REGULATORY COMMISSION

BIBLIOGRAPHIC DATA SHEET

SEE INSTRUCTIONS ON THE REVERSE.

1. REPORT NUMBER *(Assigned by TIDC, add Vol. No., if any)*

NUREG/CP-0075
CSNI Report No. 97

2. TITLE AND SUBTITLE

Proceedings of the CSNI/NRC Workshop on Ductile Piping Fracture Mechanics

3. LEAVE BLANK

4. DATE REPORT COMPLETED

MONTH | YEAR

5. AUTHOR(S)

Compiled by M. F. Kanninen

6. DATE REPORT ISSUED

MONTH: June | YEAR: 1988

7. PERFORMING ORGANIZATION NAME AND MAILING ADDRESS *(Include Zip Code)*

Southwest Research Institute
P.O. Drawer 28510
San Antonio, TX 78284

8. PROJECT/TASK/WORK UNIT NUMBER

9. FIN OR GRANT NUMBER

B0119

10. SPONSORING ORGANIZATION NAME AND MAILING ADDRESS *(Include Zip Code)*

Div. of Engineering
Office of Nuclear Regulatory Research
U.S. Nuclear Regulatory Commission
Washington, DC 20555

Heavy Section Steel Technology Program
Oak Ridge National Laboratory
P.O. Box Y, Bldg. 9201
Oak Ridge, TN 37832

Nuclear Safety Div.
Nuclear Energy Agency
Organ. for Economic Co-Operation and Development (OECD)
38, Boulevard Suchet
75016 Paris, France

11a. TYPE OF REPORT

Conference Proceedings

b. PERIOD COVERED *(Inclusive dates)*

13. ABSTRACT *(200 words or less)*

This report contains the papers presented at a workshop meeting that was conducted to compare the various different elastic-plastic fracture mechanics analysis methods that can be applied to assess the margin of safety in cracked nuclear plant pipes. A specific problem - a circumferentially cracked Type 304 stainless steel pipe in combined axial tension and bending - was addressed. The applied bending moments at crack growth initiation and at fracture instability were sought. Seven estimation type solutions were performed along with a benchmark elastic-plastic finite element solution.

It was learned that precise specification of the material stress-strain curve must be made to obtain meaningful results. But, when applied under controlled conditions, the different estimation method solutions do provide reasonably consistent results. These results appear to be conservative in comparison with an elastic-plastic finite element solution that was performed to provide a comparison with these results.

14. DOCUMENT ANALYSIS – a. KEYWORDS/DESCRIPTORS

elastic-plastic fracture mechanics

b. IDENTIFIERS/OPEN-ENDED TERMS

elastic-plastic finite element
deformation plasticity
elastic-plastic analysis methods
ductile piping fracture analyses
leak-before-break
J-integral
Double-Ended Guillotine Break (DEGB)
Loss of Coolant Accident (LOCA)
benchmark problem
through-wall crack
true-stress, true-strain curve

15. AVAILABILITY STATEMENT

Unlimited

16. SECURITY CLASSIFICATION

(This page) Unclassified

(This report) Unclassified

17. NUMBER OF PAGES

18. PRICE

UNITED STATES
NUCLEAR REGULATORY COMMISSION
WASHINGTON, D.C. 20555

SPECIAL FOURTH-CLASS RATE
POSTAGE & FEES PAID
USNRC
PERMIT No. G-67